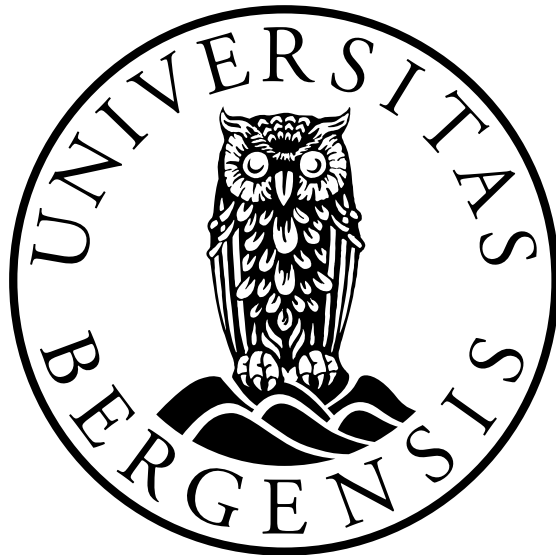


# **Numerical methods for nonlinear nonlocal water wave models**

**Daulet Moldabayev**



Dissertation for the degree of Philosophiae Doctor (PhD)

Department of Mathematics  
University of Bergen  
Norway

April 2017



# **Preface**

This dissertation is submitted as a partial fulfillment of the requirements for the degree Doctor of Philosophy (PhD) at the Department of Mathematics, University of Bergen. The research was supported by the Research Council of Norway on grant no. 213474/F20.

The advisory committee has consisted of Henrik Kalisch (University of Bergen, Bergen, Norway), Dmitry Pelinovsky (McMaster University, Hamilton, Ontario, Canada) and Angel Durán (Universidad de Valladolid, Valladolid, Spain).



# Acknowledgements

First of all I would like to thank Henrik Kalisch and Magnus Svärd who carried out the selection process of candidates for the PhD position. I am sincerely thankful to Professor Henrik Kalisch, my main supervisor, for sharing knowledge and guiding me, for his enthusiasm, support and encouragement. The thesis would not have been possible without you.

In the course of the doctorate studies, I have had fruitful collaboration with Olivier Verdier, Evgueni Dinvay, Denys Dutykh, Ben Segal and others. I would like to thank them for productive discussions, advices on research questions and some inspiring ideas we came up with.

As a PhD Candidate I have been lucky to meet my colleagues and fellow students at the Department of Mathematics. They have always provided a friendly and supportive environment. I appreciate everything we have experienced during the time of our studies.

I would like to express my gratitude to my family for their continuous support and encouragement over the years of my studies. I am also thankful for all of my teachers and professors from schools and universities I studied at.

I am heartily grateful for my wife Assem. You have always been there for me. Without your love, support and understanding I would not have been able to go that far.



# **Abstract**

Nonlinear water wave models



# Outline

This thesis is organised in the following way. Part I contains general theoretical background on nonlinear wave models as well as description of methods used to solve the equations involved. Some properties of solutions to the equations and a summary of results are also given in the first part. Part 2 consists of the research papers that present scientific results in detail.

## List of research papers included in Part II

### Paper A:

Moldabayev, D., Kalisch, H., Dutykh, D.: *The Whitham equation as a model for surface water waves*, Phys. D **309**, 99–107 (2015),  
<http://dx.doi.org/10.1016/j.physd.2015.07.010>.

### Paper B:

Dinvay, E., Moldabayev, D., Dutykh, D., Kalisch, H.: *The Whitham equation with surface tension*, Nonlinear Dynamics, 1–14 (2017),  
<http://dx.doi.org/10.1007/s11071-016-3299-7>.

### Paper C:

Henrik Kalisch, Daulet Moldabayev, Olivier Verdier: *A numerical study of nonlinear dispersive wave models with SpecTravVave*, specify status of the paper.

### Paper D:

Benjamin Segal, Daulet Moldabayev, Henrik Kalisch, Bernard Deconinck: *Explicit solutions for a long-wave model with constant vorticity*, submitted to European Journal of Mechanics - B/Fluids.



# Contents

<b>Preface</b>	<b>i</b>
<b>Acknowledgements</b>	<b>iii</b>
<b>Abstract</b>	<b>v</b>
<b>Outline</b>	<b>vii</b>
<b>I Background</b>	<b>1</b>
<b>1 Introduction</b>	<b>3</b>
<b>Bibliography</b>	<b>5</b>
<b>II Scientific results</b>	<b>7</b>
<b>Paper A The Whitham equation as a model for surface water waves</b>	<b>9</b>
<b>Paper B The Whitham equation with surface tension</b>	<b>21</b>
<b>Paper C A numerical study of nonlinear dispersive wave models with Spec-TraVVave</b>	<b>37</b>
<b>Paper D Explicit solutions for a long-wave model with constant vorticity</b>	<b>67</b>



# **Part I**

## **Background**



# **Chapter 1**

## **Introduction**

This is the introduction [1–3]...



# Bibliography

- [1] BIRKELAND, T., AND NEPSTAD, R. Pyprop. <http://pyprop.googlecode.com>. 1
- [2] DE BOOR, C. *A Practical Guide to Splines*. Springer-Verlag, New York, 2001. 1
- [3] DINVAY, E., MOLDABAYEV, D., DUTYKH, D., AND KALISCH, H. The whitham equation with surface tension. *Nonlinear Dynamics* (2017), 1–14, doi: [10.1007/s11071-016-3299-7](https://doi.org/10.1007/s11071-016-3299-7). 1



## **Part II**

## **Scientific results**



# **Paper A**

## **The Whitham equation as a model for surface water waves**

Daulet Moldabayev, Henrik Kalisch, Denys Dutyh

*Physica D* **309**, (2015)

<http://dx.doi.org/10.1016/j.physd.2015.07.010>





## The Whitham Equation as a model for surface water waves



Daulet Moldabayev<sup>a</sup>, Henrik Kalisch<sup>a,\*</sup>, Denys Dutykh<sup>b</sup>

<sup>a</sup> Department of Mathematics, University of Bergen, Postbox 7800, 5020 Bergen, Norway

<sup>b</sup> LAMA, UMR5127, CNRS – Université Savoie Mont Blanc, 73376 Le Bourget-du-Lac Cedex, France

### HIGHLIGHTS

- Definition of Whitham scaling regime.
- Derivation of a Hamiltonian Whitham system.
- Asymptotic derivation of the Whitham equation.
- Comparison of Whitham, KdV, BBM and Padé models with inviscid free surface dynamics.

### ARTICLE INFO

#### Article history:

Received 16 October 2014

Received in revised form

9 June 2015

Accepted 24 July 2015

Available online 31 July 2015

Communicated by J. Bronski

#### Keywords:

Nonlocal equations  
Nonlinear dispersive equations  
Hamiltonian models  
Solitary waves  
Surface waves

### ABSTRACT

The Whitham equation was proposed as an alternate model equation for the simplified description of unidirectional wave motion at the surface of an inviscid fluid. As the Whitham equation incorporates the full linear dispersion relation of the water wave problem, it is thought to provide a more faithful description of shorter waves of small amplitude than traditional long wave models such as the KdV equation.

In this work, we identify a scaling regime in which the Whitham equation can be derived from the Hamiltonian theory of surface water waves. A Hamiltonian system of Whitham type allowing for two-way wave propagation is also derived. The Whitham equation is integrated numerically, and it is shown that the equation gives a close approximation of inviscid free surface dynamics as described by the Euler equations. The performance of the Whitham equation as a model for free surface dynamics is also compared to different free surface models: the KdV equation, the BBM equation, and the Padé (2,2) model. It is found that in a wide parameter range of amplitudes and wavelengths, the Whitham equation performs on par with or better than the three considered models.

© 2015 The Authors. Published by Elsevier B.V.  
This is an open access article under the CC BY-NC-ND license  
(<http://creativecommons.org/licenses/by-nc-nd/4.0/>).

### 1. Introduction

In its simplest form, the water-wave problem concerns the flow of an incompressible inviscid fluid with a free surface over a horizontal impenetrable bed. In this situation, the fluid flow is described by the Euler equations with appropriate boundary conditions, and the dynamics of the free surface are of particular interest in the solution of this problem.

There are a number of model equations which allow the approximate description of the evolution of the free surface without having to provide a complete solution of the fluid flow below the surface. In the present contribution, interest is focused

on the derivation and evaluation of a nonlocal water-wave model known as the Whitham equation. The equation is written as

$$\eta_t + \frac{3}{2} \frac{c_0}{h_0} \eta \eta_x + K_{h_0} * \eta_x = 0, \quad (1)$$

where the convolution kernel  $K_{h_0}$  is given in terms of the Fourier transform by

$$\mathcal{F}K_{h_0}(\xi) = \sqrt{\frac{g \tanh(h_0 \xi)}{\xi}}, \quad (2)$$

$g$  is the gravitational acceleration,  $h_0$  is the undisturbed depth of the fluid, and  $c_0 = \sqrt{gh_0}$  is the corresponding long-wave speed. The convolution can be thought of as a Fourier multiplier operator, and (2) represents the Fourier symbol of the operator.

The Whitham equation was proposed by Whitham [1] as an alternative to the well known Korteweg-de Vries (KdV) equation

$$\eta_t + c_0 \eta_x + \frac{3}{2} \frac{c_0}{h_0} \eta \eta_x + \frac{1}{6} c_0 h_0^2 \eta_{xxx} = 0. \quad (3)$$

\* Corresponding author.

E-mail addresses: [daulet.moldabayev@math.uib.no](mailto:daulet.moldabayev@math.uib.no) (D. Moldabayev), [henrik.kalisch@math.uib.no](mailto:henrik.kalisch@math.uib.no) (H. Kalisch), [Denys.Dutykh@univ-savoie.fr](mailto:Denys.Dutykh@univ-savoie.fr) (D. Dutykh).

<http://dx.doi.org/10.1016/j.physd.2015.07.010>

0167-2789/© 2015 The Authors. Published by Elsevier B.V. This is an open access article under the CC BY-NC-ND license (<http://creativecommons.org/licenses/by-nc-nd/4.0/>).

The validity of the KdV equation as a model for surface water waves can be described as follows. Suppose a wave field with a prominent amplitude  $a$  and characteristic wavelength  $l$  is to be studied. The KdV equation is known to produce a good approximation of the evolution of the waves if the amplitude of the waves is small and the wavelength is large when compared to the undisturbed depth, and if in addition, the two non-dimensional quantities  $a/h_0$  and  $h_0^2/l^2$  are of similar size. The latter requirement can be written in terms of the Stokes number as

$$\delta = \frac{al^2}{h_0^3} \sim 1.$$

While the KdV equation is a good model for surface waves if  $\delta \sim 1$ , one notorious problem with the KdV equation is that it does not model accurately the dynamics of shorter waves. Recognizing this shortcoming of the KdV equation, Whitham proposed to use the same nonlinearity as the KdV equation, but couple it with a linear term which mimics the linear dispersion relation of the full water-wave problem. Thus, at least in theory, the Whitham equation can be expected to yield a description of the dynamics of shorter waves which is closer to the solutions of the more fundamental Euler equations which govern the flow.

The Whitham equation has been studied from a number of vantage points during recent years. In particular, the existence of traveling and solitary waves has been established in [2,3]. Well posedness of a similar equation was investigated in [4–6], and a model with variable depth has been studied numerically in [7]. Moreover, it has been shown in [8,9] that periodic solutions of the Whitham equation feature modulational instability for short enough waves in a similar way as small-amplitude periodic wave solutions of the water-wave problem. However, even though the equation is routinely mentioned in texts on nonlinear waves [10, 11], it appears that the performance of the Whitham equation in the description of surface water waves has not been investigated so far.

The purpose of the present article is to give an asymptotic derivation of the Whitham equation as a model for surface water waves, and to confirm Whitham's expectation that the equation is a fair model for the description of time-dependent surface water waves. For the purpose of the derivation, we introduce an exponential scaling regime in which the Whitham equation can be derived asymptotically from an approximate Hamiltonian principle for surface water waves. In order to motivate the use of this scaling, note that the KdV equation has the property that wide classes of initial data decompose into a number of solitary waves and small-amplitude dispersive residue [12]. For the KdV equations, solitary-wave solutions are known in closed form, and are given by

$$\eta = \frac{a}{h_0} \operatorname{sech}^2 \left( \sqrt{\frac{3a}{4h_0^3}} (x - ct) \right) \quad (4)$$

for a certain wave celerity  $c$ . These waves clearly comply with the amplitude-wavelength relation  $a/h_0 \sim h_0^2/l^2$  which was mentioned above. It appears that the Whitham equation – as indeed do many other nonlinear dispersive equations – also has the property that broad classes of initial data rapidly decompose into ordered trains of solitary waves (see Fig. 1). Quantifying the amplitude-wavelength relation for these solitary waves yields an asymptotic regime which is expected to be relevant to the validity of the Whitham equation as a water wave model.

As the curve fit in the right panel of Fig. 1 shows, the relationship between wavelength and amplitude of the Whitham solitary waves can be approximately described by the relation  $\frac{a}{h_0} \sim e^{-\kappa(l/h_0)^v}$  for certain values of  $\kappa$  and  $v$ . Since the Whitham solitary waves are not known in exact form, the values of  $\kappa$  and  $v$  have to be found numerically. Then one may define a Whitham scaling regime

$$\mathcal{W}(\kappa, v) = \frac{a}{h_0} e^{\kappa(l/h_0)^v} \sim 1, \quad (5)$$

and it will be shown in Sections 2 and 3 that this scaling can be used advantageously in the derivation of the Whitham equation. The derivation proceeds by examining the Hamiltonian formulation of the water-wave problem due to Zakharov, Craig and Sulem [13,14], and by restricting to wave motion which is predominantly in the direction of increasing values of  $x$ . The approach is similar to the method of [15], but relies on the new relation (5).

First, in Section 2, a Whitham system is derived which allows for two-way propagation of waves. The Whitham equation is found in Section 3. Finally, in Section 4, a comparison of modeling properties of the KdV and Whitham equations is given. The comparison also includes the regularized long-wave equation

$$\eta_t + c_0 \eta_x + \frac{3}{2} \frac{c_0}{h_0} \eta \eta_x - \frac{1}{6} h_0^2 \eta_{xxt} = 0, \quad (6)$$

which was put forward in [16] and studied in depth in [17], and which is also known as the BBM or PBBM equation. The linearized dispersion relation of this equation is not an exact match to the dispersion relation of the full water-wave problem, but it is much closer than the KdV equation, and it might also be expected that this equation may be able to model shorter waves more successfully than the KdV equation. In order to obtain an even better match of the linear dispersion relation, one may make use of Padé expansions. In the context of simplified evolutions equations, this approach was pioneered in [18]. For uni-directional models, this approach was advocated in [19], and in particular, the equation based on the Padé (2,2) approximation was studied in depth. In dimensional variables, this model takes the form

$$\eta_t + c_0 \eta_x + \frac{3}{2} \frac{c_0}{h_0} \eta \eta_x - \frac{3}{20} c_0 h_0^2 \eta_{xxx} - \frac{19}{60} h_0^2 \eta_{xxt} = 0. \quad (7)$$

The dispersion relations for the KdV, BBM and Padé (2,2) models are respectively

$$\begin{aligned} c(k) &= c_0 - \frac{1}{6} c_0 h_0^2 k^2 && (\text{KdV}), \\ c(k) &= \frac{1}{1 + \frac{1}{6} h_0^2 k^2} && (\text{BBM}), \\ c(k) &= c_0 \frac{1 + \frac{3}{20} h_0^2 k^2}{1 + \frac{19}{60} h_0^2 k^2} && (\text{Padé (2,2)}). \end{aligned}$$

These approximate dispersion relations are compared to the full dispersion relation in Fig. 2. It appears clearly that the Padé (2,2) approximation remains much closer to the full dispersion relation than the dispersion relations based on either the linear KdV or linear BBM equations. As will be seen in Section 4, solutions of both the Whitham and Padé (2,2) equations give closer approximations to solutions of the full Euler equations than either the KdV or BBM equations in most cases investigated. However, the Whitham equation still keeps a slight edge over the Padé model.

## 2. Derivation of evolution systems of Whitham type

The surface water-wave problem is generally described by the Euler equations with slip conditions at the bottom, and kinematic and dynamic boundary conditions at the free surface. Assuming weak transverse effects, the unknowns are the surface elevation  $\eta(x, t)$ , the horizontal and vertical fluid velocities  $u_1(x, z, t)$  and  $u_2(x, z, t)$ , respectively, and the pressure  $P(x, z, t)$ . If the assumption of irrotational flow is made, then a velocity potential  $\phi(x, z, t)$  can be used. In order to nondimensionalize the problem, the undisturbed depth  $h_0$  is taken as a unit of distance, and the

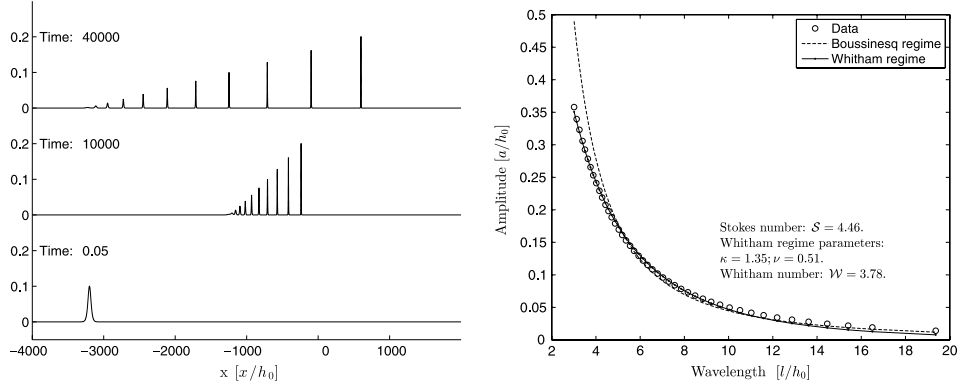


**Fig. 1.** Left panel: Formation of solitary waves of the Whitham equation from Gaussian initial data. Right panel: Curve fit for the Whitham regime and for the Boussinesq regime to amplitude/wavelength data from Whitham solitary waves. The wavelength is defined as  $l = \frac{1}{a} \int_{-\infty}^{\infty} \eta(x) dx$ .

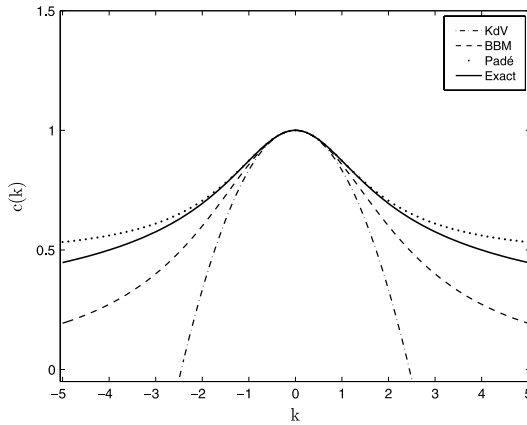


**Fig. 2.** Approximate models to the exact dispersion relation of the full water-wave problem.

parameter  $\sqrt{h_0/g}$  as a unit of time. For the remainder of this article, all variables appearing in the water-wave problem are considered as being non-dimensional. The problem is posed on a domain  $\{(x, z)^T \in \mathbb{R}^2 \mid -1 < z < \eta(x, t)\}$  which extends to infinity in the positive and negative  $x$ -direction. Due to the incompressibility of the fluid, the potential then satisfies Laplace's equation in this domain. The fact that the fluid cannot penetrate the bottom is expressed by a homogeneous Neumann boundary condition at the flat bottom. Thus we have

$$\begin{aligned} \phi_{xx} + \phi_{zz} &= 0 \quad \text{in } -1 < z < \eta(x, t) \\ \phi_z &= 0 \quad \text{on } z = -1. \end{aligned}$$

The pressure is eliminated with the help of the Bernoulli equation, and the free-surface boundary conditions are formulated in terms of the potential and the surface excursion by

$$\left. \begin{aligned} \eta_t + \phi_x \eta_x - \phi_z &= 0, \\ \phi_t + \frac{1}{2} (\phi_x^2 + \phi_z^2) + \eta &= 0, \end{aligned} \right\} \text{on } z = \eta(x, t).$$

The total energy of the system is given by the sum of kinetic energy and potential energy, and normalized such that the potential energy is zero when no wave motion is present at the surface. Accordingly the Hamiltonian function for this problem is

$$H = \int_{\mathbb{R}} \int_0^\eta z dz dx + \int_{\mathbb{R}} \int_{-1}^\eta \frac{1}{2} |\nabla \phi|^2 dz dx. \quad (8)$$

Defining the trace of the potential at the free surface as  $\Phi(x, t) = \phi(x, \eta(x, t), t)$ , one may integrate in  $z$  in the first integral and use the divergence theorem on the second integral in order to arrive at the formulation

$$H = \frac{1}{2} \int_{\mathbb{R}} [\eta^2 + \Phi G(\eta) \Phi] dx. \quad (9)$$

This is the Hamiltonian formulation of the water wave problem as found in [13,20,14], and written in terms of the Dirichlet–Neumann operator  $G(\eta)$ . As shown in [21], the Dirichlet–Neumann operator can be expanded in a series of the form

$$G(\eta) \Phi = \sum_{j=0}^{\infty} G_j(\eta) \Phi. \quad (10)$$

In order to proceed, we need to understand the first few terms in this series. As shown in [15,13], the first two terms in this series can be written with the help of the operator  $D = -i\partial_x$  as

$$G_0(\eta) = D \tanh(D), \quad G_1(\eta) = D\eta D - D \tanh(D) \eta D \tanh(D).$$

Note that it can be shown that the terms  $G_j(\eta)$  for  $j \geq 2$  are of quadratic or higher-order in  $\eta$ , and will therefore not be needed in the current analysis.

It will be convenient for the present purpose to formulate the Hamiltonian in terms of the dependent variable  $u = \Phi_x$ . To this end, we define the operator  $\mathcal{K}(\eta)$  by

$$G(\eta) = D \mathcal{K}(\eta) D.$$

As was the case with  $G(\eta)$ , the operator  $\mathcal{K}(\eta)$  can be expanded in a Taylor series around zero as

$$\mathcal{K}(\eta) \xi = \sum_{j=0}^{\infty} \mathcal{K}_j(\eta) \xi, \quad \mathcal{K}_j(\eta) = D^{-1} G_j(\eta) D^{-1}. \quad (11)$$

In particular, note that  $\mathcal{K}_0 = \frac{\tanh D}{D}$ . In non-dimensional variables, we write the operator with the integral kernel  $K_{h_0}$  as  $K = \sqrt{\frac{\tanh D}{D}}$ , so that we have  $\mathcal{K}_0 = K^2$ . The Hamiltonian is then expressed as

$$H = \frac{1}{2} \int_{\mathbb{R}} [\eta^2 + u \mathcal{K}(\eta) u] dx. \quad (12)$$

The water-wave problem can then be written as a Hamiltonian system using the variational derivatives of  $H$  and posing the Hamiltonian equations

$$\eta_t = -\partial_x \frac{\delta H}{\delta u}, \quad u_t = -\partial_x \frac{\delta H}{\delta \eta}. \quad (13)$$

This system is not in canonical form as the associated structure map  $J_{\eta,u}$  is symmetric:

$$J_{\eta,u} = \begin{pmatrix} 0 & -\partial_x \\ -\partial_x & 0 \end{pmatrix}.$$

We now proceed to derive a system of equations which is similar to the Whitham equation (1), but allows bi-directional wave propagation. This system will be a stepping stone on the way to a derivation of (1), but may also be of independent interest. Consider a wave-field having a characteristic wavelength  $l$  and a characteristic amplitude  $a$ . Taking into account the nondimensionalization, the two scalar parameters  $\lambda = l/h_0$  and  $\alpha = a/h_0$  appear. In order to introduce the long-wave and small amplitude approximation into the non-dimensional problem, we use the scaling  $\tilde{x} = \frac{1}{\lambda}x$ , and  $\eta = \alpha\tilde{\eta}$ . This induces the transformation  $\tilde{D} = \lambda D = -\lambda i\partial_x$ . If the energy is nondimensionalized in accord with the nondimensionalization mentioned earlier, then the natural scaling for the Hamiltonian is  $\tilde{H} = \alpha^2 H$ . In addition, the unknown  $u$  is scaled as  $u = \alpha\tilde{u}$ . The scaled Hamiltonian (12) is then written as

$$\begin{aligned} \tilde{H} = & \frac{1}{2} \int_{\mathbb{R}} \tilde{\eta}^2 dx + \frac{1}{2} \int_{\mathbb{R}} \tilde{u} \left[ 1 - \frac{1}{3} \lambda^{-2} \tilde{D}^2 + \dots \right] \tilde{u} dx \\ & + \frac{\alpha}{2} \int_{\mathbb{R}} \tilde{\eta} \tilde{u}^2 dx - \frac{\alpha}{2} \int_{\mathbb{R}} \tilde{u} \left[ \lambda^{-1} \tilde{D} - \frac{1}{3} \lambda^{-3} \tilde{D}^3 + \dots \right] \\ & \times \tilde{\eta} \left[ \lambda^{-1} \tilde{D} - \frac{1}{3} \lambda^{-3} \tilde{D}^3 + \dots \right] \tilde{u} dx. \end{aligned}$$

Let us now introduce the small parameter  $\mu = \frac{1}{\lambda}$ , and assume for simplicity that  $\alpha = e^{-\kappa/\mu^v}$ , which corresponds to the case where  $\mathcal{W}(\kappa, v) = 1$ . Then the Hamiltonian can be written in the following form:

$$\begin{aligned} \tilde{H} = & \frac{1}{2} \int_{\mathbb{R}} \tilde{\eta}^2 dx + \frac{1}{2} \int_{\mathbb{R}} \tilde{u} \left[ 1 - \frac{1}{3} \mu^2 \tilde{D}^2 + \dots \right] \tilde{u} dx \\ & + \frac{e^{-\kappa/\mu^v}}{2} \int_{\mathbb{R}} \tilde{\eta} \tilde{u}^2 dx - \frac{e^{-\kappa/\mu^v}}{2} \int_{\mathbb{R}} \tilde{u} \left[ \mu \tilde{D} - \frac{1}{3} \mu^3 \tilde{D}^3 + \dots \right] \\ & \times \tilde{\eta} \left[ \mu \tilde{D} - \frac{1}{3} \mu^3 \tilde{D}^3 + \dots \right] \tilde{u} dx. \end{aligned}$$

Disregarding terms of order  $\mathcal{O}(\mu^2 e^{-\kappa/\mu^v})$ , but not of order  $\mathcal{O}(e^{-\kappa/\mu^v})$  yields the expansion

$$\begin{aligned} \tilde{H} = & \frac{1}{2} \int_{\mathbb{R}} \tilde{\eta}^2 dx + \frac{1}{2} \int_{\mathbb{R}} \tilde{u} \left[ 1 - \frac{1}{3} \mu^2 \tilde{D}^2 + \dots \right] \tilde{u} dx \\ & + \frac{e^{-\kappa/\mu^v}}{2} \int_{\mathbb{R}} \tilde{\eta} \tilde{u}^2 dx. \end{aligned} \quad (14)$$

Note that by taking  $\mu$  small enough, an arbitrary number of terms of algebraic order in  $\mu$  may be kept in the asymptotic series, so that the truncated version of the Hamiltonian in dimensional variables may be written as

$$H = \frac{1}{2} \int_{\mathbb{R}} [\eta^2 + u \mathcal{K}_0^N(\eta)u + u\eta u] dx dz. \quad (15)$$

However, the difference between  $\mathcal{K}_0$  and  $\mathcal{K}_0^N$  is below the order of approximation, so that it is possible to formally define the truncated Hamiltonian with  $\mathcal{K}_0$  instead of  $\mathcal{K}_0^N$ .

Hence, the Whitham system is obtained from the Hamiltonian (15) as follows:

$$\eta_t = -\partial_x \frac{\delta H}{\delta u} = -\mathcal{K}_0 u_x - (\eta u)_x, \quad (16)$$

$$u_t = -\partial_x \frac{\delta H}{\delta \eta} = -\eta_x - uu_x. \quad (17)$$

One may also derive a higher-order equation by keeping terms of order  $\mathcal{O}(\mu^2 e^{-\kappa/\mu^v})$ , but discarding terms of order  $\mathcal{O}(\mu^4 e^{-\kappa/\mu^v})$ . In this case we find the system

$$\eta_t = -\mathcal{K}_0 u_x - (\eta u)_x - (\eta u_x)_{xx},$$

$$u_t = -\eta_x - uu_x + u_x u_{xx}.$$

### 3. Derivation of evolution equations of Whitham type

In order to derive the Whitham equation for uni-directional wave propagation, it is important to understand how solutions of the Whitham system (16)–(17) can be restricted to either left or right-going waves. As it will turn out, if  $\eta$  and  $u$  are such that  $\eta = Ku$ , then this pair of functions represents a solution of (16)–(17) which is propagating to the right. Indeed, let us analyze the relation between  $\eta$  and  $u$  in the linearized Whitham system

$$\eta_t = -\mathcal{K}_0 u_x, \quad (18)$$

$$u_t = -\eta_x. \quad (19)$$

Considering a solution of the system (18)–(19) in the form

$$\eta(x, t) = Ae^{(i\xi x - i\omega t)}, \quad u(x, t) = Be^{(i\xi x - i\omega t)}, \quad (20)$$

gives rise to the matrix equation

$$\begin{pmatrix} -\omega & \tanh \xi \\ \xi & -\omega \end{pmatrix} \begin{pmatrix} A \\ B \end{pmatrix} = \begin{pmatrix} 0 \\ 0 \end{pmatrix}. \quad (21)$$

If existence of a nontrivial solution of this system is to be guaranteed, the determinant of the matrix has to be zero, so that we have  $\omega^2 - \frac{\tanh \xi}{\xi} \xi^2 = 0$ . Defining the phase speed as  $c = \omega/\xi$ , we obtain the dispersion relation

$$c = \pm \sqrt{\frac{\tanh \xi}{\xi}}. \quad (22)$$

The choice of  $c > 0$  corresponds to right-going wave solutions of the system (18)–(19), and the relation between  $\eta$  and  $u$  can be deduced from (19). Accordingly, it is expedient to separate solutions into a right-going part  $r$  and a left-going part  $s$  which are defined by

$$r = \frac{1}{2}(\eta + Ku), \quad s = \frac{1}{2}(\eta - Ku).$$

According to the transformation theory detailed in [22], if the unknowns  $r$  and  $s$  are used instead of  $\eta$  and  $u$ , the structure map changes to

$$J_{r,s} = \left( \frac{\partial F}{\partial(r, u)} \right) J_{\eta,u} \left( \frac{\partial F}{\partial(\eta, u)} \right)^T = \begin{pmatrix} -\frac{1}{2} \partial_x K & 0 \\ 0 & \frac{1}{2} \partial_x K \end{pmatrix}. \quad (23)$$

We now use the same scaling for both dependent and independent variables as before. Thus we have  $r = \alpha\tilde{r}$  and  $s = \alpha\tilde{s}$ . The Hamiltonian is written in terms of  $\tilde{r}$  and  $\tilde{s}$  as

$$\begin{aligned} \tilde{H} = & \frac{1}{2} \int_{\mathbb{R}} (\tilde{r} + \tilde{s})^2 dx \\ & + \frac{1}{2} \int_{\mathbb{R}} \tilde{K}^{-1}(\tilde{r} - \tilde{s}) \left[ 1 - \frac{1}{3} \mu^2 \tilde{D}^2 + \dots \right] \tilde{K}^{-1}(\tilde{r} - \tilde{s}) dx \\ & + \frac{\alpha}{2} \int_{\mathbb{R}} (\tilde{r} + \tilde{s}) \left( \tilde{K}^{-1}(\tilde{r} - \tilde{s}) \right)^2 dx \\ & - \frac{\alpha}{2} \int_{\mathbb{R}} \tilde{K}^{-1}(\tilde{r} - \tilde{s}) \left[ \mu \tilde{D} - \frac{1}{3} \mu^3 \tilde{D}^3 + \dots \right] (\tilde{r} + \tilde{s}) \\ & \times \left[ \mu \tilde{D} - \frac{1}{3} \mu^3 \tilde{D}^3 + \dots \right] \tilde{K}^{-1}(\tilde{r} - \tilde{s}) dx. \end{aligned}$$

Following the transformation rules, the structure map transforms to  $J_{\tilde{r},\tilde{s}} = 1/\alpha^2 J_{r,s}$ . In addition, the time scaling  $t = \lambda \tilde{t}$  is employed. Since the focus is on right-going solutions, the equation to be considered is

$$\lambda \tilde{r}_{\tilde{t}} = -\frac{1}{2\alpha^2} \lambda \partial_{\tilde{x}} \tilde{K} \left[ \frac{\delta(\alpha^2 \tilde{H})}{\delta \tilde{r}} \right]. \quad (24)$$

So far, this equation is exact. If we now assume that  $s$  is of the order of  $\mathcal{O}(\mu^2 e^{-\kappa/\mu^\nu})$ , then the equation for  $\tilde{r}$  is

$$\begin{aligned} \tilde{r}_{\tilde{t}} = & -\frac{1}{2} \partial_{\tilde{x}} \left[ 1 - \frac{1}{6} \mu^2 \tilde{D}^2 + \dots \right] \left\{ 2\tilde{r} + \frac{\alpha}{2} \left( [1 + \frac{1}{6} \mu^2 \tilde{D}^2 + \dots] \tilde{r} \right)^2 \right. \\ & + \alpha \left[ 1 + \frac{1}{6} \mu^2 \tilde{D}^2 + \dots \right] \left( \tilde{r} [1 + \frac{1}{6} \mu^2 \tilde{D}^2 + \dots] \tilde{r} \right) \\ & - \frac{\alpha}{2} \left( [\mu \tilde{D} - \frac{1}{3} \mu^3 \tilde{D}^3 + \dots] [1 + \frac{1}{6} \mu^2 \tilde{D}^2 + \dots] \tilde{r} \right)^2 \\ & - \alpha \left[ \mu \tilde{D} - \frac{1}{3} \mu^3 \tilde{D}^3 + \dots \right] \left[ 1 + \frac{1}{6} \mu^2 \tilde{D}^2 + \dots \right] \\ & \times \left( \tilde{r} [\mu \tilde{D} - \frac{1}{3} \mu^3 \tilde{D}^3 + \dots] [1 + \frac{1}{6} \mu^2 \tilde{D}^2 + \dots] \tilde{r} \right) \left. \right\} \\ & + \mathcal{O}(\alpha \mu^2). \end{aligned}$$

As in the case of the Whitham system, we use  $\alpha = \mathcal{O}(e^{-\kappa/\mu^\nu})$ , and disregard terms of order  $\mathcal{O}(\mu^2 e^{-\kappa/\mu^\nu})$ , but not of order  $\mathcal{O}(e^{-\kappa/\mu^\nu})$ . This procedure yields the Whitham equation (1) which is written in nondimensional variables as

$$r_t = -Kr_x - \frac{3}{2}rr_x.$$

As was the case for the system found in the previous section, it is also possible here to include terms of order  $\mathcal{O}(\mu^2 e^{-\kappa/\mu^\nu})$ , resulting in the higher-order equation

$$r_t = -Kr_x - \frac{3}{2}rr_x - \frac{13}{12}r_x r_{xx} - \frac{5}{12}rr_{xxx}.$$

#### 4. Numerical results

In this section, the performance of the Whitham equation as a model for surface water waves is compared to the KdV equation (3), the BBM equation (6), and the Padé (2,2) equation (7). For this purpose initial data are imposed, the Whitham, KdV, BBM, and Padé equations are solved numerically, and the solutions are compared to numerical solutions of the full Euler equations with free-surface boundary conditions. We continue to work in normalized variables, such as stated in the beginning of Section 2.

The numerical treatment of the three model equations is by a standard pseudo-spectral scheme, such as explained in [23,24] for example. For the time stepping, an efficient fourth-order implicit method developed in [25] is used. The numerical treatment of the free-surface problem for the Euler equations is based on a conformal mapping of the fluid domain into a rectangle. In the time-dependent case, this method has roots in the work of Ovsyannikov [26], and was later used in [27–30]. The particular method used for the numerical experiments reported here is a pseudo-spectral scheme which is detailed in [31].

Initial conditions for the Euler equations are chosen in such a way that the solutions are expected to be right moving. This is achieved by posing an initial surface disturbance  $\eta_0(x)$  together with the trace of the potential  $\Phi(x) = \int_0^x \eta_0(x') dx'$ . In order to normalize the data, we choose  $\eta_0(x)$  in such a way that the average of  $\eta_0(x)$  over the computational domain is zero. The experiments are performed with several different amplitudes  $\alpha$  and wavelengths

**Table 1**

Summary of the Stokes number, nondimensional amplitude and nondimensional wavelength of the initial data used in the numerical experiments.

Experiment	Stokes number	$\alpha$	$\lambda$
A	0.2	0.1	$\sqrt{2}$
B	0.2	0.2	1
C	1	0.1	$\sqrt{10}$
D	1	0.2	$\sqrt{5}$
E	5	0.1	$\sqrt{50}$
F	5	0.2	5

(for the purpose of this section, we define the wavelength  $\lambda$  as the distance between the two points  $x_1$  and  $x_2$  at which  $\eta_0(x_1) = \eta_0(x_2) = \alpha/2$ ). Both positive and negative initial disturbances are considered. While disturbances with positive main part have been studied widely, an initial wave of depression is somewhat more exotic, but nevertheless important, as shown for instance in [32]. A summary of the experiments' settings is given in Table 1. Experiments run with an initial wave of elevation are labeled as *positive*, and experiments run with an initial wave of depression are labeled as *negative*. The domain for the computations is  $-L \leq x \leq L$ , with  $L = 50$ . The function initial data in the *positive* cases is given by

$$\eta_0(x) = \alpha \operatorname{sech}^2(f(\lambda)x) - C, \quad (25)$$

where

$$f(\lambda) = \frac{2}{\lambda} \log \left( \frac{1 + \sqrt{1/2}}{\sqrt{1/2}} \right), \quad \text{and} \quad C = \frac{1}{L} \frac{\alpha}{f(\lambda)} \tanh \left( \frac{L}{f(\lambda)} \right)$$

and  $C$  and  $f(\lambda)$  are chosen so that  $\int_{-L}^L \eta_0(x) dx = 0$ , and the wavelength  $\lambda$  is the distance between the two points  $x_1$  and  $x_2$  at which  $\eta_0(x_1) = \eta_0(x_2) = \alpha/2$ . The velocity potential in this case is given by

$$\Phi(x) = \frac{\alpha}{f(\lambda)} \tanh(f(\lambda)x) - Cx. \quad (26)$$

In the *negative* case, the initial data are given by

$$\eta_0(x) = -\alpha \operatorname{sech}^2(f(\lambda)x) + C.$$

The definitions for  $f(\lambda)$  and  $C$  are the same, and the velocity potential is

$$\Phi(x) = -\frac{\alpha}{f(\lambda)} \tanh(f(\lambda)x) + Cx.$$

In Figs. 3 and 4, the time evolution of a wave with an initial narrow peak and one with an initial narrow depression at the center is shown. The amplitude is  $\alpha = 0.2$ , and the wavelength is  $\lambda = \sqrt{5}$ . In Fig. 3, the time evolution according to the Euler, Whitham, KdV and BBM equations are shown, and in Fig. 4, the time evolution according to the Euler, Whitham, and Padé (2,2) equations are shown.

It appears in Fig. 3 that the KdV equation produces a significant number of spurious oscillations, the BBM equation also produces a fair number of spurious oscillations, and the Whitham equation produces fewer small oscillations than Euler equations. Moreover, while the highest peak in the upper panels in Fig. 3 is underpredicted by the KdV and BBM equation, the Whitham equation produces peaks which are slightly too high. In the case of an initial depression, the Whitham equation also produces some peaks which are too high, but on the other hand, the KdV and the BBM equations introduce phase errors in the main oscillations. As is visible in Fig. 4, the Padé (2,2) equation reproduces the leading wave fairly accurately, but overpredicts the trailing oscillations in the case of a positive disturbance, and underpredicts the trailing oscillations in the case of a negative initial disturbance. Nevertheless, since the Padé (2,2) does not introduce a phase error, the overall performance is better than that of the KdV and BBM equations.

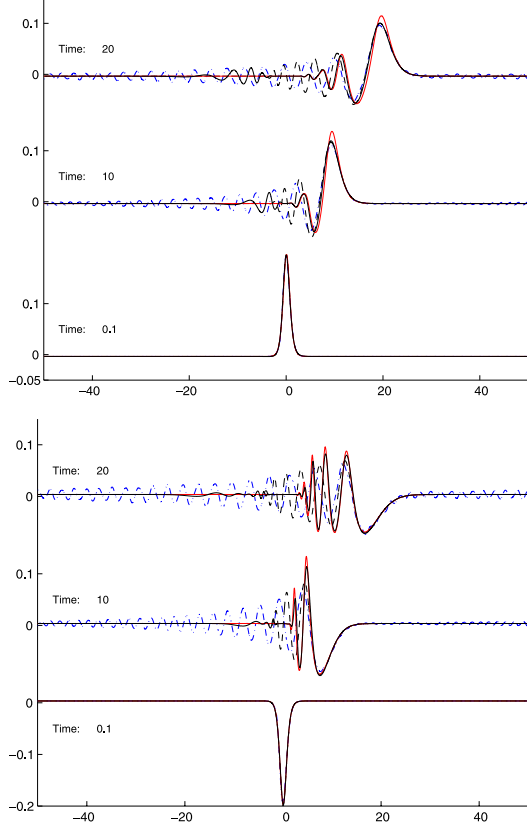


**Fig. 3.** Wave profiles at three different times: – Euler (black line), --- KdV, - - BBM, – Whitham (red line). Experiment D:  $\delta = 1$ ,  $\alpha = 0.2$ ,  $\lambda = \sqrt{5}$ . Upper panel: positive case; lower panel: negative case. Horizontal axis:  $x/h_0$ , vertical axis:  $z/h_0$ . Snapshots are given at nondimensional time  $t/\sqrt{h_0/g}$ .

In order to compare the performance of the four approximate equations in a more quantitative manner, the discrepancies between solutions of the model equations and the prediction due to solving the Euler equations are measured in an integral norm. In the center right panels of Figs. 5 and 6, the computations from Figs. 3 and 4 are summarized by plotting the normalized  $L^2$ -error between the KdV, BBM, Padé and Whitham, respectively, and the Euler solutions as a function of non-dimensional time. Using this quantitative measure of comparison, it appears that the Whitham equation gives the best overall rendition of the free surface dynamics predicted by the Euler equations.

In the center left panels of Figs. 5 and 6, a similar computation with  $\delta = 1$ , but smaller amplitude is analyzed. Also in these cases, it appears that the Whitham equation gives a good approximation to the corresponding Euler solutions, and in particular, a much better approximation than either the KdV or the BBM equation. The Padé equation also does better than both KdV and BBM equations, but not better than the Whitham equation.

Figs. 5 and 6 show comparisons in several other cases of both positive and negative initial amplitude, and Stokes numbers  $\delta = 0.2$ ,  $\delta = 1$  and  $\delta = 5$ . In most cases, the normalized  $L^2$ -error between the Whitham and Euler solutions is similar or smaller than the errors between the Euler solutions and the other three model equations. However, the Padé equation generally outperforms both the KdV and the BBM equation by some measure.

The only case in this study in which the KdV, BBM and Padé equations outperform the Whitham equation is in the case of

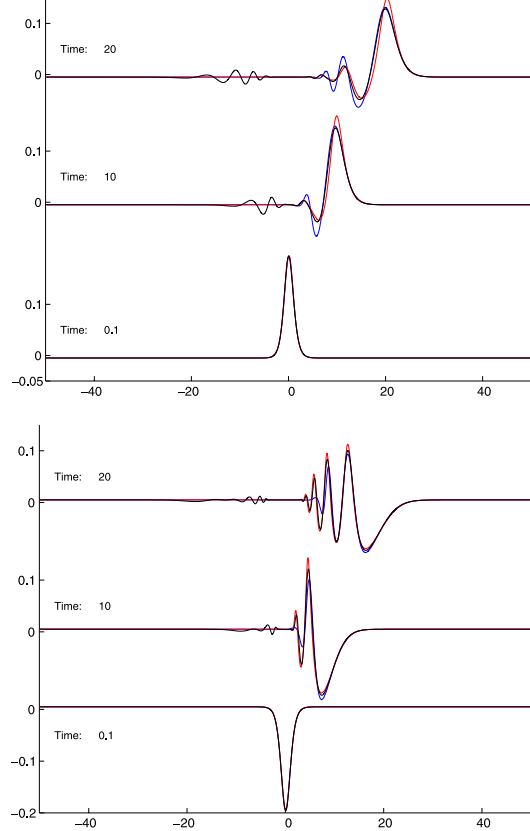


**Fig. 4.** Wave profiles at three different times: – Euler (black line), – Padé (blue line), – Whitham (red line). Experiment D:  $\delta = 1$ ,  $\alpha = 0.2$ ,  $\lambda = \sqrt{5}$ . Upper panel: positive case; lower panel: negative case. Horizontal axis:  $x/h_0$ , vertical axis:  $z/h_0$ . Snapshots are given at nondimensional time  $t/\sqrt{h_0/g}$ .

very long positive initial disturbances. The case when  $\delta = 5$  is shown in the lower panels of Fig. 5. However, even in this case, the Whitham equation yields approximations of the Euler solutions which are similar or better than in the case of smaller wavelengths. In addition, in the case of negative initial data, the performance of the Whitham equation is on par with the KdV, BBM and Padé equations in the case when  $\delta = 5$  (lower panels of Fig. 5).

## 5. Conclusion

In this article, the Whitham equation (1) has been studied as an approximate model equation for wave motion at the surface of a perfect fluid. Numerical integration of the equation suggests that broad classes of initial data decompose into individual solitary waves. The wavelength–amplitude ratio of these approximate solitary waves has been studied, and it was found that this ratio can be described by an exponential relation of the form  $\frac{a}{h_0} \sim e^{-\kappa(l/h_0)^\nu}$ . Using this scaling in the Hamiltonian formulation of the water-wave problem, a system of evolution equations has been derived which contains the exact dispersion relation of the water-wave problem in its linear part. Restricting to one-way propagation, the Whitham equation emerged as a model which combines the usual quadratic nonlinearity with one branch of the exact dispersion relation of the water-wave problem. The performance of the Whitham equation in the approximation of

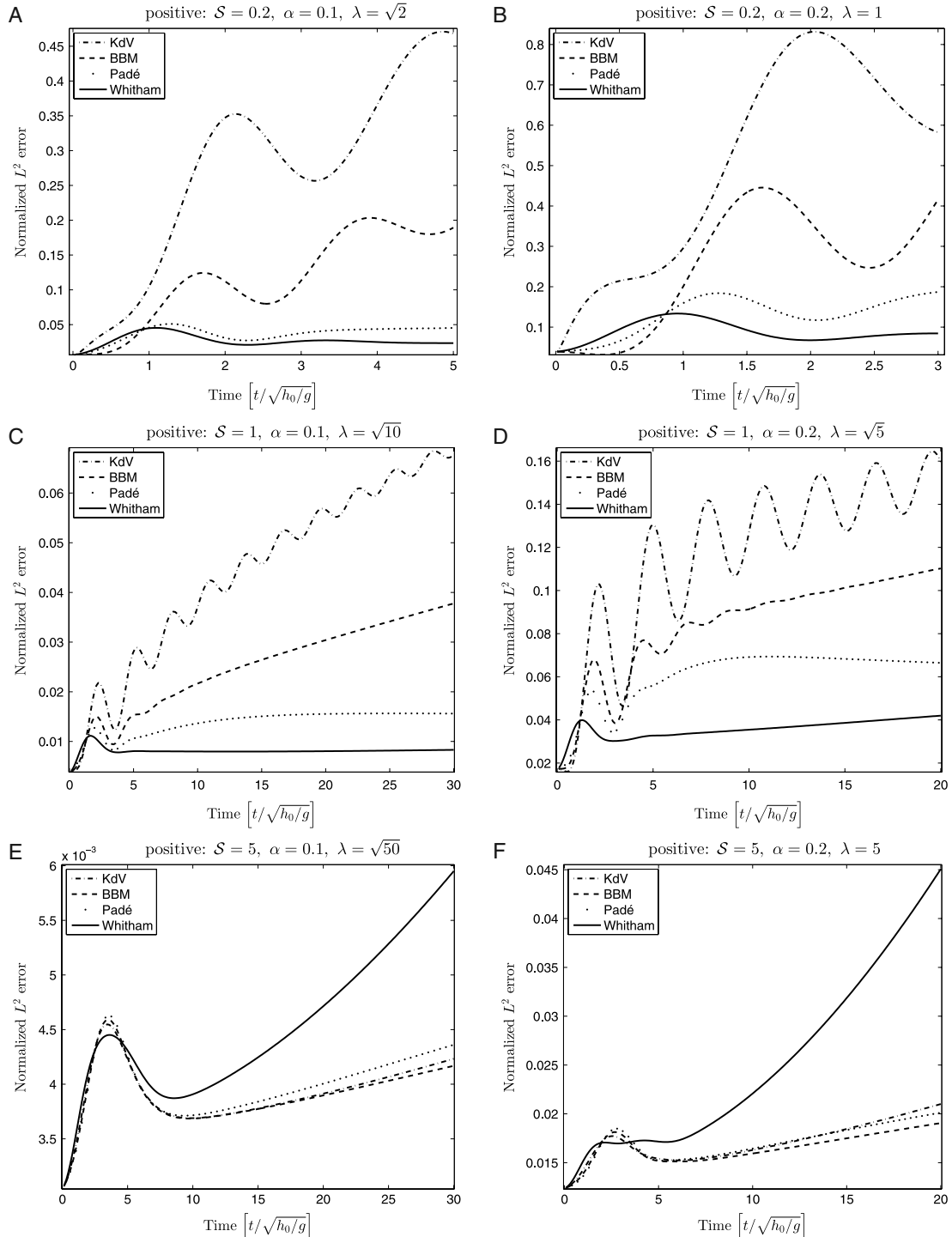


**Fig. 5.**  $L^2$  errors in approximation of solutions to full Euler equations by different model equations: cases A and B ( $\delta = 0.2$ ), cases C and D ( $\delta = 1$ ), cases E and F ( $\delta = 5$ ), positive.

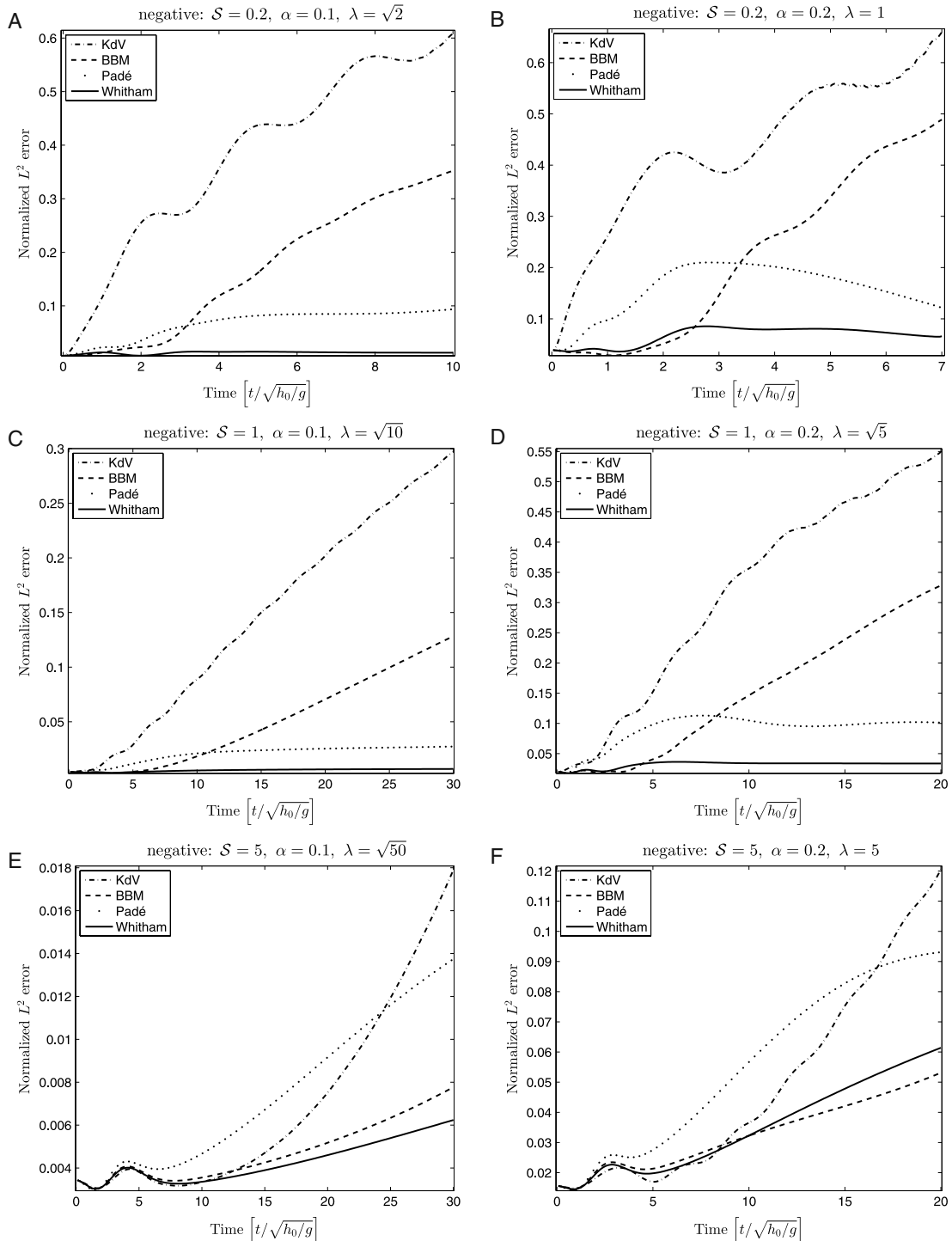


**Fig. 6.**  $L^2$  errors in approximation of solutions to full Euler equations by different model equations: cases A and B ( $\delta = 0.2$ ), cases C and D ( $\delta = 1$ ), cases E and F ( $\delta = 5$ ), negative.

solutions of the Euler equations free-surface boundary conditions was analyzed, and compared to the performance of the KdV and BBM equations, and to the Padé (2,2) model. It was found that the Whitham equation gives a more faithful representation of the solutions of the Euler equations than either the KdV or the BBM equations, except in the case of very long waves with positive main part. In this last case, the KdV and BBM equations have the upper hand over the Whitham equation. The Padé (2,2) model also outperforms the KdV and BBM equations, but does not quite as well as the Whitham equation for shorter waves and negative disturbances. However, in the case of very long waves with positive main part, the Padé model stays on par with the KdV and BBM equations.

### Acknowledgment

This research was supported by the Research Council of Norway (213474/F20).

### References

- [1] G.B. Whitham, Variational methods and applications to water waves, Proc. R. Soc. Lond. Ser. A 299 (1967) 6–25.
- [2] M. Ehrnström, M.D. Groves, E. Wahlén, Solitary waves of the Whitham equation – a variational approach to a class of nonlocal evolution equations and existence of solitary waves of the Whitham equation, Nonlinearity 25 (2012) 2903–2936.
- [3] M. Ehrnström, H. Kalisch, Traveling waves for the Whitham equation, Differential Integral Equations 22 (2009) 1193–1210.
- [4] D. Lannes, The Water Waves Problem, in: Mathematical Surveys and Monographs, vol. 188, Amer. Math. Soc, Providence, 2013.
- [5] D. Lannes, J.-C. Saut, Remarks on the full dispersion Kadomtsev-Petviashvili equation, Kinet. Relat. Models 6 (2013) 989–1009.
- [6] C. Klein, J.-C. Saut, A numerical approach to blow-up issues for dispersive perturbations of Burgers' equation, Physica D 295 (2015) 46–65.
- [7] P. Aceves-Sánchez, A.A. Minzoni, P. Panayotaros, Numerical study of a nonlocal model for water-waves with variable depth, Wave Motion 50 (2013) 80–93.
- [8] V.M. Hur, M.A. Johnson, Modulational instability in the Whitham equation of water waves, Stud. Appl. Math. 134 (1) (2015) 120–143.
- [9] N. Sanford, K. Kodama, J.D. Carter, H. Kalisch, Stability of traveling wave solutions to the Whitham equation, Phys. Lett. A 378 (2014) 2100–2107.
- [10] P.G. Drazin, R.S. Johnson, Solitons: an introduction, in: Cambridge Texts in Applied Mathematics, Cambridge University Press, Cambridge, 1989.
- [11] G.B. Whitham, Linear and Nonlinear Waves, Wiley, New York, 1974.
- [12] M. Ablowitz, H. Segur, Solitons and the inverse scattering transform, in: SIAM Studies in Applied Mathematics, vol. 4, SIAM, Philadelphia, 1981.
- [13] W. Craig, C. Sulem, Numerical simulation of gravity waves, J. Comput. Phys. 108 (1993) 73–83.
- [14] V.E. Zakharov, Stability of periodic waves of finite amplitude on the surface of a deep fluid, J. Appl. Mech. Tech. Phys. 9 (1968) 190–194.
- [15] W. Craig, M.D. Groves, Hamiltonian long-wave approximations to the water-wave problem, Wave Motion 19 (1994) 367–389.
- [16] D.H. Peregrine, Calculations of the development of an undular bore, J. Fluid Mech. 25 (1966) 321–330.
- [17] T.B. Benjamin, J.L. Bona, J.J. Mahony, Model equations for long waves in nonlinear dispersive systems, Philos. Trans. R. Soc. Lond., Ser. A 272 (1972) 47–78.
- [18] J.M. Witting, A unified model for the evolution of nonlinear water waves, J. Comput. Phys. 56 (1984) 203–236.
- [19] R. Fetecau, D. Levy, Approximate model equations for water waves, Commun. Math. Sci. 3 (2) (2005) 159–170.
- [20] A.A. Petrov, Variational statement of the problem of liquid motion in a container of finite dimensions, Prikl. Math. Mekh. 28 (1964) 917–922.
- [21] D.P. Nicholls, F. Reitich, A new approach to analyticity of Dirichlet-Neumann operators, Proc. Roy. Soc. Edinburgh Sect. A 131 (2001) 1411–1433.
- [22] W. Craig, P. Guyenne, H. Kalisch, Hamiltonian long-wave expansions for free surfaces and interfaces, Comm. Pure Appl. Math. 58 (2005) 1587–1641.
- [23] M. Ehrnström, H. Kalisch, Global bifurcation for the Whitham equation, Math. Mod. Nat. Phenomena 8 (2013) 13–30.
- [24] B. Fornberg, G.B. Whitham, A numerical and theoretical study of certain nonlinear wave phenomena, Phil. Trans. Roy. Soc. A 289 (1978) 373–404.
- [25] J. De Frutos, J.M. Sanz-Serna, An easily implementable fourth-order method for the time integration of wave problems, J. Comput. Phys. 103 (1992) 160–168.
- [26] L.V. Ovsyannikov, To the shallow water theory foundation, Arch. Mech. 26 (1974) 407–422.
- [27] A.I. Dyachenko, E.A. Kuznetsov, M.D. Spector, V.E. Zakharov, Analytical description of the free surface dynamics of an ideal fluid (canonical formalism and conformal mapping), Phys. Lett. A 221 (1996) 73–79.
- [28] Y.A. Li, J.M. Hyman, W. Choi, A numerical study of the exact evolution equations for surface waves in water of finite depth, Stud. Appl. Math. 113 (2004) 303–324.
- [29] W. Choi, R. Camassa, Exact evolution equations for surface waves, J. Eng. Mech. 125 (1999) 756–760.
- [30] P. Milewski, J.-M. Vanden-Broeck, Z. Wang, Dynamics of steep two-dimensional gravity-capillary solitary waves, J. Fluid Mech. 664 (2010) 466–477.
- [31] D. Mitsotakis, D. Dutykh, J.D. Carter, On the nonlinear dynamics of the traveling-wave solutions of the Serre equations (2014) submitted for publication, <http://arxiv.org/abs/1404.6725>.
- [32] J.L. Hammack, H. Segur, The Korteweg-de Vries equation and water waves. Part 2. Comparison with experiments, J. Fluid Mech. 65 (1974) 289–314.



# **Paper B**

## **The Whitham equation with surface tension**

Evgueni Dinvay, Daulet Moldabayev, Denys Dutykh, Henrik Kalisch

*Nonlinear Dynamics*, 1–14 (2017)

<http://dx.doi.org/10.1007/s11071-016-3299-7>



## The Whitham equation with surface tension

Evgueni Dinvay · Daulet Moldabayev ·  
Denys Dutykh · Henrik Kalisch

Received: 23 September 2016 / Accepted: 10 December 2016  
© Springer Science+Business Media Dordrecht 2017

**Abstract** The viability of the Whitham equation as a nonlocal model for capillary-gravity waves at the surface of an inviscid incompressible fluid is under study. A nonlocal Hamiltonian system of model equations is derived using the Hamiltonian structure of the free-surface water-wave problem and the Dirichlet–Neumann operator. The system features gravitational and capillary effects, and when restricted to one-way propagation, the system reduces to the capillary Whitham equation. It is shown numerically that in various scaling regimes the Whitham equation gives a more accurate approximation of the free-surface problem for the Euler system than other models like the KdV and Kawahara equation. In the case of relatively strong capillarity considered here, the KdV and Kawahara equations outperform the Whitham equation with surface tension only for very long waves with negative polarity.

**Keywords** Surface waves · Fully dispersive equations · Capillarity · Hamiltonian systems

### 1 Introduction

We consider the water-wave problem for a layer of an incompressible inviscid fluid bounded by a flat impenetrable bottom from below and by a free surface from above. The layer extends to infinity in the horizontal directions. It is a matter of common knowledge that the Euler equations with appropriate boundary conditions give a complete description of the liquid dynamics. However, in many cases the dynamics of the surface of solutions is of particular interest. To avoid heavy computations and concentrate attention only on the free surface, several models approximating evolution of the surface fluid displacement have been used. These model equations describe only the surface dynamics without providing complete solutions in the bulk of the fluid. The present work focuses on the derivation of a nonlocal water-wave model known as the Whitham equation that is fully dispersive in the linear approximation. In particular, we extend here the results of the work [26] to the case where surface tension is taken into account. The model equation under study is written as

$$\eta_t + W\eta_x + \frac{3}{2}\eta\eta_x = 0, \quad (1.1)$$

where the convolution kernel of the operator  $W\eta_x = w(-i\partial_x)\eta_x = (\mathcal{F}^{-1}w) * \eta_x$  is given in terms of the Fourier transform by

---

E. Dinvay · D. Moldabayev · H. Kalisch (✉)  
Department of Mathematics, University of Bergen, Postbox 7800, 5020 Bergen, Norway  
e-mail: henrik.kalisch@math.uib.no

E. Dinvay  
e-mail: evgueni.dinvay@math.uib.no

D. Moldabayev  
e-mail: daulet.moldabayev@math.uib.no

D. Dutykh  
LAMA, UMR5127, CNRS - Université Savoie Mont Blanc, Campus Scientifique, 73376 Le Bourget-du-Lac Cedex, France  
e-mail: Denys.Dutykh@univ-savoie.fr

$$w(\xi) = \sqrt{(1 + \varkappa \xi^2) \frac{\tanh(\xi)}{\xi}}. \quad (1.2)$$

Here it is assumed that the variables are suitably normalized so that the gravitational acceleration, the undisturbed depth of the fluid and the density are all unity. The surface fluid tension is included here by means of the capillarity parameter  $\varkappa$  which is the inverse of the Bond number. The convolution can be thought of as a Fourier multiplier operator, and (1.2) represents the Fourier symbol of the operator. It is also convenient from the analytical point of view to regard the Whitham operator  $W = w(-i\partial_x)$  as an integral with respect to the spectral measure of the self-adjoint operator  $-i\partial_x$  in  $L^2(\mathbb{R})$ . Thus after linearization (1.1) can be considered as a Schrödinger equation with the self-adjoint operator  $-i\partial_x w(-i\partial_x)$ . Indeed, introducing operator  $D = -i\partial_x$  one may rewrite (1.1) as

$$i\eta_t = Dw(D)\eta + \frac{3}{4}D\eta^2.$$

From this point of view, for example, one may deduce straight away that for any real-valued solution  $\eta \in C^1(\mathbb{R}, L^2(\mathbb{R}))$  of this equation the  $L^2$ -norm does not depend on time.

The Whitham equation was proposed by Whitham [32, 33] as an alternative to the well-known Korteweg-de Vries (KdV) equation

$$\eta_t + \eta_x + \frac{3}{2}\eta\eta_x - \frac{1}{2}\left(\varkappa - \frac{1}{3}\right)\eta_{xxx} = 0. \quad (1.3)$$

Provided  $\varkappa < 1/3$  one may rescale  $x$  and  $t$  by  $\sqrt{1 - 3\varkappa}$  and arrive at the equation

$$\eta_t + \eta_x + \frac{3}{2}\eta\eta_x + \frac{1}{6}\eta_{xxx} = 0.$$

Thus it is apparent that small capillary effect does not add anything new to the KdV model. However, when  $\varkappa$  is near  $1/3$  one cannot expect that this model be applicable. To describe surface waves in such a situation, one may use instead the fifth-order model equation

$$\begin{aligned} \eta_t + \eta_x + \frac{3}{2}\eta\eta_x - \frac{1}{2}\left(\varkappa - \frac{1}{3}\right)\eta_{xxx} \\ + \frac{1}{360}(19 - 30\varkappa - 45\varkappa^2)\eta_{xxxxx} = 0. \end{aligned} \quad (1.4)$$

In our numerical experiments we use  $\varkappa = 1/3$ , so that the equation reduces to what is known as the Kawahara equation [3, 6, 20], which has the following form:

$$\eta_t + \eta_x + \frac{3}{2}\eta\eta_x + \frac{1}{90}\eta_{xxxxx} = 0.$$

The validity of the KdV and Kawahara equations can be described in the terms of the Stokes number  $\mathcal{S} = \alpha\lambda^2$  where  $\alpha = a/h_0$  and  $\lambda/h_0$  represent a prominent amplitude and a characteristic wavelength of the wave field, respectively. The KdV equation is known to be a good model for water waves if the amplitude of the waves is small and the wavelength is large when compared to the undisturbed depth, and if in addition, the two nondimensional quantities  $\alpha$  and  $1/\lambda^2$  are of similar size which means  $\mathcal{S} \sim 1$ . With the same requirement and  $\varkappa$  near  $1/3$  the Kawahara equation gives better results for waves where capillarity is important. An alternative model where the air density above the free surface is taken into account was proposed in [31]. Another alternative model to the KdV equation (1.3) known as the BBM equation was put forward in [29] and studied in depth in [4]. The corresponding model with the capillarity  $\varkappa$  has the form

$$\eta_t + \eta_x + \frac{3}{2}\eta\eta_x + \frac{1}{2}\left(\varkappa - \frac{1}{3}\right)\eta_{xxt} = 0. \quad (1.5)$$

The linearized dispersion relation of this equation is not an exact match to the dispersion relation of the full water-wave problem, but it is much closer than the KdV equation in the case when  $\varkappa < 1/3$ , and it might also be expected that this equation may be able to model shorter waves more successfully than the KdV equation. However, the domain of its applicability is  $\mathcal{S} \sim 1$ , that coincides with the corresponding restrictions of the KdV model [4]. One may also notice that (1.5) can also be scaled to the equation without capillarity in the same way as (1.3) providing capillarity  $\varkappa$  is small.

Both KdV and Kawahara equations are generally believed to approximate very long waves quite well, but one notorious problem with these equations is that they do not model accurately the dynamics of shorter waves. Recognizing this shortcoming of the KdV equation, Whitham proposed to use the same nonlinearity as the KdV equation, but coupled with a linear term which mimics the linear dispersion relation of the full water-wave problem. Thus, at least in theory, the Whitham equation can be expected to yield a description of the dynamics of shorter waves which is closer to the governing Euler equations. The Whitham equation (1.1) has been studied from a number of vantage points during recent years. In particular, the existence of traveling and solitary waves has been studied [1, 13–15]. Well posedness of a similar equation was investi-

gated in [21], and similar full dispersion equations were also studied in [22]. Moreover, it has been shown in [18, 19, 30] that periodic solutions of Eq. (1.1) feature modulational instability for short enough waves in a similar way as small-amplitude periodic wave solutions of the water-wave problem. The performance of the Whitham equation in the description of surface water waves has been investigated in [5] in the steady case without surface tension. However, it appears that no study of the performance of the Whitham equation in the presence of capillarity has been done.

In the present note, we give an asymptotic derivation of the Whitham equation as a model for surface water waves, giving close consideration to the influence of the surface tension. The derivation proceeds by examining the Hamiltonian formulation of the water-wave problem due to Zhakarov [34], Craig and Sulem [10]. This approach is similar to the method of [8]. However, our consideration is not constrained heavily by any particular scalar regime. Firstly, a corresponding Whitham system is derived, and then the Whitham equation is found by restricting the system to one-way propagation. Secondly, we derive different models from the Whitham equation and point out the corresponding domains of their applicability.

Finally, a numerical comparison of modeling properties of the KdV, Kawahara and Whitham equations is given with respect to the Euler system.

## 2 Euler system and its Hamiltonian

The surface water-wave problem is generally described by the Euler equations with no-flow conditions at the bottom, and kinematic and dynamic boundary conditions at the free surface. Assuming weak transverse effects, the unknowns are the surface elevation  $\eta(x, t)$ , the horizontal and vertical fluid velocities  $u_1(x, z, t)$  and  $u_2(x, z, t)$ , respectively, and the pressure  $P(x, z, t)$ . If the assumption of irrotational flow is made, then a velocity potential  $\phi(x, z, t)$  can be used. Taking the undisturbed depth  $h_0 = 1$  as a unit of distance, and the parameter  $\sqrt{h_0/g} = 1$  as a unit of time, the problem may be posed on a domain  $\{(x, z) \in \mathbb{R}^2 | -1 < z < \eta(x, t)\}$  which extends to infinity in the positive and negative  $x$ -direction. Due to the incompressibility of the fluid, the potential then satisfies the Laplace's equation in this domain. The fact that the fluid cannot penetrate

the bottom is expressed by a homogeneous Neumann boundary condition at the flat bottom. Thus we have

$$\begin{aligned}\phi_{xx} + \phi_{zz} &= 0 \quad \text{in } -1 < z < \eta(x, t) \\ \phi_z &= 0 \quad \text{on } z = -1.\end{aligned}$$

The pressure is eliminated with help of the Bernoulli equation, and the free-surface boundary conditions are formulated in terms of the potential  $\varphi$  and the surface displacement  $\eta$  by

$$\left. \begin{aligned}\eta_t + \phi_x \eta_x - \phi_z &= 0, \\ \phi_t + \frac{1}{2} (\phi_x^2 + \phi_z^2) + \eta - \kappa \eta_{xx} (1 + \eta_x^2)^{-3/2} &= 0,\end{aligned}\right\} \text{on } z = \eta(x, t).$$

The first equation represents the definition of the fluid velocity with respect to the Euler coordinates. The second one is the Bernoulli equation with the capillary term.

The total energy of the system is given by the sum of the kinetic energy, the potential energy and the surface tension energy, and normalized in such a way that the total energy is zero when no wave motion is present at the surface. Accordingly, the Hamiltonian function for this problem is

$$H = \int_{\mathbb{R}} \int_0^\eta z dz dx + \int_{\mathbb{R}} \int_{-1}^\eta \frac{1}{2} |\nabla \phi|^2 dz dx \\ + \kappa \int_{\mathbb{R}} \frac{\eta_x^2}{1 + \sqrt{1 + \eta_x^2}} dx.$$

Defining the trace of the potential at the free surface as  $\Phi(x, t) = \phi(x, \eta(x, t), t)$ , one may integrate in  $z$  in the first integral and use the divergence theorem on the second integral in order to arrive at the formulation

$$H = \int_{\mathbb{R}} \left[ \frac{1}{2} \eta^2 + \frac{1}{2} \Phi G(\eta) \Phi + \kappa \frac{\eta_x^2}{1 + \sqrt{1 + \eta_x^2}} \right] dx. \quad (2.1)$$

This is the Hamiltonian of the water-wave problem with surface tension as for instance found in [2] and written in terms of the Dirichlet–Neumann operator  $G(\eta)$ . As shown in [27], the Dirichlet–Neumann operator is analytic in a certain sense and can be expanded as a power series as

$$G(\eta) \Phi = \sum_{j=0}^{\infty} G_j(\eta) \Phi.$$

In order to proceed, we need to understand the first few terms in this series. As shown in [8, 10], the first two terms in this series can be written with the help of the operator  $D = -i \partial_x$  as

$$G_0(\eta) = D \tanh(D),$$

$$G_1(\eta) = D\eta D - D \tanh(D)\eta D \tanh(D).$$

Note that it can be shown that the terms  $G_j(\eta)$  for  $j \geq 2$  are of quadratic or higher-order in  $\eta$ , and will therefore not be needed in the following analysis.

It will be convenient for the present purpose to formulate the Hamiltonian in terms of the dependent variable  $u = \Phi_x$ . This new variable is proportional to the velocity of the fluid tangential to the surface. More precisely  $u = \varphi_x + \eta_x \varphi_z = \varphi_\tau \sqrt{1 + \eta_x^2}$  where  $\varphi_\tau$  is exactly the tangential velocity component to the surface. To this end, we define the operator  $\mathcal{K}$  by

$$G(\eta) = D\mathcal{K}(\eta)D.$$

As was the case with  $G(\eta)$ , the operator  $\mathcal{K}(\eta)$  can also be expanded in a Taylor series with respect to powers of  $\eta$  and  $\eta_x$  as

$$\mathcal{K}(\eta) = \sum_{j=0}^{\infty} \mathcal{K}_j(\eta), \quad \mathcal{K}_j(\eta) = D^{-1} G_j(\eta) D^{-1}.$$

In particular, note that  $\mathcal{K}_0 = \tanh D/D$  and  $\mathcal{K}_1 = \eta - \tanh D(\eta \tanh D)$ . After integrating by parts the Hamiltonian can be expressed as

$$H = \int_{\mathbb{R}} \left[ \frac{1}{2} \eta^2 + \frac{1}{2} u \mathcal{K}(\eta) u + \kappa \frac{\eta_x^2}{1 + \sqrt{1 + \eta_x^2}} \right] dx. \quad (2.2)$$

The following analysis has the formal character of long-wave approximation. Consider a wave field having a characteristic nondimensional wavelength  $\lambda$  and a characteristic nondimensional amplitude  $\alpha$ . We also introduce the small parameter  $\mu = \frac{1}{\lambda}$ . To obtain different approximations of the discussed problem the amplitude  $\alpha$  is considered as a function of wave number  $\mu$ . Its behavior at small wave numbers defines different scaling regimes. The long-wave approximation means the scale  $\eta = O(\alpha)$ ,  $u = O(\alpha)$  and  $D = -i\partial_x = O(\mu)$  where  $\alpha = \alpha(\mu)$  depends on the small parameter  $\mu$ . Now the Hamiltonian (2.2) may be simplified as follows

$$H = H_g + H_c + O(\mu^2 \alpha^4) \quad (2.3)$$

with the gravity term

$$H_g = \frac{1}{2} \int_{\mathbb{R}} \left[ \eta^2 + u \frac{\tanh D}{D} u + \eta u^2 - u \tanh D(\eta \tanh D u) \right] dx \quad (2.4)$$

and the capillary part

$$H_c = \kappa \int_{\mathbb{R}} \frac{\eta_x^2 dx}{1 + \sqrt{1 + \eta_x^2}} = \frac{\kappa}{2} \int_{\mathbb{R}} \eta_x^2 dx + O(\mu^4 \alpha^4). \quad (2.5)$$

Before we continue with derivation of the Whitham equation we prove the following lemma about integration by parts, which is certainly well known, and we add it here only for completeness.

**Lemma 2.1** *Let  $f, g$  be real-valued square integrable functions on real axis  $\mathbb{R}$ . Regard  $D = -i\partial_x$  as self-adjoint on  $L^2(\mathbb{R}, \mathbb{C})$  and a real-valued function  $\varphi$  that is measurable and almost everywhere finite with respect to Lebesgue measure. If  $f, g$  lie in the domain of the operator  $\varphi(D)$  then*

$$\int f \varphi(D) g = \int g \varphi(-D) f$$

*Proof* It is given two proofs below. The first one is to regard  $\varphi(D) = (\mathcal{F}^{-1}\varphi)*$  as the operator of convolution in the sense of distribution theory

$$\begin{aligned} \int f \varphi(D) g &= \int f(\xi) (\mathcal{F}^{-1}\varphi)(\xi - x) g(x) dx d\xi = \\ &= \int f(\xi) (\mathcal{F}^{-1}\varphi \circ (-id)) \\ &\quad \times (x - \xi) g(x) dx d\xi = \int g \varphi(-D) f. \end{aligned}$$

The second proof is to represent  $\varphi(D) = \int \varphi dE$  as the integral with respect to spectral measure  $E$  of the operator  $D$ . The corresponding projector of the interval  $(\alpha, \beta)$  is the convolution with the function  $e_{(\alpha, \beta)}(x) = \frac{1}{2\pi i x} (e^{i\beta x} - e^{i\alpha x})$ . So the replacement of  $f$  and  $g$  changes the corresponding spectral complex measure of intervals as follows

$$\begin{aligned} \mu_{f,g}(\alpha, \beta) &= (E(\alpha, \beta) f, g) \\ &= \int e_{(\alpha, \beta)}(x - y) f(y) g(x) dx dy \\ &= \int e_{(-\beta, -\alpha)}(y - x) f(y) g(x) dx dy \\ &= \mu_{g,f}(-\beta, -\alpha) \end{aligned}$$

which implies the statement of the lemma

$$\begin{aligned} \int f \varphi(D) g &= \int \varphi(x) d\mu_{g,f}(x) \\ &= \int \varphi(-x) d\mu_{f,g}(x) \\ &= \int g \varphi(-D) f. \end{aligned}$$

□

The Whitham equation with surface tension

### 3 Derivation of the Whitham-type evolution system

The water-wave problem can be rewritten as a Hamiltonian system using the variational derivatives of  $H$ . Making reference to [8,9] note that the pair  $(\eta, \Phi)$  represents the canonical variables for the Hamiltonian function (2.1). However, it is more common to write the equations of motion in the fluid dynamics of free surface in terms of  $\eta$  and  $u = \Phi_x$ . The transformation  $(\eta, \Phi) \mapsto (\eta, u)$  is associated with the Jacobian

$$\frac{\partial(\eta, u)}{\partial(\eta, \Phi)} = \begin{pmatrix} 1 & 0 \\ 0 & \partial_x \end{pmatrix}.$$

Thus in terms of  $\eta$  and  $u$  the Hamiltonian equations have the form

$$\eta_t = -\partial_x \frac{\delta H}{\delta u}, \quad u_t = -\partial_x \frac{\delta H}{\delta \eta} \quad (3.1)$$

that is not canonical since the associated structure map  $J_{\eta, u}$  is symmetric:

$$\begin{aligned} J_{\eta, u} &= \left( \frac{\partial(\eta, u)}{\partial(\eta, \Phi)} \right) \begin{pmatrix} 0 & 1 \\ -1 & 0 \end{pmatrix} \left( \frac{\partial(\eta, u)}{\partial(\eta, \Phi)} \right)^* \\ &= \begin{pmatrix} 0 & -\partial_x \\ -\partial_x & 0 \end{pmatrix}. \end{aligned}$$

We now derive a system of equations which is similar to the Whitham equation (1.1), but admits bidirectional wave propagation. The variational derivative  $\delta H_g / \delta u$  is defined by means of any real-valued square integrable function  $h$  as follows

$$\begin{aligned} \int_{\mathbb{R}} \frac{\delta H_g}{\delta u}(x) h(x) dx &= d_u H_g h = \frac{d}{d\tau} \Big|_{\tau=0} H_g(u + \tau h, \eta) \\ &= \int_{\mathbb{R}} u \eta h dx + \\ &\quad + \frac{1}{2} \int_{\mathbb{R}} \left[ h \frac{\tanh D}{D} u + u \frac{\tanh D}{D} h \right. \\ &\quad \left. - h \tanh D (\eta \tanh Du) \right. \\ &\quad \left. - u \tanh D (\eta \tanh Dh) \right] dx. \end{aligned}$$

Making use of integration by parts described in Lemma 2.1 one obtains

$$\begin{aligned} \frac{\delta H_g}{\delta u} &= \frac{\tanh D}{D} u + \eta u - \tanh D (\eta \tanh Du) \\ &= \frac{\tanh D}{D} u + \eta u + O(\mu^2 \alpha^2) \end{aligned}$$

and in the same way

$$\frac{\delta H_g}{\delta \eta} = \eta + \frac{1}{2} u^2 + \frac{1}{2} (\tanh Du)^2$$

$$= \eta + \frac{1}{2} u^2 + O(\mu^2 \alpha^2).$$

These variational derivatives were also obtained by Moldabayev and Kalisch [26]. The capillary part  $H_c$  defined by (2.5) gives the pressure  $P$  on the surface

$$\frac{\delta H_c}{\delta \eta} = -\varkappa \frac{\eta_{xx}}{(1 + \eta_x^2)^{\frac{3}{2}}} = -\varkappa \eta_{xx} + O(\mu^4 \alpha^3).$$

At last the Hamiltonian system (3.1) is simplified to the Whitham system

$$\begin{aligned} \eta_t &= -\frac{\tanh D}{D} u_x - (\eta u)_x + \tanh D (\eta \tanh Du)_x \\ &\quad + O(\mu^3 \alpha^3), \end{aligned} \quad (3.2)$$

$$\begin{aligned} u_t &= -\eta_x - uu_x - (\tanh Du) \tanh Du_x \\ &\quad + \varkappa \eta_{xxx} + O(\mu^3 \alpha^3) \end{aligned} \quad (3.3)$$

which is in line with the system obtained in [7], and similar to the one obtained in [26]:

$$\begin{aligned} \eta_t &= -\frac{\tanh D}{D} u_x - (\eta u)_x + O(\mu^3 \alpha^2), \\ u_t &= -\eta_x - uu_x + \varkappa \eta_{xxx} + O(\mu^3 \alpha^2). \end{aligned}$$

### 4 Derivation of Whitham-type evolution equations

It turns out that the Whitham system (3.2), (3.3) might be rewritten as a system of two independent equations by further simplification. More precisely, they will be independent with respect to the linear approximation of that system. For this purpose we need to separate solutions corresponding to waves moving in other directions. In order to derive the Whitham equation for unidirectional wave propagation, it is important to understand how one-way propagation works in the Whitham system (3.2), (3.3). Regard the linearization of this system

$$\eta_t + \frac{\tanh D}{D} u_x = 0, \quad (4.1)$$

$$u_t + (1 + \varkappa D^2) \eta_x = 0. \quad (4.2)$$

Regarding solutions of this linear system in the wave form

$$\eta(x, t) = A e^{i\xi x - i\omega t}, \quad u(x, t) = B e^{i\xi x - i\omega t}$$

gives rise to the matrix equation

$$\begin{pmatrix} -\omega & \tanh \xi \\ \xi + \varkappa \xi^3 & -\omega \end{pmatrix} \begin{pmatrix} A \\ B \end{pmatrix} = \begin{pmatrix} 0 \\ 0 \end{pmatrix}.$$

This equation has a nontrivial solution, provided its determinant equals zero, so that  $\omega^2 - (\xi + \kappa \xi^3) \tanh \xi = 0$ . Defining the phase speed as  $c = \omega(\xi)/\xi$  one obtains the dispersion relation

$$c^2(\xi) = (1 + \kappa \xi^2) \frac{\tanh \xi}{\xi}$$

which coincides, up to the sign of  $c$ , with Whitham dispersion relation (1.2). Obviously, the choice  $c > 0$  corresponds to right-going wave solutions of the linear system (4.1), (4.2). And the phase speed  $c < 0$  gives left-going waves. To split up these two kinds of waves we regard the following transformation of variables

$$r = \frac{1}{2}(\eta + Ku), \quad s = \frac{1}{2}(\eta - Ku). \quad (4.3)$$

It is supposed that  $K$  is an invertible operator, namely an invertible function of the differential operator  $D$ . The inverse transformation has the form

$$\eta = r + s, \quad u = K^{-1}(r - s). \quad (4.4)$$

The question arises whether it is possible to choose such operator  $K$  that  $r$  and  $s$  correspond to right- and left-going waves, respectively. After applying the transformation (4.4) to the linear system (4.1), (4.2) one arrives to the system

$$r_t + \partial_x (A(D, K)r + B(D, K)s) = 0,$$

$$s_t - \partial_x (A(D, K)s + B(D, K)r) = 0$$

where operators  $A$  and  $B$  depend on  $D$  and  $K$  as follows

$$A = \frac{1}{2} \left( (1 + \kappa D^2)K + \frac{\tanh D}{D} K^{-1} \right),$$

$$B = \frac{1}{2} \left( (1 + \kappa D^2)K - \frac{\tanh D}{D} K^{-1} \right).$$

So to achieve independence of the obtained two equations we need to choose the transformation  $K$  in the way  $B(D, K) = 0$ , so that

$$K = \sqrt{\frac{1}{1 + \kappa D^2}} \cdot \frac{\tanh D}{D} \quad (4.5)$$

which leads to the two independent Whitham equations

$$r_t + \partial_x Wr = 0, \quad (4.6)$$

$$s_t - \partial_x Ws = 0 \quad (4.7)$$

where the Whitham operator  $W = w(D) = A(D, K)$  was introduced at the beginning of the paper by (1.2). If we again regard the wave solutions  $r(x, t) = \exp(i\xi x - i\omega_r t)$  and  $s(x, t) = \exp(i\xi x - i\omega_s t)$ , then we conclude that the first equation (4.6) describes waves moving to the right with the phase velocity  $c_r = \omega_r/\xi = w(\xi)$  and the second equation (4.7) corresponds to the left-going waves with  $c_s = \omega_s/\xi = -w(\xi)$ .

Now we regard the Hamiltonian (2.2) as a functional of  $r$  and  $s$  with the same long-wave approximation as before (2.3) where obviously  $r = O(\alpha)$  and  $s = O(\alpha)$ . The unperturbed Hamiltonian part (2.4) is

$$\begin{aligned} H_g = & \frac{1}{2} \int_{\mathbb{R}} \left[ (r + s)^2 + \left( K^{-1}(r - s) \right) \frac{\tanh D}{D} \right. \\ & \times K^{-1}(r - s) + (r + s) \left( K^{-1}(r - s) \right)^2 \\ & - \left( K^{-1}(r - s) \right) \tanh D \\ & \left. \times \left( (r + s) \tanh D K^{-1}(r - s) \right) \right] dx \end{aligned} \quad (4.8)$$

and the surface tension adding (2.5) is

$$H_c = \frac{\kappa}{2} \int_{\mathbb{R}} (r + s)_x^2 dx + O(\mu^4 \alpha^4). \quad (4.9)$$

According to the transformation theory detailed in [9], due to the changing of variables (4.3) or (4.4), the structure map changes to

$$\begin{aligned} J_{r,s} &= \left( \frac{\partial(r, s)}{\partial(\eta, u)} \right) J_{\eta,u} \left( \frac{\partial(r, s)}{\partial(\eta, u)} \right)^* \\ &= s \begin{pmatrix} -\frac{1}{2} \partial_x K & 0 \\ 0 & \frac{1}{2} \partial_x K \end{pmatrix}. \end{aligned}$$

The corresponding Hamiltonian system has the form

$$r_t + \partial_x \left( \frac{K}{2} \frac{\delta H}{\delta r} \right) = 0, \quad s_t - \partial_x \left( \frac{K}{2} \frac{\delta H}{\delta s} \right) = 0. \quad (4.10)$$

These equations are equivalent to (3.1). However, solutions  $r(x, t)$  and  $s(x, t)$  are the displacements going right and left, respectively, when a solution  $u(x, t)$ , representing the tangential velocity component up to the curvature multiplier, might not be imagined so easy. As above we calculate the Gâteaux derivative of  $H_g$  given by (4.8) with respect to  $r$  at a real-valued square integrable function

The Whitham equation with surface tension

$$\begin{aligned}
& \int_{\mathbb{R}} \frac{\delta H_g}{\delta r}(x) h(x) dx \\
&= d_r H_g h = \frac{d}{d\tau} \Big|_{\tau=0} H_g(r + \tau h, s) \\
&= \int (r + s) h + \\
&\quad + \frac{1}{2} \int (K^{-1} h) \frac{\tanh D}{D} K^{-1}(r - s) \\
&\quad + \frac{1}{2} \int (K^{-1}(r - s)) \frac{\tanh D}{D} K^{-1} h \\
&\quad + \frac{1}{2} \int h (K^{-1}(r - s))^2 \\
&\quad + \int (r + s) (K^{-1}(r - s)) K^{-1} h \\
&\quad - \frac{1}{2} \int (K^{-1} h) \tanh D ((r + s) \tanh D \\
&\quad \times K^{-1}(r - s)) \\
&\quad - \frac{1}{2} \int (K^{-1}(r - s)) \tanh D \\
&\quad \times (h \tanh D K^{-1}(r - s)) \\
&\quad - \frac{1}{2} \int (K^{-1}(r - s)) \tanh D \\
&\quad \times ((r + s) \tanh D K^{-1} h).
\end{aligned}$$

Integrating by parts as in Lemma 2.1 and taking into account that functions  $\tanh D$  are odd while  $K$  is even (4.5) with respect to  $D$ , one can obtain  $\delta H_g/\delta r$ , and in the similar way  $\delta H_c/\delta r$ ,  $\delta H_g/\delta s$ ,  $\delta H_c/\delta s$ . Thus as a result

$$\begin{aligned}
\frac{K}{2} \frac{\delta H}{\delta r} &= Wr + \frac{1}{4} K (K^{-1}(r - s))^2 \\
&\quad + \frac{1}{2} (r + s) K^{-1}(r - s) \\
&\quad + \frac{1}{4} K (\tanh D K^{-1}(r - s))^2 \\
&\quad - \frac{1}{2} \tanh D ((r + s) \tanh D K^{-1}(r - s)) \\
&\quad + O(\mu^2 \alpha^3)
\end{aligned} \tag{4.11}$$

and

$$\begin{aligned}
\frac{K}{2} \frac{\delta H}{\delta s} &= Ws + \frac{1}{4} K (K^{-1}(r - s))^2 \\
&\quad - \frac{1}{2} (r + s) K^{-1}(r - s) \\
&\quad + \frac{1}{4} K (\tanh D K^{-1}(r - s))^2
\end{aligned}$$

$$\begin{aligned}
&\quad + \frac{1}{2} \tanh D ((r + s) \tanh D K^{-1}(r - s)) \\
&\quad + O(\mu^2 \alpha^3)
\end{aligned} \tag{4.12}$$

together with (4.10) are the Whitham system describing the displacement  $\eta(x, t)$  in terms of waves going right and left. This system is entirely equivalent to (3.2), (3.3) and at the same time gives rise to solutions with more clear physical meaning. Another useful property of this system is that it can be enough to regard only one equation if we are allowed to neglect the waves going to a particular direction. More precisely, regarding only right-going waves leads to

$$\begin{aligned}
\frac{K}{2} \frac{\delta H}{\delta r} &= Wr + \frac{1}{4} K (K^{-1} r)^2 + \frac{1}{2} r K^{-1} r \\
&\quad + \frac{1}{4} K (\tanh D K^{-1} r)^2 \\
&\quad - \frac{1}{2} \tanh D (r \tanh D K^{-1} r) \\
&\quad + O(\alpha|s|) + O(\mu^2 \alpha^3)
\end{aligned} \tag{4.13}$$

and only left-going waves gives

$$\begin{aligned}
\frac{K}{2} \frac{\delta H}{\delta s} &= Ws + \frac{1}{4} K (K^{-1} s)^2 + \frac{1}{2} s K^{-1} s \\
&\quad + \frac{1}{4} K (\tanh D K^{-1} s)^2 \\
&\quad - \frac{1}{2} \tanh D (s \tanh D K^{-1} s) \\
&\quad + O(\alpha|r|) + O(\mu^2 \alpha^3).
\end{aligned} \tag{4.14}$$

As one can see, these expressions are identical up to discarded parts. Equality (4.13) together with the first equation of (4.10) corresponds to the Whitham equation describing right-going surface waves. Equality (4.14) together with the second equation of (4.10) corresponds to the Whitham equation describing left-going surface waves. Further simplifications can be made by studying concrete regimes  $\alpha(\mu)$ . As a matter of fact, examples of behavior  $\alpha(\mu)$  at small  $\mu$  that we regard below need less accurate asymptotic. So that operators  $K$  and  $\tanh D$  can still be simplified by taking into account  $D = O(\mu)$  in Equality (4.13) as follows

$$\begin{aligned}
\frac{K}{2} \frac{\delta H}{\delta r} &= Wr + \frac{3}{4} r^2 + \frac{1}{4} \left( \varkappa - \frac{5}{3} \right) r D^2 r \\
&\quad - \frac{1}{4} \left( \varkappa + \frac{4}{3} \right) (Dr)^2 \\
&\quad + O(\mu^4 \alpha^2) + O(\alpha|s|) + O(\mu^2 \alpha^3).
\end{aligned} \tag{4.15}$$

It is in line with [26] for liquids without surface tension  $\varkappa = 0$ . There is the same expression for the other variational derivative with replacement  $r$  by  $s$ .

#### 4.1 Linear approximation

Let  $r$  and  $s$  be of the same order and  $\alpha = o(1)$  as  $\mu \rightarrow 0$ . Then (4.13), (4.14) are simplified to

$$\frac{K}{2} \frac{\delta H}{\delta r} = Wr(1 + o(1)), \quad \frac{K}{2} \frac{\delta H}{\delta s} = Ws(1 + o(1))$$

that together with (4.10) represent two independent linear equations. We again arrived to (4.6), (4.7). This is the case when we do not have enough information about order relation between right- and left-going waves.

#### 4.2 The shallow-water scaling regime

Let  $\alpha = O(1)$  as  $\mu \rightarrow 0$ . Assume also that left-going waves can be discarded  $s = o(1)$ . In this case operators  $W$  can also be simplified by taking into account  $D = O(\mu)$ . Expression (4.15) becomes

$$\frac{K}{2} \frac{\delta H}{\delta r} = r + \frac{3}{4}r^2 + o(1)$$

which leads to the shallow-water equation

$$r_t + r_x + \frac{3}{2}rr_x = o(\mu).$$

#### 4.3 The Boussinesq scaling regime

Let  $\alpha = O(\mu^2)$  and  $s = o(\mu^2)$  as  $\mu \rightarrow 0$ . Expression (4.15) becomes

$$\frac{K}{2} \frac{\delta H}{\delta r} = Wr + \frac{3}{4}r^2 + o(\mu^4)$$

that can be simplified further by two different ways

$$\begin{aligned} W &= 1 + \frac{1}{2} \left( \varkappa - \frac{1}{3} \right) D^2 + O(\mu^4) \\ &= \left( 1 - \frac{1}{2} \left( \varkappa - \frac{1}{3} \right) D^2 \right)^{-1} + O(\mu^4). \end{aligned}$$

The first equality leads to the KdV equation

$$r_t + r_x - \frac{1}{2} \left( \varkappa - \frac{1}{3} \right) r_{xxx} + \frac{3}{2}rr_x = o(\mu^5).$$

The second equality gives rise to the BBM equation

$$r_t + r_x + \frac{1}{2} \left( \varkappa - \frac{1}{3} \right) r_{xxt} + \frac{3}{2}rr_x = o(\mu^5).$$

#### 4.4 The Padé (2,2) approximation

Suppose  $\alpha = O(\mu^4)$  and  $s = o(\mu^4)$  as  $\mu \rightarrow 0$ . Expression (4.15) becomes

$$\frac{K}{2} \frac{\delta H}{\delta r} = Wr + \frac{3}{4}r^2 + o(\mu^8)$$

that can be simplified further provided  $\varkappa \neq 1/3$  by the way

$$W = \frac{1 + aD^2}{1 + bD^2} + O(\mu^6)$$

where constants  $a$  and  $b$  depend on  $\varkappa$  as follows

$$a(\varkappa) = \frac{3 + 10\varkappa - 45\varkappa^2}{20(1 - 3\varkappa)},$$

$$b(\varkappa) = \frac{19 - 30\varkappa - 45\varkappa^2}{60(1 - 3\varkappa)}.$$

The corresponding equation

$$r_t + r_x - a(\varkappa)r_{xxx} - b(\varkappa)r_{xxt} + \frac{3}{2}rr_x = o(\mu^9).$$

As one can see, the order of this differential equation is the same as the order of KdV or BBM, meanwhile the Padé approximation is more accurate. In the case  $\varkappa = 1/3$  one has to use the usual Taylor approximation

$$\begin{aligned} W &= 1 + \frac{1}{2} \left( \varkappa - \frac{1}{3} \right) D^2 \\ &\quad + \frac{1}{360} (19 - 30\varkappa - 45\varkappa^2) D^4 + O(\mu^6) \end{aligned}$$

which gives rise to the equation of fifth order

$$\begin{aligned} r_t + r_x - \frac{1}{2} \left( \varkappa - \frac{1}{3} \right) r_{xxx} \\ + \frac{1}{360} (19 - 30\varkappa - 45\varkappa^2) r_{xxxxx} + \frac{3}{2}rr_x = o(\mu^9) \end{aligned}$$

that is the Kawahara equation (1.4).

#### 4.5 The Whitham scaling regime

If we now assume  $\alpha = O(\mu^N)$  for any positive integer  $N$  and  $s = o(\alpha)$  as  $\mu \rightarrow 0$ , then we arrive to an example when the Whitham operator  $W$  cannot be approximated using a simple differential operator instead. The simplest equation in this case is the Whitham equation

$$r_t + Wr_x + \frac{3}{2}rr_x = o(\mu\alpha^2).$$

An example of the function  $\alpha(\mu)$  when the Whitham equation works better than its approximations was given in [26]. At the same time that function  $\alpha(\mu)$  may be similar to the Boussinesq scale at some wave numbers  $\mu$  as was pointed out in [26].

## 5 Numerical results

The purpose of this section is to compare the performance of the Whitham equation as a model for surface water waves to both the KdV equation (1.3) and to the Kawahara equation (1.4). In other words, all these approximate models are compared to the Euler system which is considered as giving the closest description of an actual surface wave profile. For this purpose initial data are imposed, the Whitham, KdV and Kawahara equations are solved with periodic boundary conditions, and the solutions are compared to the numerical solutions of the full Euler equations with free-surface boundary conditions. This matching is made in various scaling regimes from small Stokes numbers to  $S \sim 1$ , to large Stokes numbers.

The numerical treatment of the three model equations is a standard spectral scheme, such as used in [15, 16] for example. For the time stepping, an efficient fourth-order implicit method developed in [12] is used. The numerical discretization of the free-surface problem for the Euler equations is based on a conformal mapping of the fluid domain into a rectangle. In the case of transient dynamics, this method has roots in the work of Ovsyannikov [28] and was later used in [11, 23, 24]. In the case of periodic boundary conditions, a Fourier spectral collocation method can be used for the computations, and the particular method used for the numerical experiments reported here is detailed in [25].

Initial conditions for the Euler equations are chosen in such a way that the solutions are expected to be right moving. This can be achieved by imposing an initial surface disturbance  $\eta_0$  together with the initial trace of the potential  $\Phi(x) = \int_0^x \eta_0(\xi) d\xi$ . Indeed, the right-going wave condition is  $s(x, t) = 0$  which together with (4.3) and (4.5) imply

$$\begin{aligned}\Phi(x) &= \int_0^x u(\xi, 0) d\xi \\ &= \int_0^x K^{-1} \eta_0(\xi) d\xi \approx \int_0^x \eta_0(\xi) d\xi.\end{aligned}$$

This last provision makes our numerical experiments more natural, since it is not assumed that the regarded surface waves are strictly right moving  $s = O(\mu^2 \alpha)$  and  $\eta = r + O(\mu^2 \alpha)$ . In Fig. 1 one can see the corresponding small wave  $s$  moving to the left given by solving the Euler system. In order to normalize the data, we choose  $\eta_0$  in such a way that the average of

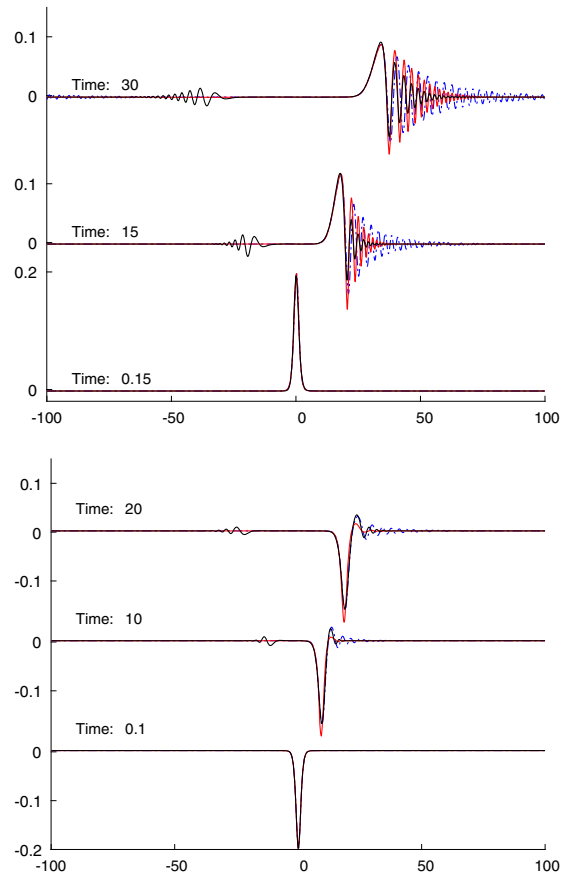


**Fig. 1** Wave profiles at three different times: the Euler (black line), Whitham (red line) and KdV (blue line) with amplitude  $\alpha = 0.2$ , wavelength  $\lambda = \sqrt{5}$  and capillarity parameter  $\kappa = 1/2$ . (Color figure online)

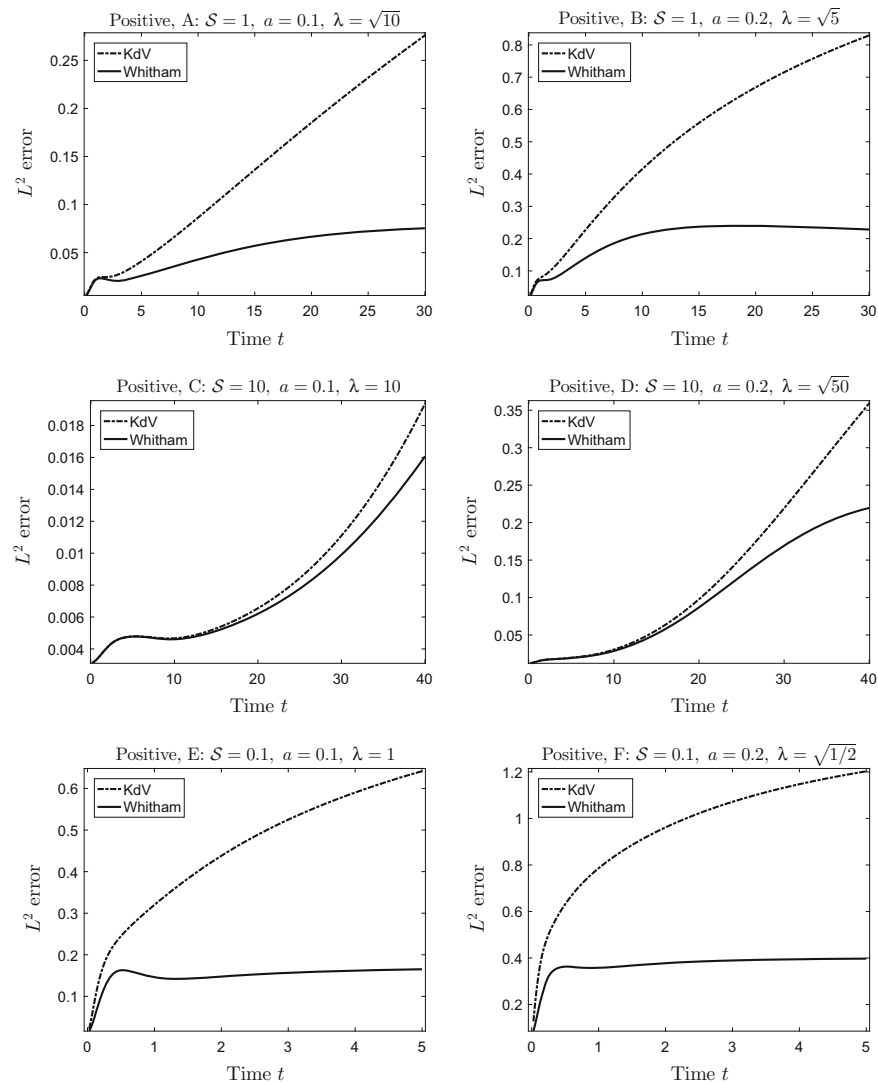
$\eta_0$  over the computational domain is zero. The experiments are performed with several different amplitudes  $\alpha$  and wavelengths  $\lambda$ . For the purpose of this section, we define the wavelength  $\lambda$  as the distance between the two points  $x_1$  and  $x_2$  at which  $\eta_0(x_1) = \eta_0(x_2) = \alpha/2$ . Both positive and negative initial disturbances are considered. Numerical experiments were performed with a range of parameters for amplitude  $\alpha$  and the wavelength  $\lambda$ . The summary of experiments' settings is given in Table 1. All experiments are made with initial wave of elevation and wave of depression, labeled as “positive” and “negative,” respectively (see [17]). The domain for computations is  $-L \leq x \leq L$ , with  $L = 100$ . The “positive” initial data are

$$\eta_0(x) = a \cdot \operatorname{sech}^2(f(\lambda)x) - C, \quad (5.1)$$

**Table 1** Summary of the Stokes number, nondimensional wavelength, nondimensional amplitude of the initial data used in the numerical experiments

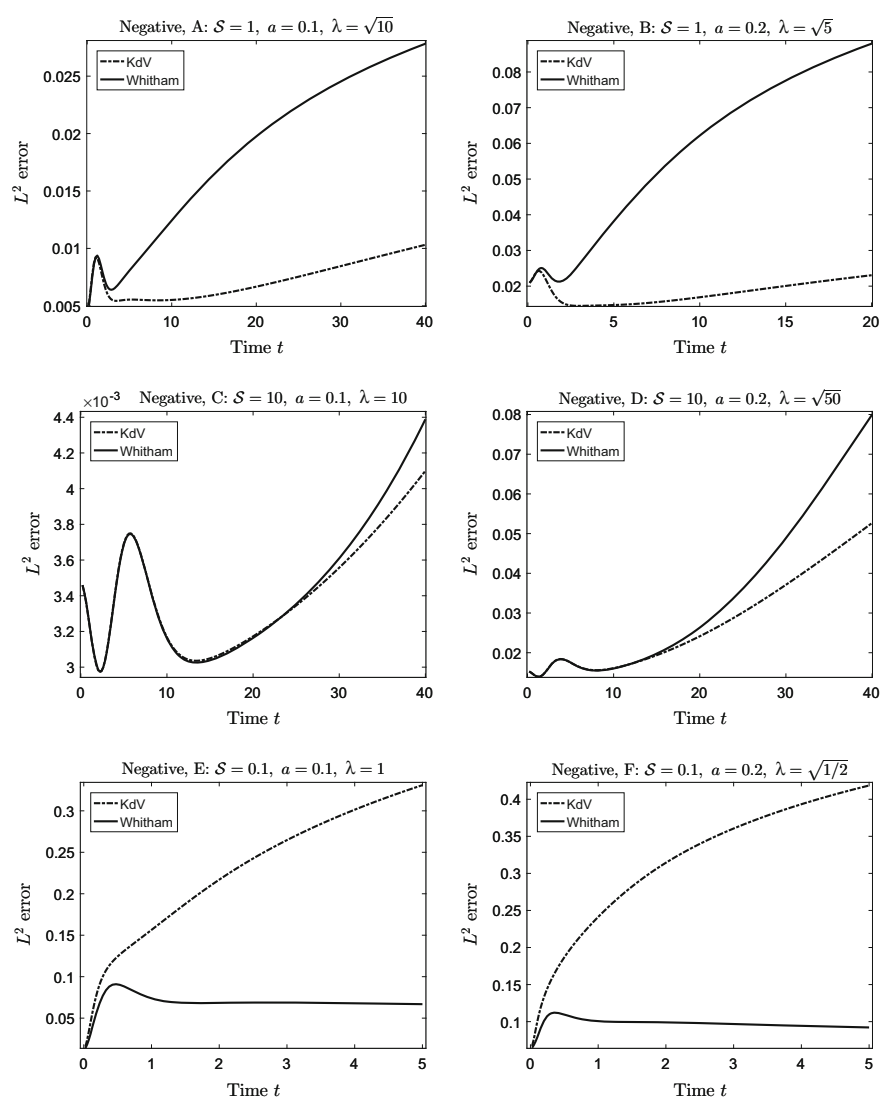
Experiment	Stokes number $\mathcal{S}$	Amplitude $\alpha$	Wavelength $\lambda$
A	1	0.1	$\sqrt{10}$
B	1	0.2	$\sqrt{5}$
C	10	0.1	10
D	10	0.2	$\sqrt{50}$
E	0.1	0.1	1
F	0.1	0.2	$\sqrt{1/2}$

**Fig. 2**  $L^2$  errors in approximation of solutions to the full Euler equations by different model equations with the positive initial wave  $\eta_0(x)$  and the surface tension  $\kappa = \frac{1}{2}$



## The Whitham equation with surface tension

**Fig. 3**  $L^2$  errors in approximation of solutions to the full Euler equations by different model equations with the negative initial wave  $\eta_0(x)$  and the surface tension  $\kappa = \frac{1}{2}$



where

$$\begin{aligned} f(\lambda) &= \frac{2}{\lambda} \log \left( \frac{1 + \sqrt{1/2}}{\sqrt{1/2}} \right), \\ C &= \frac{1}{L} \frac{a}{f(\lambda)} \tanh \left( \frac{L}{f(\lambda)} \right). \end{aligned}$$

Here  $C$  and  $f(\lambda)$  are chosen so that  $\int_{-L}^L \eta_0(x) dx = 0$ , and the wavelength  $\lambda$  is the distance between the two points  $x_1$  and  $x_2$  at which  $\eta_0(x_1) = \eta_0(x_2) = a/2$ . The velocity potential in this case is:

$$\Phi(x) = \frac{a}{f(\lambda)} \tanh(f(\lambda)x) - Cx, \quad (5.2)$$

The “negative” case function is just the “reverse” of the first one

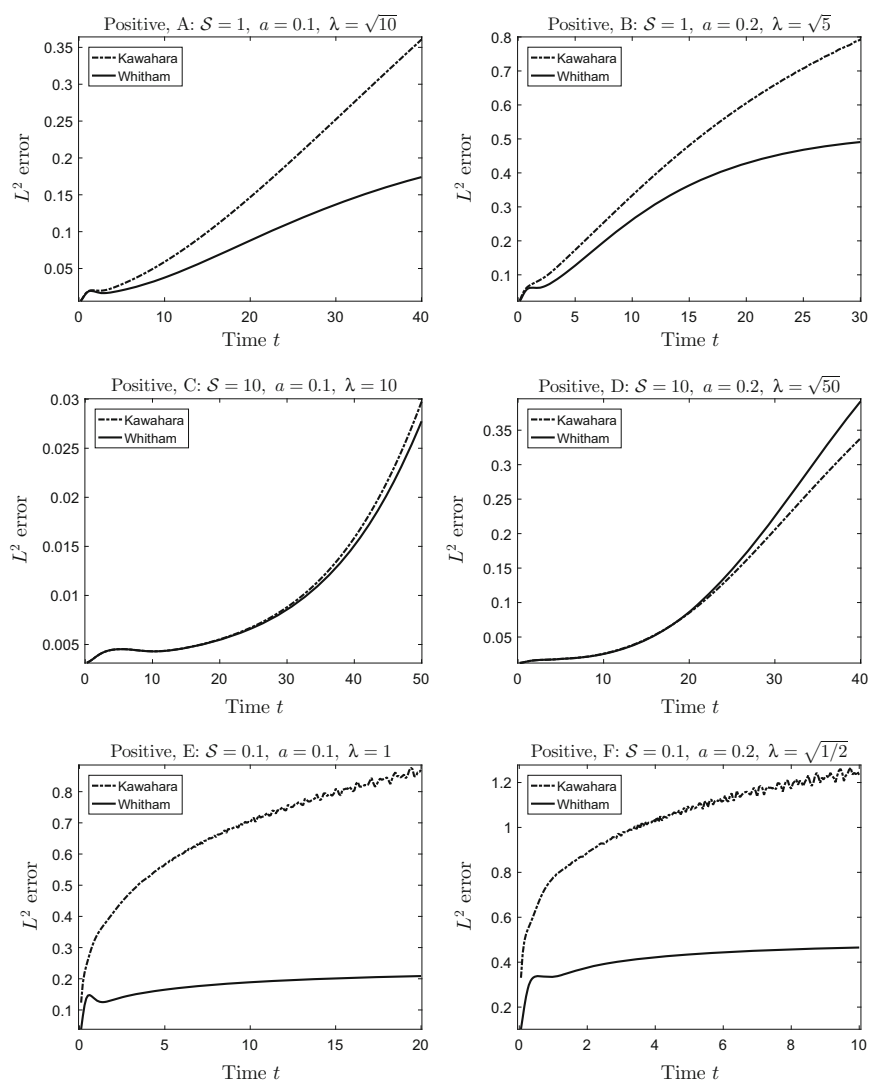
$$\eta_0(x) = -a \cdot \operatorname{sech}^2(f(\lambda)x) + C. \quad (5.3)$$

The definitions for  $f(\lambda)$  and  $C$  are the same. And the velocity potential is

$$\Phi(x) = -\frac{a}{f(\lambda)} \tanh(f(\lambda)x) + Cx, \quad (5.4)$$

We calculate solutions of the Whitham equation and the Euler system. We also calculate solutions of the

**Fig. 4**  $L^2$  errors in approximation of solutions to the full Euler equations by different model equations with the positive initial wave  $\eta_0(x)$  and the surface tension  $\kappa = \frac{1}{3}$



KdV for the capillarity  $\kappa = 1/2$  and solutions of the Kawahara in the case  $\kappa = 1/3$ .

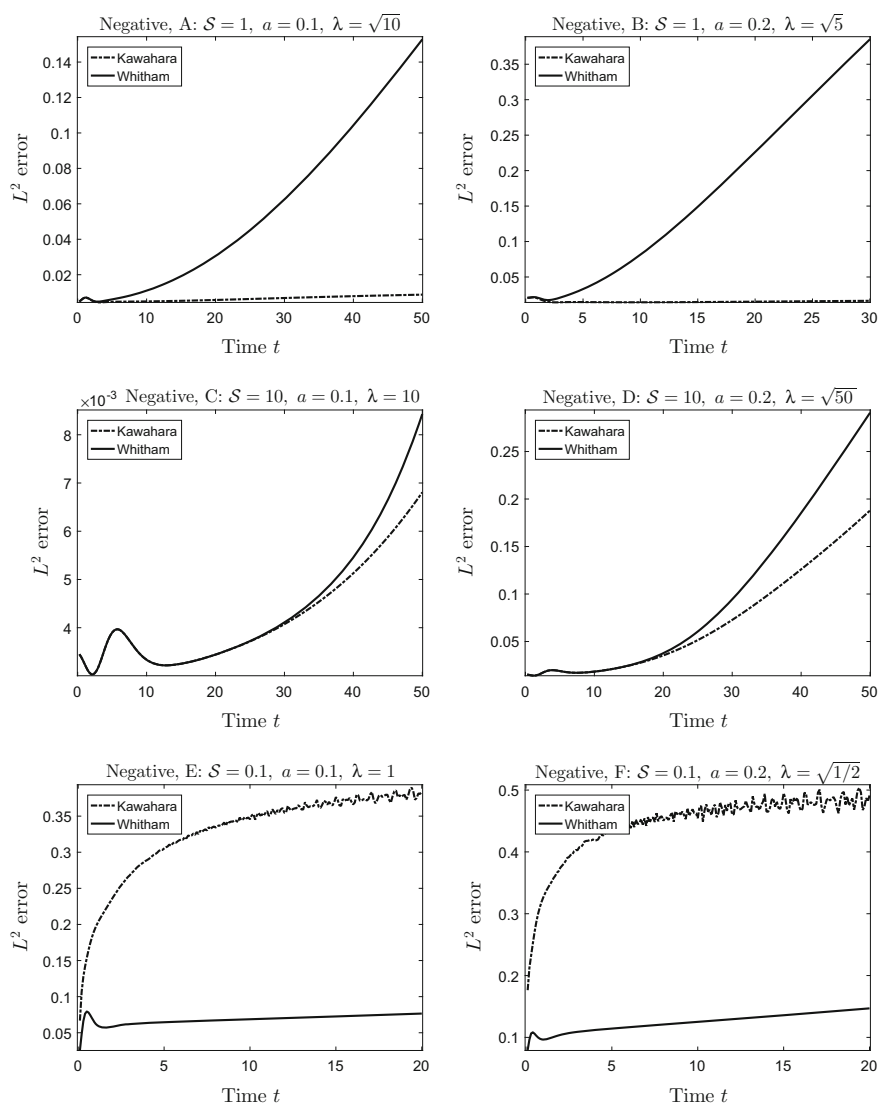
In Fig. 1, the time evolution of a wave with an initial narrow peak is shown according to the Euler (black line), Whitham (red line) and KdV (blue line) equations. Here the amplitude  $a = 0.2$ , the wavelength  $\lambda = \sqrt{5}$  and the capillary parameter  $\kappa = 1/2$  are used. This case corresponds to the Stokes number  $\mathcal{S} = 1$ . It appears that the KdV equation produces a significant amount of spurious oscillations and the Whitham equation gives the closest approximation of the corresponding Euler solution. As one can expect, the unidirectional models also lag in the description of waves going to the left.

In order to compare the accuracy of each approximate model we calculate the differences, firstly between the Whitham and Euler equations, and secondly between the KdV (or Kawahara) and Euler equations. These differences are measured in the integral  $L^2$ -norm normalized by initial condition  $\|\eta_0\|$  as follows

$$\frac{\|\eta_E(t) - \eta(t)\|}{\|\eta_0\|} = \sqrt{\frac{\int (\eta_E(x, t) - \eta(x, t))^2 dx}{\int \eta_0(x)^2 dx}}$$

## The Whitham equation with surface tension

**Fig. 5**  $L^2$  errors in approximation of solutions to the full Euler equations by different model equations with the negative initial wave  $\eta_0(x)$  and the surface tension  $\kappa = \frac{1}{3}$



where  $\eta_E(x, t)$  is the solution for the Euler system and  $\eta(x, t)$  corresponds either to the Whitham, KdV or Kawahara equation. The next Figs. 2, 3, 4, 5 show the dependence of  $L^2$ -error on time for different initial situations. Thus as one can see, the Whitham model performs better than the KdV and Kawahara equations, in nearly all situations except the cases with a negative initial wave of depression and Stokes number approximately unity.

**Acknowledgements** This research was supported in part by the Research Council of Norway under Grant Nos. 213474/F20 and 239033/F20.

## References

1. Aceves-Sánchez, P., Minzoni, A.A., Panayotaros, P.: Numerical study of a nonlocal model for water-waves with variable depth. *Wave Motion* **50**, 80–93 (2013)
2. Alazard, T., Burq, N., Zuily, C.: On the water-wave equations with surface tension. *Duke Math. J.* **158**, 413–499 (2011)
3. Biswas, A.: Solitary wave solution for the generalized Kawahara equation. *Appl. Math. Lett.* **22**, 208–210 (2009)
4. Benjamin, T.B., Bona, J.L., Mahony, J.J.: Model equations for long waves in nonlinear dispersive systems. *Philos. Trans. R. Soc. Lond. Ser. A* **272**, 47–78 (1972)
5. Borluk, H., Kalisch, H., Nicholls, D.P.: A numerical study of the Whitham equation as a model for steady surface water waves. *J. Comput. Appl. Math.* **296**, 293–302 (2016)

6. Chardard, F.: Stabilité des Ondes Solitaires. Ph.D. Thesis (2009)
7. Choi, W., Camassa, R.: Exact evolution equations for surface waves. *J. Eng. Mech.* **125**, 756–760 (1999)
8. Craig, W., Groves, M.D.: Hamiltonian long-wave approximations to the water-wave problem. *Wave Motion* **19**, 367–389 (1994)
9. Craig, W., Guyenne, P., Kalisch, H.: Hamiltonian long-wave expansions for free surfaces and interfaces. *Commun. Pure Appl. Math.* **58**, 1587–1641 (2005)
10. Craig, W., Sulem, C.: Numerical simulation of gravity waves. *J. Comput. Phys.* **108**, 73–83 (1993)
11. Dyachenko, A.I., Kuznetsov, E.A., Spector, M.D., Zakharov, V.E.: Analytical description of the free surface dynamics of an ideal fluid (canonical formalism and conformal mapping). *Phys. Lett. A* **221**, 73–79 (1996)
12. De Frutos, J., Sanz-Serna, J.M.: An easily implementable fourth-order method for the time integration of wave problems. *J. Comput. Phys.* **103**, 160–168 (1992)
13. Ehrnström, M., Groves, M.D., Wahlén, E.: Solitary waves of the Whitham equation—a variational approach to a class of nonlocal evolution equations and existence of solitary waves of the Whitham equation. *Nonlinearity* **25**, 2903–2936 (2012)
14. Ehrnström, M., Kalisch, H.: Traveling waves for the Whitham equation. *Differ. Integral Equ.* **22**, 1193–1210 (2009)
15. Ehrnström, M., Kalisch, H.: Global bifurcation for the Whitham equation. *Math. Model. Nat. Phenom.* **8**, 13–30 (2013)
16. Fornberg, B., Whitham, G.B.: A Numerical and Theoretical Study of Certain Nonlinear Wave Phenomena. *Philos. Trans. R. Soc. A* **289**, 373–404 (1978)
17. Hammack, J.L., Segur, H.: The Korteweg-de Vries equation and water waves. Part 2. Comparison with experiments. *J. Fluid Mech.* **65**, 289–314 (1974)
18. Hur, V.M., Johnson, M.: Modulational instability in the Whitham equation of water waves. *Stud. Appl. Math.* **134**, 120–143 (2015)
19. Hur, V.M., Johnson, M.: Modulational instability in the Whitham equation with surface tension and vorticity. *Nonlinear Anal.* **129**, 104–118 (2015)
20. Kawahara, T.: Oscillatory solitary waves in dispersive media. *J. Phys. Soc. Jpn.* **33**, 260–264 (1972)
21. Lannes, D.: The Water Waves Problem. Mathematical Surveys and Monographs, vol. 188. American Mathematical Society, Providence (2013)
22. Lannes, D., Saut, J.-C.: Remarks on the full dispersion Kadomtsev–Petviashvili equation. *Kinet. Relat. Models* **6**, 989–1009 (2013)
23. Li, Y.A., Hyman, J.M., Choi, W.: A numerical study of the exact evolution equations for surface waves in water of finite depth. *Stud. Appl. Math.* **113**, 303–324 (2004)
24. Milewski, P., Vanden-Broeck, J.-M., Wang, Z.: Dynamics of steep two-dimensional gravity-capillary solitary waves. *J. Fluid Mech.* **664**, 466–477 (2010)
25. Mitsotakis, D., Dutykh, D., Carter, J.D.: On the nonlinear dynamics of the traveling-wave solutions of the Serre equations. *Wave Motion* (in press)
26. Moldabayev, D., Kalisch, H., Dutykh, D.: The Whitham equation as a model for surface water waves. *Phys. D* **309**, 99–107 (2015)
27. Nicholls, D.P., Reitich, F.: A new approach to analyticity of Dirichlet–Neumann operators. *Proc. R. Soc. Edinb. Sect. A* **131**, 1411–1433 (2001)
28. Ovsyannikov, L.V.: To the shallow water theory foundation. *Arch. Mech.* **26**, 407–422 (1974)
29. Peregrine, D.H.: Calculations of the development of an undular bore. *J. Fluid Mech.* **25**, 321–330 (1966)
30. Sanford, N., Kodama, K., Carter, J.D., Kalisch, H.: Stability of traveling wave solutions to the Whitham equation. *Phys. Lett. A* **378**, 2100–2107 (2014)
31. Stepanyants, Y.: Dispersion of long gravity-capillary surface waves and asymptotic equations for solitons. *Proc. Russ. Acad. Eng. Sci. Ser. Appl. Math. Mech.* **14**, 33–40 (2005)
32. Whitham, G.B.: Variational methods and applications to water waves. *Proc. R. Soc. Lond. A* **299**, 6–25 (1967)
33. Whitham, G.B.: Linear and Nonlinear Waves. Wiley, New York (1974)
34. Zakharov, V.E.: Stability of periodic waves of finite amplitude on the surface of a deep fluid. *J. Appl. Mech. Tech. Phys.* **9**, 190–194 (1968)

# **Paper C**

## **A numerical study of nonlinear dispersive wave models with SpecTraV-Wave**

Henrik Kalisch, Daulet Moldabayev, Olivier Verdier



# A Numerical Study of Nonlinear Dispersive Wave Models with SpecTraVVave

Henrik Kalisch<sup>\*a</sup>, Daulet Moldabayev<sup>†a</sup>, and Olivier Verdier<sup>‡ b,c</sup>

<sup>a</sup>*Department of Mathematics, University of Bergen*

<sup>b</sup>*Department of Mathematics and Statistics, University of Umeå, Sweden*

<sup>c</sup>*Department of Computing Mathematics and Physics, Høgskolen i Bergen*

In nonlinear dispersive evolution equations, the competing effects of nonlinearity and dispersion make a number of interesting phenomena possible. In the current work, the focus is on the numerical approximation of traveling-wave solutions of such equations. We describe our efforts to write a dedicated **Python** code which is able to compute traveling-wave solutions of nonlinear dispersive equations in a very general form.

The **SpecTraVVave** code uses a continuation method coupled with a spectral projection to compute approximations of steady symmetric solutions of this equation. The code is used in a number of situations to gain an understanding of traveling-wave solutions. The first case is the Whitham equation, where numerical evidence points to the conclusion that the main bifurcation branch features three distinct points of interest, namely a turning point, a point of stability inversion, and a terminal point which corresponds to a cusped wave.

The second case is the so-called modified Benjamin–Ono equation where the interaction of two solitary waves is investigated. It is found that two solitary waves may interact in such a way that the smaller wave is annihilated. The third case concerns the Benjamin equation which features two competing dispersive operators. In this case, it is found that bifurcation curves of periodic traveling-wave solutions may cross and connect high up on the branch in the nonlinear regime.

---

<sup>\*</sup>[henrik.kalisch@math.uib.no](mailto:henrik.kalisch@math.uib.no)

<sup>†</sup>[daulet.moldabayev@math.uib.no](mailto:daulet.moldabayev@math.uib.no)

<sup>‡</sup>[olivier.verdier@hib.no](mailto:olivier.verdier@hib.no)

## 1. Introduction

This paper is concerned with traveling wave solutions for a class of nonlinear dispersive equations of the form

$$u_t + [f(u)]_x + \mathcal{L}u_x = 0, \quad (1)$$

where  $\mathcal{L}$  is a self-adjoint operator, and  $f$  is a real-valued function with  $f(0) = 0$  and  $f'(0) = 0$ , and which satisfies certain growth conditions. Equations of this form arise routinely in the study of wave problems in fluid mechanics and many other contexts. A prototype of such an equation is the KdV equation that appears if  $\mathcal{L} = I + \frac{1}{6}\partial_x^2$  and  $f(u) = \frac{3}{4}u^2$ . In the current work, the operator  $\mathcal{L}$  is considered to be given as a Fourier multiplier operator, such as for instance in the Benjamin–Ono equation, which arises in the study of interfacial waves. In this case, the Fourier multiplier operator is given by  $\mathcal{L} = I - \mathcal{H}\partial_x$ , where the Hilbert transform  $\mathcal{H}$  is defined as

$$\mathcal{H}u(x) = \frac{1}{\pi} \text{p.v.} \int_{-\infty}^{\infty} \frac{u(x-y)}{y} dy, \quad \widehat{\mathcal{H}u}(k) = -i \operatorname{sgn}(k) \widehat{u}(k).$$

We also study in detail traveling wave solutions of the Whitham equation, which appears when  $\mathcal{L}$  is given by convolution with the integral kernel  $K_{h_0}$  in the form

$$\mathcal{L}u(x) = \int_{-\infty}^{\infty} K_{h_0}(y)u(x-y) dy, \quad \widehat{K_{h_0}}(k) = \sqrt{\frac{g \tanh(h_0 k)}{k}}, \quad (2)$$

and  $f$  is the same function as in the KdV equation.

The particular form of equation (1) exhibits the competing effects of dispersion and nonlinearity, which gives rise to a host of interesting phenomena. The most well known special phenomenon is the existence of solitary waves and of periodic traveling waves containing higher Fourier modes. Indeed, note that in the purely dispersive model  $u_t + \mathcal{L}u_x = 0$ , the only possible permanent progressive waves are simple sinusoidal waves, while in the nonlinear model (1) higher Fourier modes must be considered to obtain solutions.

The order of the operator  $\mathcal{L}$  appearing in (1) has a major effect on the types of solutions that may be found. A higher-order operator, such as in the Korteweg–de Vries equation, acts as a smoothing operator because of its effect of spreading different frequency components out due to a strongly varying phase speed [34]. Lower-order operators such as the operator  $K_{h_0}$  in (1) appearing in the Whitham equation may allow solutions to develop singularities, such as derivative blow-up (see [27], [29]) and formation of cusps (see [24]).

On the other hand, highly nonlinear functions  $f(u)$  may lead to  $L^\infty$ -blow-up. For instance, the generalized KdV equation which is written in normalized form as

$$u_t + u^p u_x + u_x + u_{xxx} = 0,$$

features global existence of solutions for  $p = 1, 2, 3$ , but the solutions blow-up in the critical case  $p = 4$  (the case  $p \geq 5$  is open). In the case of the generalized Benjamin–Ono

equation

$$u_t + u^p u_x + u_x - \mathcal{H}u_{xx} = 0,$$

where  $\mathcal{H}$  is the Hilbert transform, numerical evidence points to singularity formation for  $p > 2$  [11], but no proofs are available at this time.

In order to study different phenomena related to equations of the form (1) and their traveling wave solutions, a Python-based solver package **SpecTraVVave** was developed by the authors [40]. The general idea behind the solver is to use a numerical continuation method [35] implemented with a pseudo-spectral algorithm. Similar previous projects include **AUTO** [20] and **Wavetrain** [48]. **AUTO** is written in *C*, whereas **Wavetrain** is written in *Fortran*. Both programs are efficient and very general, as they are able to cover a wide range of problems involving bifurcation analyses. However, from a user's perspective, such a generality coupled with low level programming languages may lead to some difficulties in utilizing these programs efficiently.

**SpecTraVVave** is designed to provide researchers with a simple yet effective tool for investigating problems on traveling waves. The package is flexible, and its functionality can be easily expanded. The availability of the **IPython** notebook [44] makes the solver very interactive, so that it should be easier for new users to get started.

In order to maximize ease of use, **SpecTraVVave** was designed to find even solutions of (1). Symmetry of steady solutions can be proved for some of the models in the form (1), but not for all [16]. Some of these equations also admit non-smooth solutions, for instance as termination points of a bifurcation branch. This happens for example for the Whitham equation, which features bifurcation curves which terminate in a solution with a cusp [24]. One of the goals of the present paper is to investigate the precise nature of the termination of the bifurcation curve.

The content of the paper is structured as follows. A mathematical description of the numerical method of **SpecTraVVave** is given in § 2. § 3 presents results of different experiments carried out with the package. Concluding remarks are given in § 4. A method for finding initial guesses for the solver is described in Appendix A. Appendix B contains a schematic of program and a description of its workflow.

## 2. Spectral scheme and construction of nonlinear system.

### 2.1. Cosine collocation method.

To compute traveling wave solutions to the equation (1) the following ansatz is employed:

$$u(x, t) = \phi(x - ct).$$

Thus, the equation takes the form

$$\phi' + [f(\phi)]' + \mathcal{L}\phi' = 0,$$

which can be integrated to give

$$-c\phi + f(\phi) + \mathcal{L}\phi = B. \quad (3)$$

The constant  $B$  is a priori undetermined. One may set the  $B$  equal to zero as a way of normalizing the solutions. Another option is to impose an additional condition, for example that the integral of  $\phi$  over one wavelength be zero. In this case,  $B$  will be found along with the solution  $\phi$ .

We consider  $\mathcal{L}$  as a Fourier multiplier operator with symbol  $\alpha(k)$ . We also assume that  $f$  is at least twice differentiable, and we have  $f(0) = 0$  and  $f'(0) = 0$ . When computing traveling-wave solutions we focus on even periodic solutions. While it can be proved in some cases that solutions of (2.1) must be even, this is not known for a general operator  $\mathcal{L}$ . Nevertheless, we make this assumption here in order to make the numerical procedure as uniform as possible. For even periodic solutions, one may use a cosine collocation instead of a Fourier method. In particular, using the cosine functions as basis elements automatically removes the inherent symmetries due to reflective and translational symmetry. Moreover, the number of unknowns is reduced by a factor of 2, and the problem of the asymmetric arrangement of nodes in the FFT is circumvented. Of course, all these problems could also be dealt with a collocation method based on the Fourier basis, but the cosine basis does all of the above automatically. In addition, the Python cosine transform is based on an integrated algorithm, which relies on an optimized version of the discrete cosine transform (DCT).

The following description of computation scheme was presented in detail in [23], but we will briefly repeat it here for consistency of the manuscript. For the purpose of clarity, we will refer to full wavelength  $L$  of a solution as the (full) wavelength, and half of fundamental wavelength will be called half-wavelength. Such a definition is required because the method computes a half of a solution profile, the other half is automatically constructed due to symmetry.

Traveling wave solutions to the equation (2.1) are to be computed in the form of a linear combination of cosine functions of different wave-numbers, i.e., in the space

$$\mathcal{S}_N = \text{span}_{\mathbb{R}} \{ \cos(lx) \mid 0 \leq l \leq N - 1 \}.$$

This is a subspace of  $L^2(0, 2\pi)$ , and the collocation points  $x_n = \pi \frac{2n-1}{2N}$  for  $n = 1, \dots, N$  are used to discretize the domain. If the required full wavelength of solutions is to be  $L \neq 2\pi$ , one can use a scaling on the  $x$ -variable. Defining the new variable

$$x' = \frac{L}{2\pi}x,$$

yields collocation points  $x'_n$  and wavenumbers  $\kappa_l$  defined by

$$x'_n = \frac{L}{2} \frac{2n-1}{2N}, \quad \kappa_l = \frac{2\pi}{L}l.$$

We are seeking a function  $\phi_N \in \mathcal{S}_N$  that satisfies the equations

$$-c\phi_N(x'_n) + f(\phi_N)(x'_n) + \mathcal{L}^N \phi_N(x'_n) = 0, \quad (4)$$

at the collocation points  $x'_n$ . The operator  $\mathcal{L}^N$  is the discrete form of the operator  $\mathcal{L}$ , and  $\phi_N$  is the discrete cosine representation of  $\phi$  which is given by

$$\begin{aligned}\phi_N(x') &= \sum_{l=0}^{N-1} \omega(\kappa_l) \Phi_N(\kappa_l) \cos(\kappa_l x'), \\ \omega(\kappa_l) &= \begin{cases} \sqrt{1/N}, & \kappa_l = 0, \\ \sqrt{2/N}, & \kappa_l > 0, \end{cases} \\ \Phi_N(\kappa_l) &= \omega(\kappa_l) \sum_{n=1}^N \phi_N(x'_n) \cos(\kappa_l x'_n),\end{aligned}$$

where  $\kappa_l = 0, \frac{2\pi}{L}, \dots, \frac{2\pi}{L}(N-1)$  are the scaled wavenumbers, and  $\Phi_N(\cdot)$  are the discrete cosine coefficients. As the equation (2.1) is enforced at the collocation points  $x'_n$ , one may evaluate the term  $\mathcal{L}^N \phi_N$  using the matrix  $\mathcal{L}^N(i, j)$  defined by

$$\begin{aligned}\mathcal{L}^N \phi_N(x'_i) &= \sum_{j=1}^N \mathcal{L}^N(i, j) \phi_N(x'_j), \\ \mathcal{L}^N(i, j) &= \sum_{l=0}^{N-1} \omega^2(\kappa_l) \alpha(\kappa_l) \cos(\kappa_l x'_i) \cos(\kappa_l x'_j),\end{aligned}$$

where  $\alpha(\cdot)$  is the Fourier multiplier function of the operator  $\mathcal{L}$ .

## 2.2. Construction of nonlinear system.

The equation (2.1) enforced at  $N$  collocation points yields a nonlinear system of  $N$  equations in  $N$  unknowns, which can be written in shorthand as

$$F(\phi_N) = 0.$$

This system can be solved by a standard iterative method, such as Newton's method. In this system, the value of phase speed  $c$  has to be fixed for computing one particular solution. Such an approach becomes impractical when a turning point on the bifurcation curve appears.

In **SpecTravVave** a different approach is employed: both the amplitude  $a$  and the phase speed  $c$  of a solution are treated as functions of a parameter  $\theta$ :  $a = a(\theta)$ ,  $c = c(\theta)$ . The parameter  $\theta$  is to be computed from the system (2.2). This construction makes it possible to follow turning points on the bifurcation branch with relative ease. Having computed two solutions, i.e., two points on the bifurcation curve  $P_1 = (c_1, a_1)$  and  $P_2 = (c_2, a_2)$ , one may find a direction vector  $\mathbf{d} = (d^c, d^a)$  of the line that contains these points:

$$\mathbf{d} : \quad d^c = c_2 - c_1, \quad d^a = a_2 - a_1.$$

Then the point  $P_3 = (c_3, a_3)$  is fixed at some (small) distance  $s$  from the point  $P_2$  in the direction  $\mathbf{d}$ .

$$P_3 : \quad c_3 = c_2 + s \cdot d^c, \quad a_3 = a_2 + s \cdot d^a.$$

The point  $P_3$  plays the role of the initial guess for velocity and amplitude when computing the next solution  $P_* = (c_*, a_*)$ . The solution point  $P_*$  is required to lay on the line with direction vector  $\mathbf{d}_\perp = (d_\perp^c, d_\perp^a)$ , which is orthogonal to the vector  $\mathbf{d}$ .

$$\begin{aligned} \mathbf{d}_\perp : \quad d_\perp^c &= -d^a, & d_\perp^a &= d^c, \\ P_* : \quad c_* &= c_3 + \theta d_\perp^c & a_* &= a_3 + \theta d_\perp^a. \end{aligned}$$

A schematic sketch of finding a new solution  $P_*$  is given in [Figure 1](#).

The variable  $\theta$  is computed by Newton's method from the extended system

$$F \begin{pmatrix} \phi_N(x_1) \\ \vdots \\ \phi_N(x_N) \\ B \\ \theta \end{pmatrix} = \begin{pmatrix} (-c + \mathcal{L}_N)\phi_N(x_1) + f(\phi_N(x_1)) - B \\ \vdots \\ (-c + \mathcal{L}_N)\phi_N(x_N) + f(\phi_N(x_N)) - B \\ \Omega(\phi_N, c, a, B) \\ \phi_N(x_1) - \phi_N(x_N) - a \end{pmatrix} = \begin{pmatrix} 0 \\ \vdots \\ 0 \\ 0 \\ 0 \end{pmatrix}. \quad (5)$$

Here a nonhomogeneous problem ( $B \neq 0$ ) is considered. The equation

$$\phi_N(x_1) - \phi_N(x_N) - a = 0,$$

makes the waveheight of the computed solution to be that of  $a$ . The equation

$$\Omega(\phi_N, c, a, B) = 0,$$

is called the *boundary condition*. It allows to enforce different specifications on the computed traveling wave solution. For example, if one sets

$$\Omega(\phi_N, c, a, B) = \phi_N(x_1) + \cdots + \phi_N(x_N),$$

then *the mean of the computed wave over a period will have to be equal to zero*. One may also experiment with

$$\Omega(\phi_N, c, a, B) = B,$$

to consider the homogeneous problem ( $B = 0$ ). It can be also interesting to set

$$\Omega(\phi_N, c, a, B) = \phi_N(x_N). \quad (6)$$

This enables us to compute traveling wave solutions that mimic solitary wave solutions.

### 2.3. Convergence.

In order to test the numerical implementation of the discretization, the method is applied to a case where the solution is known. One such case is the KdV equation

$$u_t + u_x + \frac{3}{2}uu_x + \frac{1}{6}u_{xxx} = 0,$$

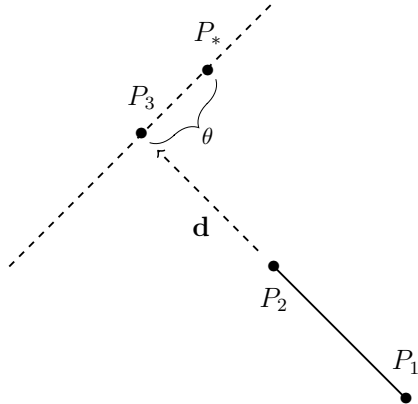


Figure 1: Navigation on the bifurcation curve.

which has a known solution, given in the form

$$u_{\text{exact}}(x, t) = a \operatorname{sech}^2 \left( \sqrt{\frac{3a}{4}}(x - ct) \right),$$

with  $c = 1 + a/2$ . Using the boundary equation (2.2), **SpecTraVVave** is capable of computing approximations to solitary wave solutions of nonlinear wave equations. Solitary wave solutions are treated as traveling waves with sufficiently long wavelength that have the wave trough at zero. In case of the KdV equation solitary wave solutions have exponential decay, and therefore, considering the symmetry of solitary solutions, the half-wavelength of 30 is considered for the comparison. Approximation errors are summarized in Table 1.

Nb. of grid points	$\log_{10}(\ u_{\text{exact}} - u\ _{L^\infty})$	$\log_{10}(\ u_{\text{exact}} - u\ _{L^2})$	Ratio of $L^2$ -errors
32	-1.389	-2.092	
64	-3.705	-4.549	286.8
128	-8.809	-9.508	90935.0
256	-15.353	-16.144	4329670.9
512	-15.353	-16.087	0.9

Table 1: Estimates of error between the exact and computed solitary wave solutions for the KdV equation. Half-wavelength 30, waveheight  $a = 1.2651$

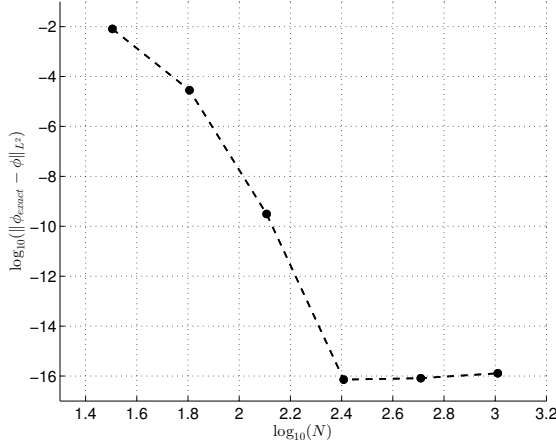


Figure 2: Graph of error estimates given in Table 1.

### 3. Experiments with SpecTraVVave.

#### 3.1. Termination of the waveheight-velocity bifurcation curve of the Whitham equation.

The waveheight-velocity bifurcation curve of the Whitham equation

$$u_t + \frac{3}{2}uu_x + Ku_x = 0, \quad \widehat{Ku}(k) = \sqrt{\tanh(k)}, \quad (7)$$

was studied numerically in [23]. An attempt was made to identify the termination point of the Whitham bifurcation curve. The investigation was limited by computational tools and complete results were not obtained. In particular, the authors could not confirm that traveling wave solutions do not exist past the point where the authors, based on pioneering work of Whitham [52] suspected a cusped solution. In this section a number of numerical results on nature of the bifurcation curve for the Whitham equation are presented. Solutions to the equation (3.1) are computed in the form of traveling waves  $u(x, t) = \phi(x - ct)$  and the homogeneous ( $B = 0$ ) integrated version the equation is considered:

$$-c\phi + \frac{3}{4}\phi^2 + K\phi = 0. \quad (8)$$

Special attention is given to relation between stability of solutions and their waveheight and velocity parameters, i.e., their position on the bifurcation curve. The following questions are under study:

- a) Where does the bifurcation curve terminate?
- b) Where on the bifurcation curve do solutions change their stability?
- c) Is there any role that the turning point on the bifurcation curve plays?

The results presented here focus on  $2\pi$ -periodic solutions to the equation (3.1), i.e., solutions of the system (2.2). Figure 3 presents Whitham bifurcation curves with numbers of grid points  $N = 512$ ,  $N = 1024$  and  $N = 2048$ . The current implementation of the **SpecTravVave** package allows fixing the number of grid points  $N$  and a so-called doubling parameter  $\mathcal{D}$ , i.e., the number by which  $N$  is doubled as computations are made. This allows us to get sets of solutions with  $N, 2N, \dots, 2^{\mathcal{D}}N$  grid points. If  $\mathcal{D} = 1$  then only two sets of solutions are computed and they are regarded as lower grid (lower resolution) and higher grid (higher resolution) solutions. While the system (2.2) is processed by Newton solver, lower grid solutions are taken as initial guesses for higher grid solutions. All curves shown in this manuscript have been produced after tests with a number of resolutions were run, and the curves shown did not change significantly under further refinement.

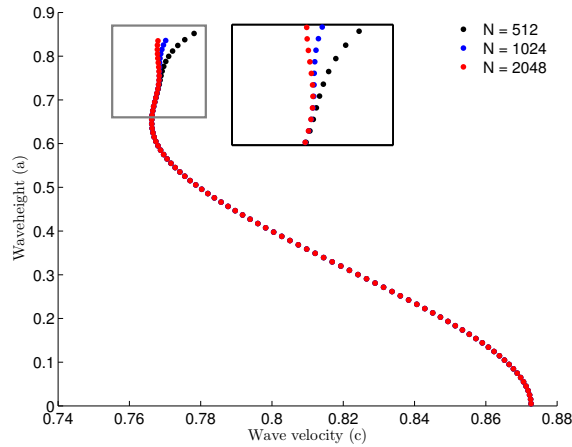


Figure 3: Whitham bifurcation curve in different grid resolutions.

Figure 4(a) presents the Whitham bifurcation curve computed by **SpecTravVave** with  $N = 1024$  and  $\mathcal{D} = 1$ . There are three solutions which deserve to be singled out:

1. Traveling wave solution with minimum velocity (rhombus);
2. Traveling wave solution with maximum  $L^2$ -norm (circle);
3. Cusped traveling wave solution (square).

Profiles of the above listed solutions are given in Figure 5(a). The solution with minimum velocity corresponds to the turning point of the bifurcation curve. The solution with maximum  $L^2$ -norm is very close to the latter one, although it has a higher waveheight and a different velocity. The solution marked by a square is called here the *terminal solution*. As already mentioned, previous studies, such as [22, 23] did not provide any conclusive analysis on the part of the bifurcation curve past the turning point. In particular, it was not clear whether solutions ceased to exist at or after the turning point, or whether solutions were stable or unstable after the turning point.

Let us first focus on the stability of solutions. Note that **SpectraVWave** has an evolution integrator routine, which enables one to check the stability of computed solutions. The current version of the package uses the fourth-order method developed in [19]. In addition one may use a more refined analysis, resting on the evaluation of invariant functionals. This analysis is based on the observation that the traveling waves can be thought of as solutions of a constrained minimization problem. This analysis is based on ideas developed by Boussinesq, first exploited in [4], and later used in [12, 14, 41], and many other works. Let us define two functionals  $V$  and  $E$ :

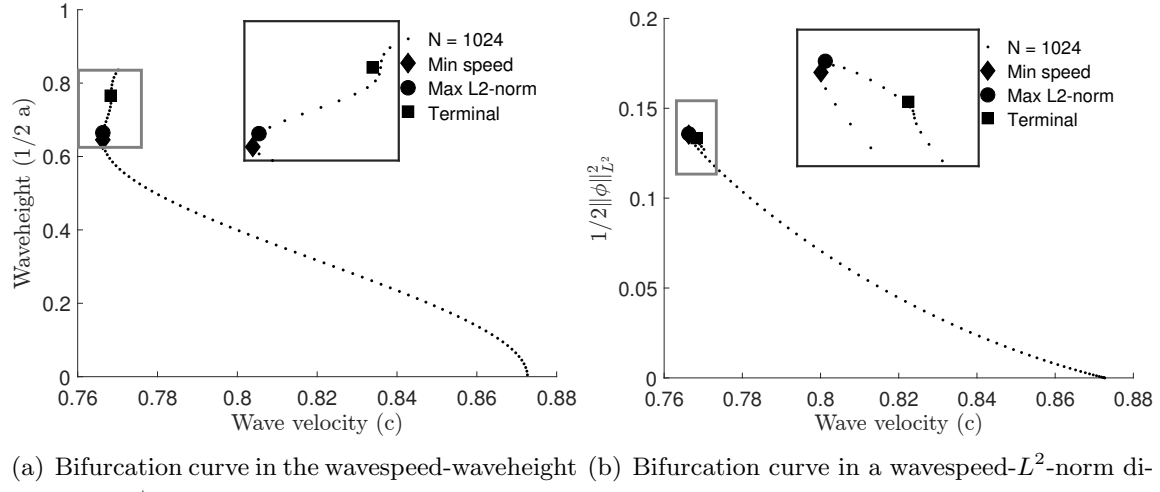


Figure 4: Whitham bifurcation curves for  $2\pi$ -periodic solutions.

$$V(\phi) = \frac{1}{2} \int_{-\infty}^{+\infty} \phi^2 d\zeta, \quad E(\phi) = \int_{-\infty}^{+\infty} \left\{ \frac{1}{2}\phi^3 - \phi K\phi \right\} d\zeta.$$

The equation (3.1) can be then written in terms of variational derivatives of  $E$  and  $V$  as

$$E'(\phi) - cV'(\phi) = 0. \quad (9)$$

It is known from [12] that under certain conditions, the stability of solitary wave solutions depends on convexity of the function  $d(c) = E(\phi) - cV(\phi)$ . Solutions with values of  $c$  for which  $d''(c) > 0$  are stable solutions, and solutions with wave speeds for which  $d''(c) < 0$  are unstable solutions.

The current numerical investigation can therefore be interpreted as an indication of the stability properties of traveling wave solutions of the Whitham equation. Note that differentiation of  $d(c)$  yields

$$d'(c) = \underbrace{E'(\phi) - cV'(\phi)}_{=0} - V(\phi).$$

Using (3.1) as indicated yields

$$d'(c) = -V(\phi) = -\frac{1}{2} \int_{-\infty}^{+\infty} \phi^2 d\zeta = -\frac{1}{2} \|\phi\|_{L^2}^2.$$

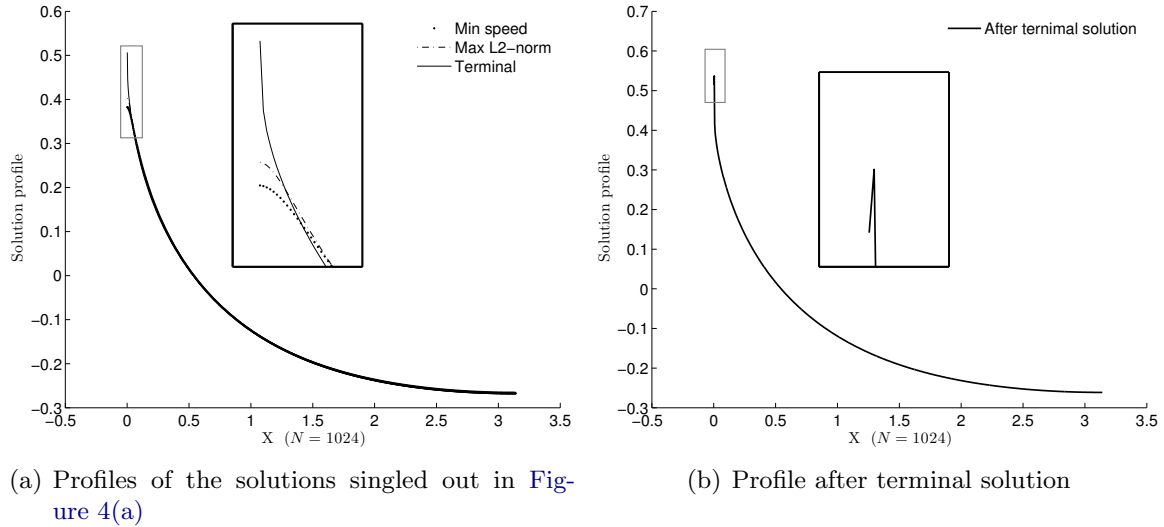


Figure 5: Profiles of specific traveling wave solutions.

Therefore, in order to understand the convexity of  $d(c)$ , it is sufficient to find points of maximum  $L^2$ -norm on the curve in the right panel of Figure 4. It is straightforward to see that  $d''(c)$  changes sign in the neighbourhood of the maximum point of this curve, i.e., around the solution with maximum  $L^2$ -norm. In particular,  $d''(c) > 0$ , i.e., solutions are stable to the left of the maximum point, and  $d''(c) < 0$ , i.e., solutions are unstable to the right of the maximum point.

In addition, the solutions were tested with the evolution integrator to confirm their stability/instability in time. The solution with maximum  $L^2$ -norm and those on the left-hand side were always found to be stable in the time-dependent computations. Solutions on the right-hand side do not preserve their shape and thus are unstable. Examples are given in Figure 6. This analysis confirms that the point corresponding to the minimum wave speed (the turning point), and the point of stability inversion are two distinct points on the bifurcation curve. Moreover, the point of stability inversion is a little further up the branch from the turning point.

Next, we turn our attention to the analysis of the terminal point. There are two main questions. Does the branch terminate, and if so, does the terminal point on the branch correspond to a cusped traveling wave. First of all, note that the solution, which is computed by `SpecTraVVave`, past the terminal solution has two crests, no matter how small the stepping on the bifurcation branch is taken. (see Figure 5(b)). Secondly, as will be explained presently, the relation

$$\frac{c}{\sup_x \phi(x)} = \frac{3}{2}$$

holds for the terminal solution with a good degree of approximation. For the most accurate runs, we obtain  $c / \sup_{x \in \mathbb{R}} \phi(x) \approx 1.51$ . To explain how this relation comes

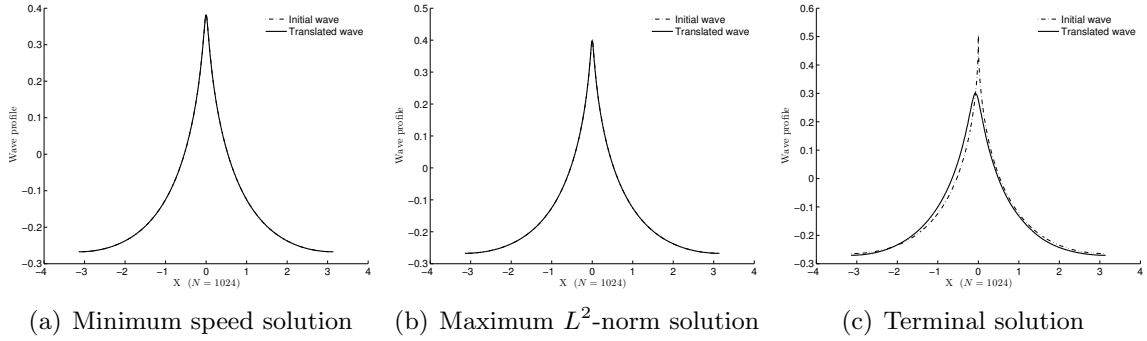


Figure 6: Evolution of specific solutions in time. Time range for each solution is three periods.

about note that the steady integrated form of the Whitham equation can be written as

$$\left(\frac{c}{\sqrt{3}} - \frac{\sqrt{3}}{2}\phi\right)^2 = \frac{1}{3}c^2 - K\phi. \quad (10)$$

It is clear that for any  $\phi < \frac{3}{2}c$ , the relation (3.1) can be used in a bootstrap argument to show that any continuous solution must be in fact smooth. However for the case  $\phi = \frac{3}{2}c$  this bootstrap argument fails since the left-hand side vanishes. It can be concluded that a solutions containing a cusp will have a maximum value of  $\frac{3}{2}c$ .

As an additional check, the discrete cosine coefficients of the solutions were examined, and fitted to the following models:

$$\mathcal{E}(k) = \nu_1 e^{-\nu_2 k^n}, \quad \mathcal{P}(k) = \frac{\mu_1}{\mu_2 + \mu_3 k^m},$$

where  $\nu_1, \nu_2, \mu_1, \mu_2, \mu_3, n$  and  $m$  are fitting parameters. A smooth function is known to have discrete cosine coefficients with exponential decay in  $k$ . On the other hand, if a function is not smooth, the discrete cosine coefficients feature polynomial decay. To identify the best fit, two parameters were used:  $L^2$ -norm of the residual and the Akaike information criterion (AIC) measure.

From the data given in the Table 2, one can deduce that for solutions with minimum speed and maximum  $L^2$ -norm exponential fit is better than polynomial. That is not the case for the terminal solution. Thus, the first two solutions are smooth and the terminal solution is nonsmooth. In fact, the polynomial fit is better than exponential for solutions that are between the maximum  $L^2$ -norm solution and the terminal solution.

The numerical evidence brought forward supports the conclusion that the Whitham bifurcation branch terminates at the terminal point indicated in Figure 3. Of course, as already mentioned, this conclusion has now also been reached using tools of mathematical analysis [24].

Model	Min speed solution		Max $L^2$ -norm solution		Terminal solution	
	$\mathcal{E}(k)$	$\mathcal{P}(k)$	$\mathcal{E}(k)$	$\mathcal{P}(k)$	$\mathcal{E}(k)$	$\mathcal{P}(k)$
Residual's $L^2$ norm	$5 \times 10^{-5}$	$4 \times 10^{-3}$	$7 \times 10^{-5}$	$3 \times 10^{-3}$	$6 \times 10^{-3}$	$6 \times 10^{-4}$
AIC	-543	-321	-529	-333	-298	-416

Table 2: Results for measures of fit.

### 3.2. Interaction of solitary wave solutions of modified Benjamin–Ono equation

In this section, we utilize the **SpecTraVVave** package to obtain high-precision approximations to solitary-wave solutions of the modified Benjamin–Ono

$$u_t + u^2 u_x + u_x - \mathcal{H}u_{xx} = 0,$$

which is a special case of the generalized Benjamin–Ono equation, with  $p = 2$ . This case corresponds to the critical scaling, i.e., invariance of the energy norm under the natural invariant scaling.

The Benjamin–Ono equation was found by Benjamin [3] as a model for long small-amplitude interfacial waves in deep water. The validity of approximating the more physically correct configuration of a continuous density distribution by the two-layer approximation has recently been justified mathematically [17].

Solitary-wave solutions of the modified Benjamin–Ono equation with  $p = 3$ ,  $p = 4$  and  $p = 5$  were approximated in [11] with a standard Newton scheme. The solutions in [11] were not very accurate, but since singularity formation of the evolution equations were under study, the accuracy of the solitary-wave approximation was not an important issue. The problem with the method of [11] and some other works was that the fft used there was not purged of possible symmetries (translational and reflective). In the current code, since a cosine formulation is chosen, these symmetries are automatically eliminated, and the resulting computations are able to render more accurate approximations.

Solitary-wave solutions of these equation could be computed with higher accuracy using a type of Petviashvili method in [43], but here we employ the **SpecTraVVave** package using the boundary equation (2.2), and treating solitary waves as traveling waves with sufficiently long wavelength that have wave trough at zero. Once these high-accuracy solutions are found, they are aligned in an evolution code using a high-order time integrator, and the interaction of two waves is studied.

Two questions are investigated. First, the interaction is investigated for evidence of integrability. Second, we are looking for possible annihilation of one of the waves, such as may happen in some other evolution equations [49].

A possible approach to studying the question of complete integrability is analyzing the interaction of two solitary wave solutions of the equation, such as carried out in [31, 33] for other nonlocal equations. In Figure 7, snapshots of interaction of two solitary waves at different times are shown. The time difference between two consecutive snapshots is constant. As it may be observed, during the process of interaction, the two initial solitary waves combine into a single wave, and an additional oscillation is produced. This

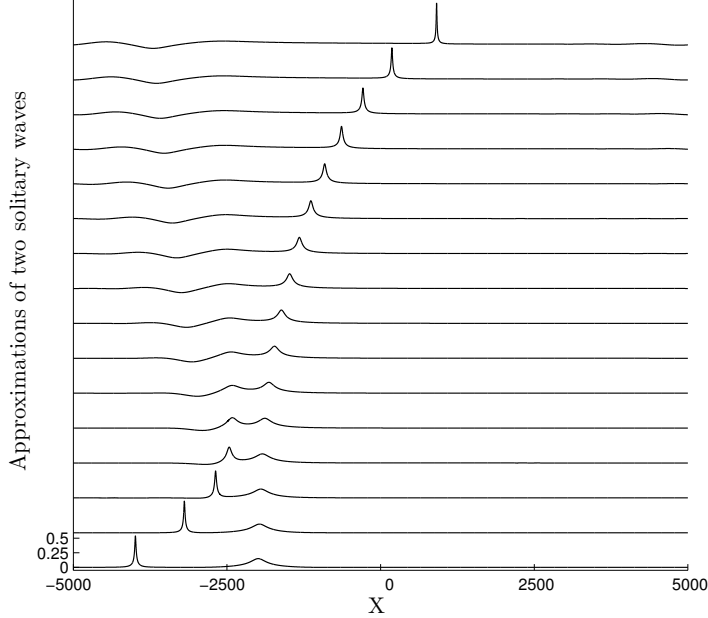


Figure 7: Interaction of two solitary waves of the modified Benjamin–Ono equation.

leads us to the conclusion that the interaction of solitary waves is not elastic and the modified Benjamin–Ono equation may not be integrable. In addition, it appears that the smaller wave disappears as most of its mass is acquired by the larger wave. Thus one may argue that the small wave is annihilated by the larger wave. It can also be observed that the larger wave starts growing, and it is likely that this growth will lead to finite-time blow-up. This question was not investigated further since blow-up phenomena have already been studied closely in [33]. Indeed, very recently, the finite-time blow-up has been proven mathematically in [38].

### 3.3. Effect of competing dispersion in the Benjamin equation

The Benjamin equation was found by Benjamin [5] as a model for two-layer flow in the case when the interface is subject to surface tension. The approximation may not be a good model for a stratified situation, but more applicable to the case where two fluids are separated by a sharp interface. The equation is

$$u_t + u_x + uu_x - \mathcal{H}u_{xx} - \tau u_{xxx} = 0, \quad (11)$$

where  $\tau$  is a parameter similar to the Bond number in free surface flow [5], [32], [50].

In this section, a study relating to the effects of competing dispersion operators on the shape of periodic traveling waves in the Benjamin equation is presented. An in-depth study of solitary waves was carried out in [21]. As will come to light, the periodic case features some new phenomena, such as secondary bifurcations, connecting and crossing branches. For the purpose of this study, we fix the parameter  $\tau = 0.1$ , so that the

dispersion relation for the linearized equation is

$$c(k) = 1 - |k| + 0.1k^2. \quad (12)$$

Traveling wave solutions with full wavelengths  $L_1 = \pi/5$ ,  $L_2 = 4\pi/19$  and  $L_3 = 4\pi$  are computed for the equation (3.3). The corresponding wavenumbers are  $k_1 = 10$ ,  $k_2 = 19/2$ , and  $k_3 = 0.5$ , respectively. A plot of the dispersion relation (3.3) is given in Figure 8. Bifurcation branches of traveling wave solutions with the selected wavelengths are given in Figure 9.

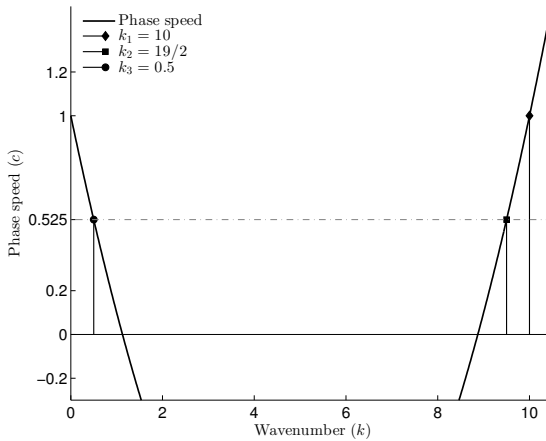


Figure 8: Dispersion relation (3.3)

The branch denoted by  $L_1$  originates at the bifurcation point located at  $c = 1$  and zero waveheight. The branches denoted by  $L_2$  and  $L_3$  originate from the same bifurcation point, located at  $c = 0.525$  and zero waveheight. These two branches continue in different directions, due to differences in wavelength. In particular, the  $L_3$  branch contains waves with shorter wavelengths, and falls into the capillary regime. On the other hand, the  $L_2$  branch falls in the gravity regime. As the waveheight grows, solutions on the  $L_3$  branch first cross the  $L_1$  branch without connecting. Additional oscillations develop in the solutions until a new fundamental wavelength  $\pi/5$  is reached, and the branch terminates as it connects to the  $L_1$  branch. The situation is depicted in Figure 10. The point where the  $L_1$  and  $L_3$  branches meet is approximately  $(c^*, a^*) = (0.945, 5.938)$ . The corresponding profiles essentially overlap, as shown on Figure 11. This point can also be interpreted as a secondary bifurcation point of the  $L_1$  branch, where solutions with wavelengths that are multiples of  $\pi/5$  develop. We should note that similar phenomena concerning crossing and connecting branches were previously observed in [46] for the Whitham equation with surface tension which was introduced in [28].

## 4. Conclusions and future work

The numerical algorithm of **SpecTravVave** features ample flexibility for researching different aspects of nonlocal dispersive wave equations and their traveling wave solutions.

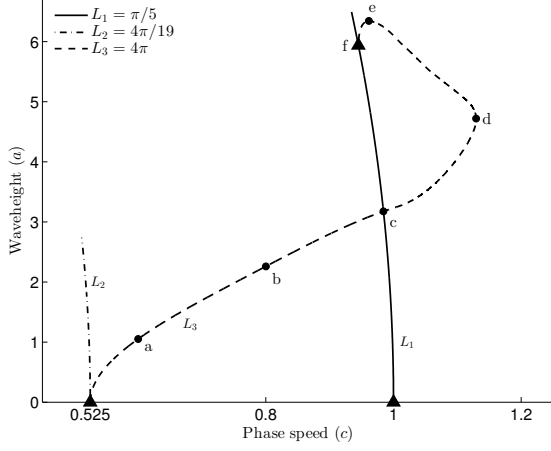


Figure 9: Bifurcation curves of the equation (3.3) with different wavelengths,  $\blacktriangle$  – points of bifurcation,  $\bullet$  – selected solutions (see Figure 10).

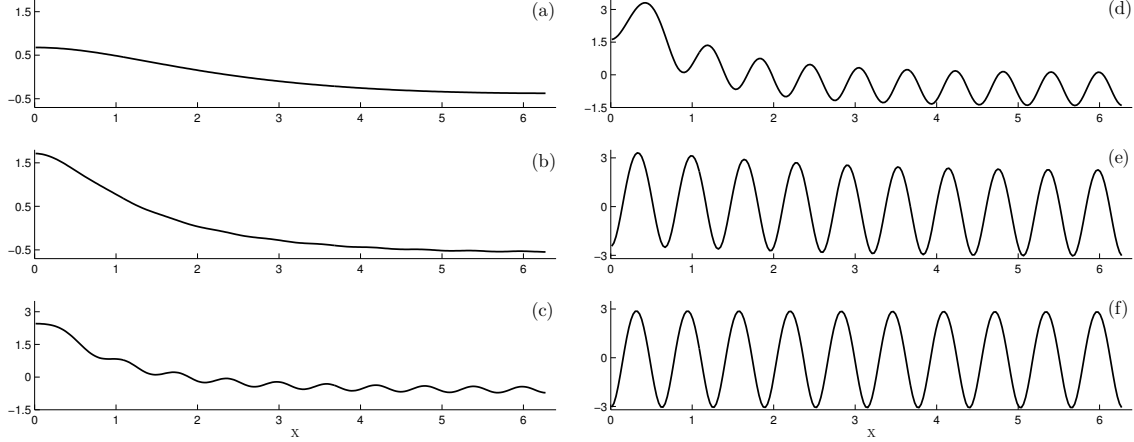


Figure 10: Selected solutions of the equation (3.3). Labels preserved as shown in Figure 9.

The solver package is simpler in use when compared with programs such as **AUTO** and **Wavetrain**, however it does not have the same level of generality. Moreover, **AUTO** and **Wavetrain** are programmed in low-level programming languages and will therefore run more efficiently. **SpecTraVVave** is implemented in an object-oriented fashion [25], which makes the program easily expandable. **IPython** provides means for interactive work with the package, and enables users to create convenient notebook-programs. A parametric approach in defining amplitude and phase speed makes it possible to follow turning points on bifurcation curves. Specification of different boundary conditions allows computing solutions with certain features, such as traveling waves with zero mean, or approximations to solitary waves.

In this work, the **SpecTraVVave** package has been put to use for the study of a number on nonlinear evolution equations: the Whitham equation, the modified Benjamin–Ono

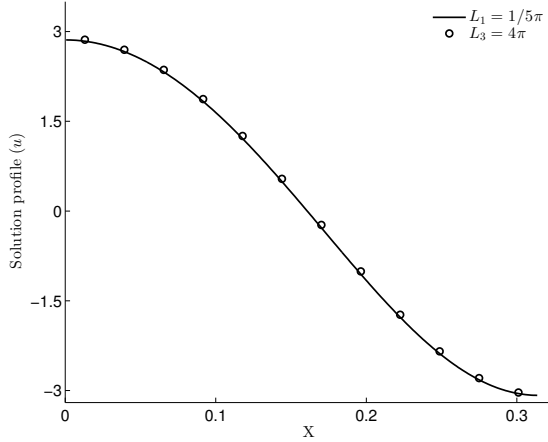


Figure 11: Solution profiles at the point  $(c^*, a^*)$  where the  $L_1$  and  $L_3$  branches meet (see Figure 9).

equation and the Benjamin equation. For the chosen set of parameters, experiments on the Whitham equation resulted in numerical confirmation of the conjecture on cusped solutions. It was also possible to identify the point of stability inversion of traveling wave solutions of the equation and the termination point of its bifurcation curve.

In case of the modified Benjamin–Ono equation, the study on solitary wave solutions lead us to conclude that interaction process ended with annihilation of one of the two waves. The experiment on the Benjamin equation showed one more example of the effect of competing dispersion. As the amplitude increased, traveling wave solutions of wavelength  $4\pi$  developed additional oscillations, and later connected up with a branch of solutions with wavelength  $\pi/5$ .

Future work on the **SpectraVWave** package will be focused on development of its functionality and broadening the range of problems that can be studied. Possible extensions may include implementation of algorithms based on the Petviashvili method [7]–[8] and generalization to systems of equations.

**Acknowledgments.** The authors would like to thank Mats Ehrnström and Erik Wahlén for fruitful discussions on the subject of the current paper. This research was supported by the Research Council of Norway on grant no. 213474/F20 and by the J C Kempe Memorial Fund on grant no. SMK-1238.

## Appendices

### A. Computing initial guesses from Stokes expansion.

$$u_t + [f(u)]_x + \mathcal{L}u_x = 0, \quad (13)$$

The goal of this section is to explain how the idea of Stokes's approximation works in providing the initial data (guess) on wave and phase velocity for solving the equation (A) numerically.

We will consider  $\mathcal{L}$  being linear and self-adjoint Fourier multiplier operator, and a function  $f$  that has degree of zeros  $p \geq 2$ :

$$\begin{aligned}\widehat{\mathcal{L}u}(k) &= \alpha(k) \cdot \widehat{u}(k), \\ \langle \mathcal{L}u, v \rangle_{L^2(0,L)} &= \langle u, \mathcal{L}v \rangle_{L^2(0,L)}, \\ p = \min_{k \in \mathbb{N}} f^{(k-1)}(0) &= 0 \text{ and } f^{(k)}(0) \neq 0\end{aligned}$$

Consider the equation (A) and its solution in the form  $u(x, t) = \phi(x - ct)$ , which is a traveling wave solution. Inserting  $\phi(x - ct)$  into (A) leads to the equation:

$$-c\phi' + f'(\phi)\phi' + \mathcal{L}\phi' = 0,$$

which can be integrated to give:

$$-c\phi + f(\phi) + \mathcal{L}\phi = B, \quad B = \text{const.} \quad (14)$$

Consider  $B = 0$  in equation (A), and expansions of  $\phi$  and  $c$ :

$$\phi = \xi = \varepsilon\xi_1 + \varepsilon^2\xi_2 + \dots, \quad (15)$$

$$c = c_0 + \varepsilon c_1 + \varepsilon^2 c_2 + \dots. \quad (16)$$

The next step is to insert (A) and (A) to the equation (A) and write out the terms at powers of  $\varepsilon$ . The function  $f(\phi)$  is expanded around zero and, therefore, will appear only in  $\varepsilon^p$  terms. Thus, the term at the first power of  $\varepsilon$  reads:

$$\varepsilon : -c_0\xi_1 + \mathcal{L}\xi_1 = 0, \quad (17)$$

Hence,  $c_0$  is an eigenvalue of the operator  $\mathcal{L}$ , regarded as defined on  $L$ -periodic functions. Taking the Fourier transform of the equation (A) gives:

$$-c_0\widehat{\xi}_1(k) + \alpha(k)\widehat{\xi}_1(k) = 0. \quad (18)$$

The equation (A) has two trivial solutions: either  $\xi_1(k) \equiv 0$  or  $\alpha(k) \equiv c_0$ . If we assume non-trivial  $\xi_1$  and  $\alpha(k) \neq \text{const}$ , the following solves the problem:

$$\widehat{\xi}_1(k) = 2\pi\delta(k - k_0), \quad \text{and} \quad c_0 = \alpha(k_0), \quad (19)$$

for some  $k_0 \in \mathbb{R}$ . Since  $\xi_1$  is the first-order approximation to  $\phi$ , the corresponding wave number should be equal to 1. The  $L$ -periodicity condition entails that  $k_0 = 2\pi/L \cdot 1$ . The spatial variable  $x$  has to be scaled to  $x' = L/2\pi x$ , accordingly. From the solutions in (A) we have

$$\xi_1(x') = e^{ik_0x'} = \cos(k_0x') + \sin(k_0x').$$

Considering the projection onto the space  $\mathcal{S}_N$ , we are led to choose  $\xi_1(x') = \cos(k_0x')$ .

For further analysis, let us define an operator  $\mathcal{A}$

$$\mathcal{A} := -c_0\mathcal{E} + \mathcal{L},$$

where  $\mathcal{E}$  is the identity operator. The operator  $\mathcal{A}$  inherits the property of being self-adjoint from  $\mathcal{L}$ . Moreover, it follows from (A) that  $\mathcal{A}\xi_1 = 0$  and  $\xi_1 \in \ker(\mathcal{A})$ . If  $p > 2$  then  $f''(0) = 0$  and the terms at  $\epsilon^2$  are:

$$\mathcal{A}\xi_2 - c_1\xi_1 = 0.$$

Taking scalar multiplication of the latter with  $\xi_1$ , one obtains:

$$\begin{aligned} \langle \xi_1, \mathcal{A}\xi_2 \rangle_{L^2(0,L)} &= c_1 \|\xi_1\|_{L^2(0,L)}^2, \\ \langle \xi_1, \mathcal{A}\xi_2 \rangle_{L^2(0,L)} &= \langle \mathcal{A}\xi_1, \xi_2 \rangle_{L^2(0,L)} = \langle 0, \xi_2 \rangle_{L^2(0,L)} = 0. \end{aligned}$$

As a result, one has  $c_1 \|\xi_1\|_{L^2(0,L)}^2 = 0$  and, hence,  $c_1 = 0$ . Repeating the same argument, it becomes clear that  $c_k = 0$  for any  $k \leq p-1$ . Besides that,  $\xi_2$  is in the kernel of  $\mathcal{A}$ , so it may be assumed to be proportional to  $\xi_1$ . The terms at order  $\epsilon^p$  are:

$$\mathcal{A}\xi_p - c_{p-1}\xi_1 + \frac{f^{(p)}(0)}{p!}\xi_1^p = 0. \quad (20)$$

Let us denote for brevity

$$f_p := \frac{f^{(p)}(0)}{p!}.$$

Pairing (A) with  $\xi_1$  (and assuming  $\|\xi_1\|_{L^2(0,L)} = 1$ ) gives

$$c_{p-1} = f_p \cdot \langle \xi_1^p, \xi_1 \rangle_{L^2(0,L)}, \quad (21)$$

which gives us the value of  $c_{p-1}$ . It only remains to solve the following problem numerically in order to obtain  $\xi_p$ :

$$\mathcal{A}\xi_p = c_{p-1}\xi_1 - f_p\xi_1^p \quad (22)$$

For the last equation to be solved, the operator  $\mathcal{A}$  has to be invertible. It is also required that  $\langle \xi_1, \xi_p \rangle_{L^2(0,L)} = 0$ . Therefore the solution is sought in the space orthogonal to  $\ker(\mathcal{A})$ . Since  $\mathcal{A}$  is still a Fourier multiplier operator, one can take the Fourier transform of the equation (A) to find

$$\begin{aligned} \widehat{\mathcal{A}}(k)\widehat{\xi}_p(k) &= c_{p-1}\widehat{\xi}_1(k) - f_p\widehat{\xi}_1^p(k), \\ \widehat{\xi}_p(k) &= \widehat{\mathcal{A}}(k)^{-1} \left( c_{p-1}\widehat{\xi}_1(k) - f_p\widehat{\xi}_1^p(k) \right). \end{aligned}$$

Taking the inverse Fourier transform of  $\widehat{\xi}_p(k)$  gives  $\xi_p$ . Since only even solutions of the problem are considered the cosine part of the Fourier transforms will be required. It is sufficient to use  $\xi_1$  and  $c_0$  as the initial guesses for the Newton method. However, it should be noted that for different values of  $p$  the pair of parameters  $\xi_p$  and  $c_{p-1}$  are computed in different ways.

- a) If  $p = 2$ , then  $\xi_2$  is computed from (A), but  $c_{p-1}$  here becomes zero. Therefore one has to consider the next level of the expansion  $\varepsilon^p$ .
- b) For odd values of  $p$  the parameter  $c_{p-1}$  can be computed from (A) and  $\xi_p$  from (A).
- c) For even values of  $p \geq 4$  the parameter  $\xi_p$  can be computed, but  $c_{p-1}$  may not be non-zero in general. In such cases a different strategy of fixing the initial guess should be used.

## B. Presentation of SpecTravVave and its workflow

### B.1. Overview

There are several classes in the **SpecTravVave** package. An overview of the program is shown in [Figure 12](#). The workflow begins with defining a flux function  $f$  and the Fourier multiplier function  $\alpha$  to set up an equation. The traveling wave solution is characterized by the wavelength  $L$  and a boundary condition  $\Omega(c, a, \phi_N, B)$ . These parameters are fixed for a given problem. The defined equation is then discretized. The **Discretization** object contains all required elements such as grid points, wave-numbers and the discrete linear operator.

The initial guess and the equation's residual are passed from the **Discretization** to the **Solver** object. The **Navigation** object is responsible for finding good initial guesses for  $c$  and  $a$  that are passed to the **Solver** object. The **Solver** object applies Newton's method to find a solution to the system of equations (2.2).

The new solution is sent back to the **Discretization** and **Navigation** objects, where variables get updated. All computed solutions are stored for further analysis. This finishes one iteration. For the next iteration the updated variables are used and a new solution is found. The process may be continued as long as the Jacobian of the problem is non-singular.

### B.2. Class Description

We present an overview of the classes used in **SpecTravVave** package. Note that, since the package is under continuous modification and development, we describe here only the basic classes and functions the package. We refer to the package repository [40] for up-to-date tutorials and installation instructions.

The **Equation** class is the general class for all model equations. Its only role is to store a parameter  $L$ , the wavelength:

```
class Equation(object):
    def __init__(self, L):
        self.length = L
```

A subclass of the **Equation** class has to implement two functions, **compute\_kernel** and **flux**.

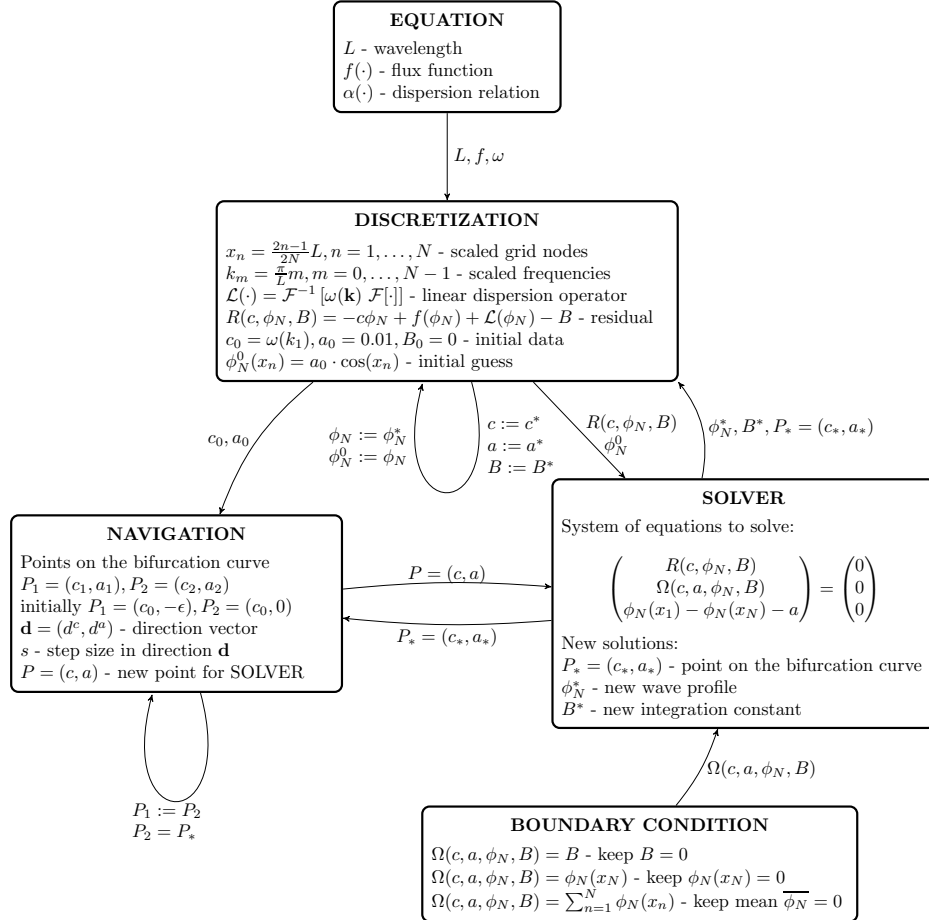


Figure 12: Overview of the SpecTravVwave package.

The KdV model equation

$$u_t + \frac{3}{2} u u_x + u_x + \frac{1}{6} u_{xxx} = 0$$

with  $f(u) = \frac{3}{4}u^2$  and  $\widehat{\mathcal{L}}u(k) = (1 - \frac{1}{6}k^2)\widehat{u}(k)$  is presented in the program as a subclass of the **Equation** class:

```

class KDV(Equation):
    def compute_kernel(self, k):
        return 1-1/6*k**k

    def flux(self, u):
        return 3/4*u*u
    
```

One can then create an object of the class **KDV** with the command:

```
kdv = KDV(L=np.pi)
```

The solver will compute only a half of a solutions profile. The full wavelength of the solutions of the defined equation will be equal to  $2\pi$ .

In order to find solutions with specific features, boundary conditions are introduced as separate classes. For instance, the boundary condition specifying a constant of integration is implemented as follows:

```
class Const(object):
    """ The boundary condition under which the constant of integration
(B) is always set to zero. """
    def __init__(self, level=0):
        self.level = level

    def enforce(self, wave, variables, parameters):
        """ Enforces the Const boundary condition. """
        return np.hstack([variables[0] - self.level])

    def variables_num(self):
        """ The number of additional variables that are required to construct
the Const boundary condition. """
        return 1
```

A `Const` boundary condition object is created as follows:

```
boundary_condition = Const()
```

The next step is to create an object of `Discretization` class, which is initialized with a model equation such as `kdv_model` and the number of grid points. The main parts of the class are the following:

```
class Discretization(object):
    def __init__(self, model_equation, grid_size):
        self.equation = model_equation
        self.size = grid_size

    def operator(self, u):
        u_ = scipy.fftpack.dct(u, norm='ortho')
        Lv = self.fourier_multiplier()*u_
        result = scipy.fftpack.idct(Lv, norm='ortho')
        return result

    def residual(self, u, wavespeed, const_B):
        residual = - wavespeed*u + self.equation.flux(u)
                           + self.operator(u) - const_B
        return residual
```

The call `Discretization.operator(u)` computes  $\mathcal{L}u$  as the inverse transform of a transformed convolution

$$\mathcal{L}u = \mathcal{F}^{-1}[\widehat{\mathcal{L}u}(k)] = \mathcal{F}^{-1}[\alpha(k) \cdot \widehat{u}(k)].$$

The result of the call `Discretization.residual(u, wavespeed, const_B)` is then used in the `Solver` class. An object of the `Solver` class is initialized with an object of the `Discretization` class, and a boundary condition object.

```

class Solver(object):
    def __init__(self, discrete_problem, boundary_condition):
        self.discretization = discrete_problem
        self.boundary = boundary_condition

    def solve(self, guess_wave, parameter_anchor, direction):
        """ Runs a Newton solver on a system of nonlinear equations once.
        Takes the residual(vector) as the system to solve. parameter_anchor
        is the initial guess for (c,a) values and it is taken from the
        Navigation class. """
        size = len(guess_wave)
        self.discretization.size = size

        def residual(vector):
            """ Constructs a system of nonlinear equations. First part,
            main_residual, is from given wave equation; second part,
            boundary_residual, comes from the chosen boundary conditions. """
            . .
            return np.hstack([main_residual, boundary_residual,
                             amplitude_residual])

        . .
        return new_wave, new_boundary_variables, new_parameter

```

Some omitted parts in the above script are substituted by '...' sign. Each iteration on a Solver object is run from a Navigation object, which takes the Solver object for initialization.

```

class Navigation(object):
    """ Runs the Solver and stores the results. """

    def __init__(self, solver_object, size=32):
        self.solve = solver_object.solve # function to run Newton method
        self.size = size # size for navigation
    . .
    def run_solver(self, current_wave, pstar, direction):
        new_wave, variables, p3 = self.solve(current_wave, pstar, direction)
        return new_wave, variables, p3

```

All the above classes can be modified and developed further, new classes may be defined as well.

### B.3. Detailed Workflow

The workflow with the package consists of three basic steps:

1. Once the necessary classes have been imported in the current namespace, generate all necessary objects:

```

equation = KDV(L=np.pi)
boundary_condition = Const()
discretization = Discretization(equation, grid_size=64)
solver = Solver(discretization, boundary_condition)
navigator = Navigation(solver)

```

2. Choose a number of iterations, i.e., the number of solutions to compute, and run the solver:

```
n_iter = 50
navigator.run(n_iter)
```

3. All computed solutions are stored in `navigator_object`

```
last_computed = -1
wave_profile = navigator[last_computed]['solution']
wave_speed = navigator[last_computed]['current'][0]
wave_amplitude = navigator[last_computed]['current'][1]
```

We further refer to the code repository <https://github.com/olivierverdier/SpecTraVVave> for up-to-date instructions on how to run the code.

## References

- [1] Abdelouhab, L. Bona, J.L., Felland, M. and Saut, J.-C. *Nonlocal models for nonlinear dispersive waves*. Physica D **40**, 360–392 (1989)
- [2] Albert, J.P., Bona, J.L. and Restrepo, J.M. *Solitary-wave solutions of the Benjamin equation*. SIAM J. Appl. Math. **59**, 2139–2161 (1999)
- [3] Benjamin, T.B. *Internal Waves of permanent form in fluids of great depth*. J. Fluid Mech. **29**, 559–592 (1967)
- [4] Benjamin, T.B. *The stability of solitary waves*. Proc. Roy. Soc. London A **328**, 153–183 (1972)
- [5] Benjamin, T.B. *A new kind of solitary wave*. J. Fluid Mech. **245**, 401–411 (1992)
- [6] Álvarez, J. and Durán, A. *A numerical scheme for periodic travelling-wave simulations in some nonlinear dispersive wave models*. J. Comput. Appl. Math. **235**, 1790–1797 (2011)
- [7] Álvarez, J. and Durán, A. *An extended Petviashvili method for the numerical generation of traveling and localized waves*. Commun. Nonlinear Sci. Numer. Simul. **19**, 2272–2283 (2014)
- [8] Álvarez, J. and Durán, A. , *Petviashvili type methods for traveling wave computations: I. Analysis of convergence*. J. Comput. Appl. Math. **266**, 39–51 (2014)
- [9] Álvarez, J. and Durán, A. *Corrigendum to "Petviashvili type methods for traveling wave computations: I. Analysis of convergence"*, [J. Comput. Appl. Math. 266 (2014) 39–51]. J. Comput. Appl. Math. **277**, 215–216 (2015)

- [10] Bona, J.L., Dougalis, V.A., Karakashian, O.A. and McKinney, W.R. *Conservative, high-order numerical schemes for the generalized Korteweg–de Vries equation*, Philos. Trans. Royal Soc. London Ser. A, **351**, 107–164 (1995)
- [11] Bona, J.L. and Kalisch, H. *Singularity formation in the generalized Benjamin–Ono equation*. Discrete Contin. Dyn. Syst. **11**, 779–785 (2004)
- [12] Bona, J.L., Souganidis, P.E. and Strauss, W.A. *Stability and instability of solitary waves of Korteweg–de Vries type*. Proc. R. Soc. Lond. A **411**, 395–412 (1987)
- [13] Borluk, H., Kalisch, H. and Nicholls, D.P. *A numerical study of the Whitham equation as a model for steady surface water waves*. J. Comput. Appl. Math. **296**, 293–302 (2016)
- [14] Bridges, T.J. *Superharmonic instability, homoclinic torus bifurcation and water-wave breaking*. J. Fluid Mech. **505**, 153–162 (2004)
- [15] Chen, H. *Existence of periodic travelling-wave solutions of nonlinear, dispersive wave equations*. Nonlinearity **17**, 2041–2056 (2004)
- [16] Chen H. and Bona, J.L. *Existence and asymptotic properties of solitary-wave solutions of Benjamin-type equations*. Adv. Diff. Eq. **3**, 51–84 (1998)
- [17] Chen, R.M. and Walsh, S. *Continuous dependence on the density for stratified steady water waves*. Arch. Ration. Mech. Anal. **219**, 741–792 (2016)
- [18] Choi, W. and Camassa, R. *Fully nonlinear internal waves in a two-fluid system*. J. Fluid Mech. **396**, 1–36 (1999)
- [19] de Frutos, J. and Sanz-Serna, J. M. *An easily implementable fourth-order method for the time integration of wave problems*. J. Comp. Phys. **103**, 160–168 (1992)
- [20] Doedel, E.J., Champneys, A.R., Fairgrieve, T.F., Kuznetsov, Y.A., Sandstede, B. and Wang, X.-J., *AUTO97 : Continuation and bifurcation software for ordinary differential equations*, available at <http://indy.cs.concordia.ca/auto/>, Department of Computer Science and Software Engineering, Concordia University, Montreal, Canada, 1997.
- [21] Dougalis, V.A., Duran, A. and Mitsotakis, D. *Numerical solution of the Benjamin equation*. Wave Motion **52**, 194–215 (2015)
- [22] Ehrnström, M. and Kalisch, H. *Traveling waves for the Whitham equation*. Differential Integral Equations **22**, 1193–1210 (2009)
- [23] Ehrnström, M. and Kalisch, H. *Global bifurcation for the Whitham equation*. Math. Mod. Nat. Phenomena **8**, 13–30 (2013)
- [24] Ehrnström, M. and Wahlén, E. *On Whitham’s conjecture of a highest cusped wave for a nonlocal dispersive equation*. arXiv:1602.05384 (2016).

- [25] Führer, C., Solem, J.E., Verdier, O. Computing with Python: An introduction to Python for science and engineering, Pearson (2014)
- [26] Grujić, Z. and Kalisch, H. *Gevrey regularity for a class of water-wave models*. Nonlinear Analysis **71**, 1160–1170 (2009)
- [27] Hur, V.M. *Breaking in the Whitham equation for shallow water waves*. arXiv:1506.04075 (2015).
- [28] Hur, V.M. and Johnson, M. *Modulational instability in the Whitham equation of water waves*. Studies in Applied Mathematics **134**, 120–143 (2015)
- [29] Hur, V.M. and Tao, L. *Wave breaking for the Whitham equation with fractional dispersion*. arXiv:1410.1570, 2014.
- [30] Fornberg, B. and Whitham, G. B. *A numerical and theoretical study of certain nonlinear wave phenomena*. Phil. Trans. Roy. Soc. A **289**, 373–404 (1978)
- [31] Kalisch, H. *Error analysis of a spectral projection of the regularized Benjamin-Ono equation*. BIT Numerical Mathematics **45**, 69–89 (2005)
- [32] Kalisch, H. *Derivation and comparison of model equations for interfacial capillary-gravity waves in deep water*. Math. Comput. Simulation **74**, 168–178 (2007)
- [33] Kalisch, H. and Bona, J.L. *Models for internal waves in deep water*. Discrete and Continuous Dynamical Systems **6**, 1–20 (2000)
- [34] Kato, T. *On the Cauchy problem for the (generalized) Korteweg-de Vries equation*. Studies in applied mathematics, 93–128, Adv. Math. Suppl. Stud., **8** (Academic Press, New York, 1983).
- [35] Keller H.B., *Numerical solution of bifurcation and nonlinear eigenvalue problems*. Applications of Bifurcation Theory, Rabinowitz, P. H., Academic Press, (1977), pp. 359–384.
- [36] Lannes, D. and Saut, J.-C. *Remarks on the full dispersion Kadomtsev-Petviashvili equation*. Kinet. Relat. Models **6**, 989–1009 (2013)
- [37] Martel, Y. and Merle, F. *Blow up in finite time and dynamics of blow up solutions for the  $L^2$ -critical generalized KdV equation*. J. Amer. Math. Soc. **15**, 617–664 (2002)
- [38] Martel, Y. and Pilod, D. *Construction of a minimal mass blow up solution of the modified Benjamin-Ono equation*. arXiv:1605.01837 (2016).
- [39] Moldabayev, D., Kalisch, H. and Dutykh, D. *The Whitham Equation as a model for surface water waves*. Phys. D **309**, 99–107 (2015)
- [40] Moldabayev, D., Verdier, O. and Kalisch, H. *SpecTraVVave*, available at <https://github.com/olivierverdier/SpecTraVVave>.

- [41] Nguyen, N.T. and Kalisch, H. *Orbital stability of negative solitary waves*. Mathematics and Computers in Simulation **80**, 139–150 (2009)
- [42] Ono, H. *Algebraic Solitary Waves in Stratified Fluids*. J. Phys. Soc. of Japan **39**, 1082–1091 (1975)
- [43] Pelinovsky, D.E. and Stepanyants, Y.A. *Convergence of Petviashvili's iteration method for numerical approximation of stationary solutions of nonlinear wave equations*. SIAM J. Numer. Anal. **42**, 1110–1127 (2004)
- [44] Fernando Pérez, Brian E. Granger *IPython: A System for Interactive Scientific Computing*, Computing in Science and Engineering, vol. 9, no. 3, pp. 21–29, May/June 2007. URL: <http://ipython.org>
- [45] Petviashvili, V.I. *Equation of an extraordinary soliton*, Sov. J. Plasma Phys. **2**, 257–258 (1976)
- [46] Remonato, F. and Kalisch, H. *Numerical bifurcation for the capillary Whitham equation*. arXiv:1604.08324 (2016).
- [47] Sanford, N., Kodama, K., Carter, J.D. and Kalisch, H. *Stability of traveling wave solutions to the Whitham equation*. Phys. Lett. A **378**, 2100–2107 (2014)
- [48] Sherratt, J.A. *Numerical continuation methods for studying periodic travelling wave (wavetrain) solutions of partial differential equations*. Appl. Math. Comp. **218**, 4684–4694 (2012)
- [49] Courtenay Lewis, J. and Tjon, J.A. *Resonant production of solitons in the RLW equation*. Phys. Lett. A **73**, 275–279 (1979)
- [50] Walsh, S. *Steady stratified periodic gravity waves with surface tension I: Local bifurcation*. Discrete Contin. Dyn. Syst. **34**, 3241–3285 (2014)
- [51] Walsh, S. *Steady stratified periodic gravity waves with surface tension II: global bifurcation*. Discrete Contin. Dyn. Syst. **34**, 3287–3315 (2014)
- [52] Whitham, G.B. *Variational methods and applications to water waves*. Proc. Roy. Soc. London A **299**, 6–25 (1967)
- [53] Whitham, G.B. Linear and Nonlinear Waves. Wiley, New York, (1974)



# **Paper D**

## **Explicit solutions for a long-wave model with constant vorticity**

Benjamin Segal, Daulet Moldabayev, Henrik Kalisch, Bernard Deconinck



# Explicit Solutions for a Long-Wave Model with Constant Vorticity

Benjamin Segal\*, Daulet Moldabayev†, Henrik Kalisch† and Bernard Deconinck\*

## Abstract

Explicit parametric solutions are found for a nonlinear long-wave model describing steady surface waves propagating on an inviscid fluid of finite depth in the presence of a linear shear current. The exact solutions, along with an explicit parametric form of the pressure and streamfunction give a complete description of the shape of the free surface and the flow in the bulk of the fluid. The explicit solutions are compared to numerical approximations previously given in [1], and to numerical approximations of solutions of the full Euler equations in the same situation [31]. These comparisons show that the long-wave model yields a fairly accurate approximation of the surface profile as given by the Euler equations up to moderate waveheights. The fluid pressure and the flow underneath the surface are also investigated, and it is found that the long-wave model admits critical layer recirculating flow and non-monotone pressure profiles similar to the flow features of the solutions of the full Euler equations.

## 1 Introduction

Background vorticity can have a significant effect on the properties of waves at the surface of a fluid [19, 24, 26, 30, 32, 35]. In particular, in the seminal paper of Teles da Silva and Peregrine [31], it was found that the combination of strong background vorticity and large amplitude leads to a number of unusual wave shapes, such as narrow and peaked waves and overhanging bulbous waves. In the present contribution, we continue the study of a simplified model equation which admits some of the features found in [31]. The equation, which has its origins in early work of Benjamin [3], has the form

$$\left(Q + \frac{\omega_0}{2}u^2\right)^2 \left(\frac{du}{dx}\right)^2 = -3 \left(\frac{\omega_0^2}{12}u^4 + gu^3 - (2R - \omega_0 Q)u^2 + 2Su - Q^2\right), \quad (1)$$

where we denote the volume flux per unit span by  $Q$ , the momentum flux per unit span and unit density corrected for pressure force by  $S$ , and the energy density per unit span by  $R$ . The gravitational acceleration is  $g$  and the constant vorticity is  $-\omega_0$ . The total flow depth as measured from the free surface to the rigid bottom is given by the function  $u(x)$ .

Equation (1) was recently studied in [1]. It was found that solutions of this equation exhibit similar properties as solutions of the full Euler equations displayed in [31]. In particular, in [1] an expression for the pressure was developed, and it was shown that the pressure may become non-monotone in the case of strong background vorticity. Indeed, it was shown in [1] that if

---

\*Department of Applied Mathematics, University of Washington, Seattle, WA 98195-2420, USA

†Department of Mathematics, University of Bergen, Postbox 7800, 5020 Bergen, Norway

$|\omega_0|$  is big enough, the maximum fluid pressure at the bed is not located under the wavecrest. Such behavior is usually only found in transient problems (cf. [33]). Moreover in some cases, the pressure near the crest of the wave may be below atmospheric pressure.

The purpose of the present work is two-fold. First, we develop a method by which equation (1) can be solved *exactly*. The resulting solutions are compared to the numerical approximations found in [1] and to some of the solutions of the full Euler equations from [31]. Secondly, more features of the solutions of (1) are discussed. Using a similar analysis as in [1], the streamfunction is constructed, and it is found that solutions of (1) may feature recirculating flow and pressure inversion. These features may have an impact on the study of sediment resuspension. Indeed, while it is generally accepted that the main mechanism for sediment resuspension is turbulence due to flow separation in the presence of strong viscous shear stresses [7, 27, 29], the strongly non-monotone pressure profiles exhibited by the solutions of (1) may represent a more fundamental mechanism for particle suspension than the viscous theory.

The geometric setup of the problem is explained as follows. Consider a background shear flow  $U_0 = \omega_0 z$ , where  $\omega$  can be positive or negative (cf. Figure 1). Superimposed on this background flow is wave motion at the surface of the fluid. One may argue that the wave motion itself introduces variations into the shear flow due to the Stokes drift [16, 25]. However for very long waves, the Stokes drift can be compared to the Stokes drift in the KdV equation [5], and it becomes negligible in the long-wave limit. Moreover, as observed by a number of authors [3, 31, 32], a linear shear current can be taken as a first approximation of more realistic shear flows with more complex structures.

If it is assumed that the free surface describes a steady periodic oscillatory pattern, then the flow underneath the free surface can be uniquely determined [10, 23], even in the presence of vorticity. Thus for the purpose of studying periodic traveling waves, one may use a reference frame moving with the wave. This change of reference frame leads to a stationary problem in the fundamental domain of one wavelength. The incompressibility guarantees the existence of the streamfunction  $\psi$  and if constant vorticity  $\omega = -\omega_0$  is stipulated, the streamfunction satisfies the Poisson equation

$$\Delta\psi = \psi_{xx} + \psi_{zz} = \omega_0, \text{ in } 0 < z < \eta(x) = \psi|_{z=\eta}. \quad (2)$$

As explained in [2, 4], the three parameters  $Q$ ,  $S$  and  $R$  are defined as follows. If  $\psi = 0$  on the streamline along the flat bottom, then  $Q$  denotes the total volume flux per unit width given by

$$Q = \int_0^\eta \psi_z dz. \quad (3)$$

Thus  $Q$  is the value of the streamfunction  $\psi$  at the free surface. The flow force per unit width  $S$  is defined by

$$S = \int_0^\eta \left\{ \frac{P}{\rho} + \psi_z^2 \right\} dz, \quad (4)$$

and the energy per unit mass is given by

$$R = \frac{1}{2}\psi_z^2 + \frac{1}{2}\psi_x^2 + g\eta \text{ on } z = \eta(x). \quad (5)$$

Finally, the pressure can be expressed as

$$P = \rho \left( R - gz - \frac{1}{2}(\psi_x^2 + \psi_z^2) + \omega_0\psi - \omega_0 Q \right), \quad (6)$$

It is well known that the quantities  $Q$  and  $S$  do not depend on the value of  $x$  [4]. Using the fact that  $S$  is a constant, the derivation of the model equation (1) can be effected by assuming that the waves are long, scaling  $z$  by the undisturbed depth  $h_0$ ,  $x$  by a typical wavelength  $L$ , and expanding in the small parameter  $\beta = h_0^2/L^2$ . This yields (1) as an approximate model equation describing the shape of the free surface. In order to distinguish from the free surface  $\eta$  in the full Euler description, we call the unknown of equation (1)  $u$  which is an approximation of  $\eta$ . The derivation of (1) was given in [1, 4], where it was shown that (1) is expected to be valid as an approximate model equation describing waves on the surface of the shear flow if the wavelength is long compared to the undisturbed depth of the fluid. On the other hand, a detailed analysis of the derivation explained in [1, 4] shows that there are no assumptions on the amplitude of the waves. Thus at least formally, the model (1) can be expected to model waves of intermediate amplitude.

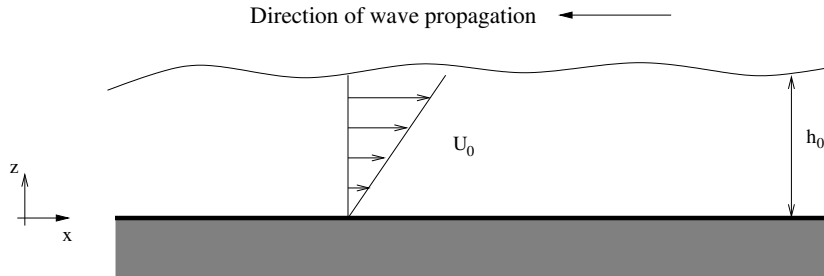


Figure 1: This figure shows the background shear flow  $U_0 = \omega_0 z$ . In the figure,  $\omega_0$  is positive, and the waves which are superposed onto this background current propagate to the left.

## 2 Explicit solutions

In order to obtain solutions of (1) given in explicit form, we apply the change of variables

$$\frac{dy}{ds} = \frac{du}{dx} \left( Q + \frac{\omega_0}{2} u^2 \right),$$

$$y(s) = u(x).$$

This gives us a new equation for  $y(s)$  in the form

$$\left( \frac{dy}{ds} \right)^2 = -3 \left( \frac{\omega_0^2}{12} y^4 + gy^3 - (2R - \omega_0 Q)y^2 + 2Sy - Q^2 \right), \quad (7)$$

and the relation

$$\frac{ds}{dx} = \frac{1}{Q + y^2 \omega_0 / 2}. \quad (8)$$

Integrating (8) we have

$$x(s) = \int^s \left( Q + \frac{\omega_0}{2} y^2 \right) d\xi - x_1. \quad (9)$$

where  $x_1$  is a constant of integration, written explicitly for convenience. We want to solve (7) for  $y(s)$  and plug our solution into (9). We notice that in the variables  $y$  and  $\frac{dy}{ds}$  the equation describes an elliptic curve of genus one [14]. Hermite's Theorem [34, p. 394] states that for a uniform solution to exist we need  $\int ds$  to be an abelian integral of the first kind. This condition

is indeed satisfied and we proceed with using a birational transformation to put (7) in the standard Weierstraß form

$$\left(\frac{dy_0}{dx_0}\right)^2 = 4y_0^3 - g_2y_0 - g_3, \quad (10)$$

where the transformation is given as

$$x_0 = -\frac{24(-2\sqrt{12}Q^2y^2\omega_0 - \sqrt{12}Qgy^3 + 4\sqrt{12}QRy^2 + 4\sqrt{12}Q^3 - 6\sqrt{12}QSy + 8Q^2\frac{dy}{ds} - 4\frac{dy}{ds}Sy)}{y^3},$$

$$y_0 = \frac{4(-Qy^2\omega_0 + 2Ry^2 + \frac{dy}{ds}\sqrt{12}Q + 6Q^2 - 6Sy)}{y^2}, \quad (11)$$

and  $g_2$  and  $g_3$  are the lattice invariants

$$g_2 = -768QR\omega_0 + 768R^2 - 1152Sg,$$

$$g_3 = 2048Q^3\omega_0^3 - 6144Q^2R\omega_0^2 - 6912Q^2g^2 + 6144QR^2\omega_0 - 4608QSg\omega_0 + 2034S^2\omega_0^2 - 4096R^3 + 9216RSg.$$

It is well known that the solution to (10) is  $y_0(x_0) = \wp(x_0 + c_0; g_2, g_3)$ , where  $\wp$  is the Weierstraß P function and  $c_0$  is an arbitrary constant [6, 14]. We invert the birational transformation to determine the exact solution to (7) as

$$y(s) = \frac{A + B\wp'((s + c_0)/4; g_2, g_3) + C\wp((s + c_0)/4; g_2, g_3)}{\wp^2((s + c_0)/4; g_2, g_3) + D\wp((s + c_0)/4; g_2, g_3) + E},$$

with

$$A = -288Q^2g - 96Q\omega_0S + 192RS,$$

$$B = \sqrt{12}Q,$$

$$C = -24S,$$

$$D = 8Q\omega_0 - 16R,$$

$$E = 64Q^2\omega_0^2 - 64QR\omega_0 + 64R^2.$$

This gives us  $u(x(s))$  in the form

$$u(x(s)) = \frac{A + B\wp'((s + c_0)/4; g_2, g_3) + C\wp((s + c_0)/4; g_2, g_3)}{\wp^2((s + c_0)/4; g_2, g_3) + D\wp((s + c_0)/4; g_2, g_3) + E}, \quad (12)$$

as a function of the parameter  $s$ . If we express  $x(s)$  as a function of  $s$ , then we have a parametric representation for  $u(x)$ , the surface elevation. From (9) we have

$$x(s) = Qs - x_1 + \frac{\omega_0}{2} \int^s y^2(\xi) d\xi. \quad (13)$$

Expanding and simplifying  $y(s)^2$  gives

$$y^2 = \frac{4B\wp^3 + C^2\wp^2 + (2AC - B^2g_2)\wp + (A^2 - B^2g_3)}{(\wp^2 + D\wp + E)^2} + \frac{2AB - 2BC\wp}{(\wp^2 + D\wp + E)^2}\wp', \quad (14)$$

making use of the shorthand  $\wp = \wp((s + c_0)/4; g_2, g_3)$  and  $\wp' = \wp'((s + c_0)/4; g_2, g_3)$ . Plugging (14) into (13) and integrating gives

$$\begin{aligned} x(s) &= Qs - x_1 + \omega_0 B \left[ \frac{8(2A - CD) \arctan \left( \frac{D+2\wp}{\sqrt{-D^2+4E}} \right)}{(-D^2 + 4E)^{3/2}} + \frac{-4AD + 8CE + (-8A + 4CD)\wp}{(D^2 - 4E)(\wp^2 + D\wp + E)} \right] \\ &\quad + \frac{\omega_0}{2} \int^s \frac{4B\wp^3 + C^2\wp^2 + (2AC - B^2g_2)\wp + (A^2 - B^2g_3)}{(\wp^2 + D\wp + E)^2} d\xi. \end{aligned} \quad (15)$$

To evaluate the integral in (15) we let

$$\begin{aligned} m_1 &= -\frac{D}{2} - \frac{\sqrt{D^2 - 4E}}{2}, \\ n_1 &= -\frac{D}{2} + \frac{\sqrt{D^2 - 4E}}{2}, \end{aligned}$$

denote the roots of  $\wp^2 + D\wp + E = 0$ . The integrand can be split into its components

$$\frac{4B\wp^3 + C^2\wp^2 + (2AC - B^2g_2)\wp + (A^2 - B^2g_3)}{(\wp - m_1)^2(\wp - n_1)^2} = \frac{J(m_1, n_1)}{(\wp - m_1)^2} + \frac{K(m_1, n_1)}{\wp - m_1} + \frac{J(n_1, m_1)}{(\wp - n_1)^2} + \frac{K(n_1, m_1)}{\wp - n_1},$$

with

$$\begin{aligned} J(m_1, n_1) &= \frac{A^2 - B^2g_3 + 2ACm_1 - B^2g_2m_1 + C^2m_1^2 + 4B^2m_1^3}{D^2 - 4E}, \\ K(m_1, n_1) &= \frac{-2A^2 + 2B^2g_3 - 2ACm_1 + B^2g_2m_1 + 4B^2m_1^3 - 2ACn_1 + B^2g_2n_1 - 2C^2m_1n_1 - 12B^2m_1^2n_1}{(4E - D^2)^{3/2}}. \end{aligned}$$

Letting

$$\begin{aligned} \alpha &= \wp^{-1}(m_1), \\ \beta &= \wp^{-1}(n_1), \end{aligned}$$

and

$$x_1 = -c_0 Q + x_2,$$

where  $x_2$  is another arbitrary constant, we express  $x(s)$  as

$$\begin{aligned} x(s) &= Q(s + c_0) - x_2 + \omega_0 B \left[ \frac{8(2A - CD) \arctan \left( \frac{D+2\wp}{\sqrt{-D^2+4E}} \right)}{(-D^2 + 4E)^{3/2}} + \frac{-4AD + 8CE + (-8A + 4CD)\wp}{(D^2 - 4E)(\wp^2 + D\wp + E)} \right] \\ &\quad + 2\omega_0 [J(m_1, n_1)I_2((s + c_0)/4, \alpha) + K(m_1, n_1)I_1((s + c_0)/4, \alpha) \\ &\quad + J(n_1, m_1)I_2((s + c_0)/4, \beta) + K(n_1, m_1)I_1((s + c_0)/4, \beta)], \end{aligned} \quad (16)$$

where  $I_1$  and  $I_2$  come from [6] and [21] and are expressed as

$$\begin{aligned} I_1(u, \gamma) &= \frac{1}{\wp'(\gamma)} \left[ \log \left( \frac{\sigma(u - \gamma)}{\sigma(u + \gamma)} \right) + 2u\zeta(\gamma) \right], \\ I_2(u, \gamma) &= \frac{\wp''(\gamma)}{\wp'^3(\gamma)} \log \left( \frac{\sigma(u + \gamma)}{\sigma(u - \gamma)} \right) - \frac{1}{\wp'^2(\gamma)} (\zeta(u + \gamma) + \zeta(u - \gamma)) - \left( \frac{2\wp(\gamma)}{\wp'^2(\gamma)} + \frac{2\wp''(\gamma)\zeta(\gamma)}{\wp'^3(\gamma)} \right) u. \end{aligned}$$

Here  $\zeta$  is the Weierstraß zeta function and  $\sigma$  is the Weierstraß sigma function. Thus we have  $x(s)$  given in (16) and  $u(x(s))$  given in (12) both as functions of  $s$ . This gives a parametric representation of our solution as a function of  $s$

$$\begin{cases} y = u(x(s)), & \text{given in (12),} \\ x = x(s), & \text{given in (16).} \end{cases} \quad (17)$$

The approximation to the pressure given in [1] is

$$P = \rho \left\{ R - gz - \frac{1}{2} \left( \frac{Q}{u^2} + \frac{\omega_0}{2} \right)^2 (z^2 u'^2 + u^2) + \frac{1}{2} \left( \frac{\omega_0}{6} u^3 - \frac{\omega_0}{2} z^2 u - \frac{2}{3} \omega_0 z^3 - \frac{Q}{3} u + z^2 \frac{Q}{u} \right) \times \left( 2Q \frac{u'^2}{u^3} - u'' \left( \frac{Q}{u^2} + \frac{\omega_0}{2} \right) \right) \right\}. \quad (18)$$

This leads to a parametric representation of the pressure as a function of  $s$

$$\begin{cases} y = P(u(x(s)), z), & \text{given in (18),} \\ x = x(s), & \text{given in (16),} \end{cases} \quad (19)$$

where  $z$  is the distance from the channel bed.

Finally, note that an expression for the streamfunction can be derived using the techniques of [1]. Since this was not done in [1], the derivation is outlined in the appendix for the sake of completeness. The expression for the streamfunction is

$$\psi = \frac{1}{2} z^2 \omega_0 + z \left( \frac{Q}{u} - \frac{u \omega_0}{2} + \frac{Qu'^2}{3u} - \frac{Qu''}{6} - \frac{\omega_0 u^2 u''}{12} \right) - \frac{z^3}{6} \left( \frac{2Qu'^2}{u^3} - \frac{Qu''}{u^2} - \frac{\omega_0 u''}{2} \right), \quad (20)$$

which gives a parametric representation of the streamfunction as a function of  $s$  as

$$\begin{cases} y = \psi(u(x(s)), z), & \text{given in (20),} \\ x = x(s), & \text{given in (16).} \end{cases} \quad (21)$$

### 3 Matching the explicit solutions to previous works

First, we verify the explicit solutions found here and the numerical approximations given in [1] by comparing them to each other. Following the analysis of [1], we first note that (1) can be written in the form

$$u'^2 = \frac{\mathcal{G}(u)}{\mathcal{F}(u)}. \quad (22)$$

Letting  $Z_1$ ,  $Z_2$ ,  $m$  and  $M$  represent the roots of the numerator  $\mathcal{G}$  on the right-hand side of (22) we write

$$\begin{aligned} \mathcal{G}(u) &= -3 \left( \frac{\omega_0^2}{12} u^4 + gu^3 - (2R - \omega_0 Q)u^2 + 2Su - Q^2 \right) \\ &= \frac{\omega_0^2}{4} (M - u)(u - m)(u - Z_1)(u - Z_2). \end{aligned} \quad (23)$$

By comparing the coefficients of (23) and assuming that  $Q$ ,  $m$ , and  $M$  are given, the two additional roots  $Z_1$  and  $Z_2$  are found as (note that a small typo in [1] has been corrected here)

$$Z_1 = \frac{1}{2} \left\{ - \left( \frac{12}{\omega_0^2} g + (M + m) \right) - \sqrt{\left( \frac{12}{\omega_0^2} g + (M + m) \right)^2 + \frac{48Q^2}{\omega_0^2 m M}} \right\},$$

$$Z_2 = \frac{1}{2} \left\{ - \left( \frac{12}{\omega_0^2} g + (M + m) \right) + \sqrt{\left( \frac{12}{\omega_0^2} g + (M + m) \right)^2 + \frac{48Q^2}{\omega_0^2 m M}} \right\}.$$

The total head  $R$  and the flow force  $S$  are obtained as

$$R = \frac{\omega_0 Q}{2} - \frac{\omega_0^2}{24} (Z_1 Z_2 + m M + (M + m)(Z_1 + Z_2)),$$

$$S = -\frac{\omega_0^2}{24} ((M + m) Z_1 Z_2 + m M (Z_1 + Z_2)).$$

Following the work in [1] there are two cases depending on the sign of  $\omega_0$ . If  $\omega_0 > 0$ , then  $u'^2$  has no singularities and there is a smooth periodic solution if  $Z_2 < m < M$ . If  $\omega_0 < 0$ , then  $u'^2$  has two singularities and the parameter space is more restricted. To find the conditions for smooth solutions to exist, we let  $\mathcal{F}(u)$  be expressed as

$$\mathcal{F}(u) = \left( Q + \frac{\omega_0}{2} u^2 \right)^2 = \frac{\omega_0^2}{4} (u - A_+)^2 (u - A_-)^2, \quad (25)$$

which reveals that the derivative is singular when  $u$  takes the values  $A_+ = \sqrt{\frac{2Q}{-\omega_0}}$  and  $A_- = -\sqrt{\frac{2Q}{-\omega_0}}$ . In the case  $\omega_0 < 0$ , smooth solutions exist when  $M < A_+$ . To better understand this condition, we introduce the non-dimensional Froude number

$$F = \frac{\omega_0 M^2}{2Q}.$$

Substituting  $F$  for  $\omega_0$  we find four cases:

$$\begin{cases} 0 < F : & \text{smooth solutions exist if } Z_2 < m < M, \\ -1 < F < 0 : & \text{smooth solutions exist,} \\ F = -1 : & \text{limiting case of smooth solutions ceasing to exist,} \\ F < -1.1 : & \text{smooth solutions do not exist but overhanging waves are possible.} \end{cases} \quad (26)$$

Only solutions of the first two cases above are seen in [1]. Below we show one representative example of each of the cases. As in [1], we use the parameters

$$g = 9.81; \rho = 1; m = 1.1; Q = 1.2\sqrt{g}; h_0 = \sqrt[3]{g^{-1}Q^2}; \omega_0 = \frac{2QF}{M^2}. \quad (27)$$

For the following figures, we use the following parameters:

$$\begin{cases} 0 < F : & M = 1.3 \text{ and } F = 1.15, \\ -1 < F < 0 : & M = 1.7 \text{ and } F = -0.3, \\ F = -1 : & M = 1.7 \text{ and } F = -1, \\ F < -1.1 : & M = 1.7 \text{ and } F = -1.1. \end{cases}$$

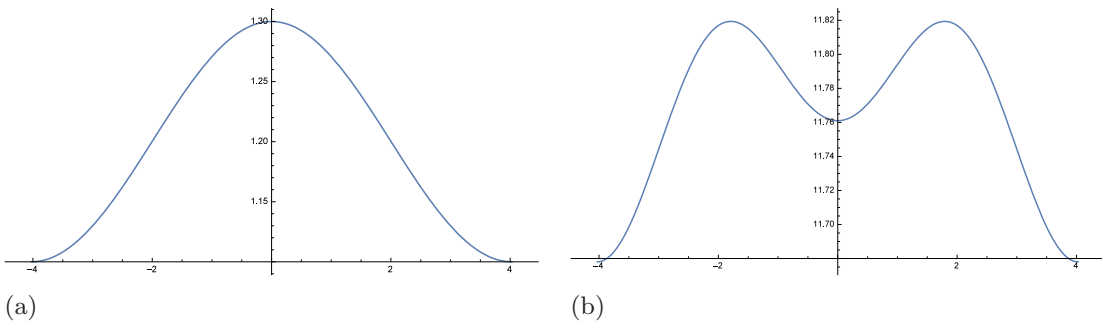


Figure 2: (a)  $u(x)$  as a function of  $x$ . (b)  $P(u(x), 0)$  as a function of  $x$ .  
 $0 < F, M = 1.3, F = 1.15$ , and  $-1/2 \leq s \leq 1/2$ . Smooth solutions exist.

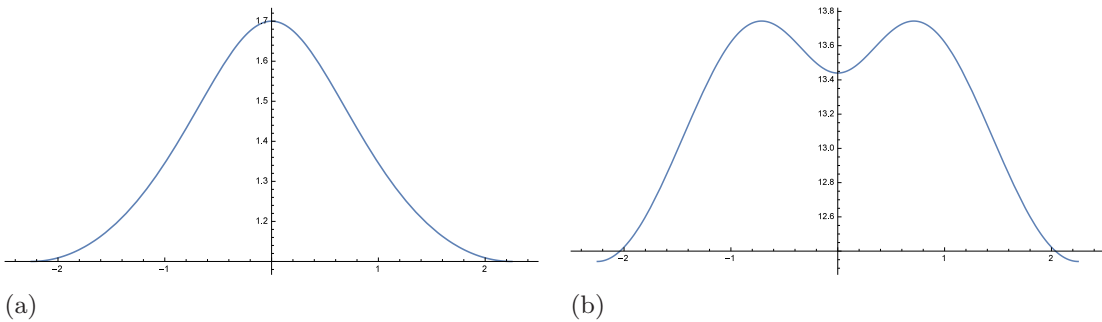


Figure 3: (a)  $u(x)$  as a function of  $x$ . (b)  $P(u(x), 0)$  as a function of  $x$ .  
 $-1 < F < 0, M = 1.7, F = -0.3$ , and  $-1/2 \leq s \leq 1/2$ . Smooth solutions exist.

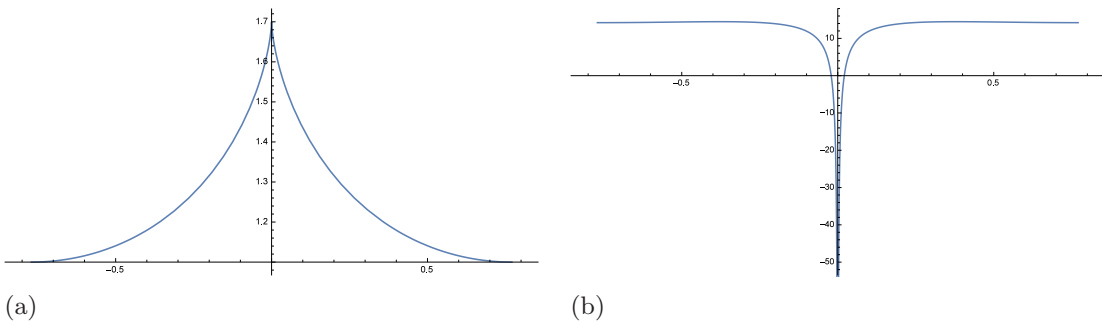


Figure 4: (a)  $u(x)$  as a function of  $x$ . (b)  $P(u(x), 0)$  as a function of  $x$ .  
 $F = -1, M = 1.7, F = -1$ , and  $-1/2 \leq s \leq 1/2$ . Cusp solution.

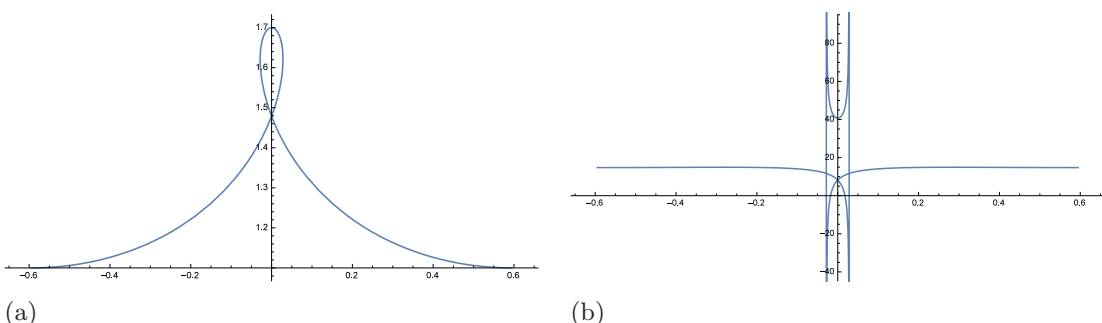


Figure 5: (a)  $u(x)$  as a function of  $x$ . (b)  $P(u(x), 0)$  as a function of  $x$ .  
 $F < -1, M = 1.7, F = -1.1$ , and  $-1/2 \leq s \leq 1/2$ . Overhanging solutions.

Additionally, in order to obtain periodic solutions with  $m < u(x) < M$  and with zero imaginary part, we need to set

$$c_0 = 4\omega_2(g_2, g_3), \quad (28)$$

where  $\omega_2$  is a Weierstraß half period corresponding to the lattice invariants  $g_2$  and  $g_3$  with non-zero imaginary part.

We produce plots of the explicit solutions for the various cases of (26) with the parameters given in (27), (28) and (32). Two plots for each case will be shown:

1.  $u(x)$  as a function of  $x$ ,
2.  $P(u(x), 0)$  as a function of  $x$ .

Note that since our solutions are symmetric under spacial translations (varying  $x_2$ ) we can shift the waves so they coincide with those in [1]. Figures 2 and 3 show two curves found in [1], and no visual difference can be detected between the explicit solutions and the numerical approximations of [1]. We notice that  $x(s)$  is a monotone function of  $s$  as  $F > -1$  decreases up until the critical value of  $F = -1$ . Beyond the critical point where  $F = -1$ ,  $x(s)$  is no longer monotone and as a result the solutions are no longer smooth. Figure 4 shows the limiting case of a cusped solution. Note that the evaluation of the pressure at the bottom under the wavecrest appears to yield extremely low and apparently non-physical values. Figure 5 shows a looped (or self-intersecting) solution which is allowed in equations (10) and (11), but not possible in (1). Since it was assumed in the derivation that the free surface is a single-valued function of  $x$ , the solution shown in Figure 5 is beyond the physical validity of the equation.

Next we investigate whether the solutions of (1) are close to the solutions of the full Euler equations with a background shear flow found in [31]. Figure 6 and 7 show a sequence of large waveheight solutions with waveheight  $H = 1.2$ , and for the set of parameters  $g = 9.81, \rho = 1.0, h_0 = 1.0$ . Note also that by rearranging the variables, we can make the self-intersecting solution look like an overhanging solution. Even though the curves shown in Figure 7 look similar to the free surface profiles shown in Figure 6 of [31], strictly speaking, the curves in Figure 7 do not represent solutions of (1).

We can also set our solutions to be  $2\pi$  periodic. For this we need to examine the periods of  $x(s)$  and  $u(s)$ . Let  $\omega_1$  be the Weierstraß half period corresponding to the lattice invariants  $g_2$  and  $g_3$  with non-zero real part. We note that

$$u(s + T_u) = u(s),$$

where

$$T_u = 8\omega_1,$$

denotes the period of  $u(x)$ , since both  $\wp((s + c_0)/4; g_2, g_3)$  and  $\wp'((s + c_0)/4; g_2, g_3)$  are periodic of period  $8\omega_1$ . Next we notice that

$$x(s + T_u) = x(s) + T_x,$$

where

$$T_x = QT_u + 2\omega_0 [J(m_1, n_1)J_2(\alpha) + K(m_1, n_1)J_1(\alpha) + J(n_1, m_1)J_2(\beta) + K(n_1, m_1)J_1(\beta)],$$

with

$$J_1(\gamma) = \frac{1}{\wp'(\gamma)} (-4\zeta(\omega_1)\gamma + 4\omega_1\zeta(\gamma)),$$

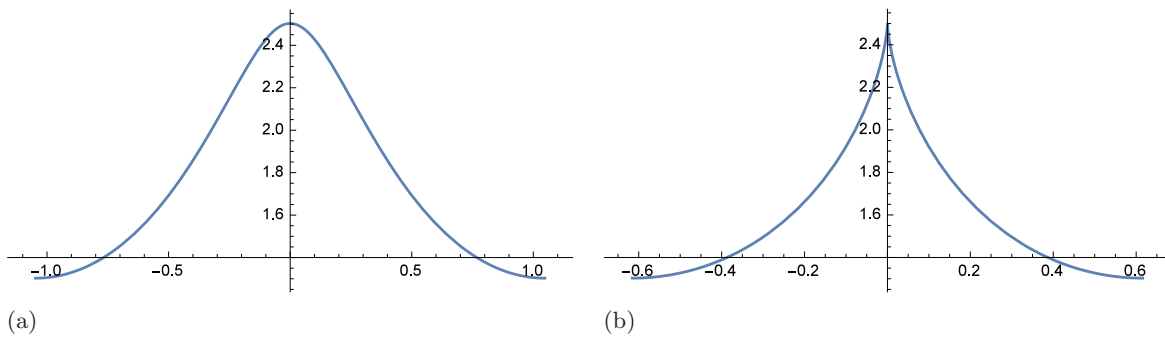


Figure 6:  $u(x)$  as a function of  $x$ : (a) smooth solution  $F = -0.5$ , (b) peaked solution  $F = -1.0$ .

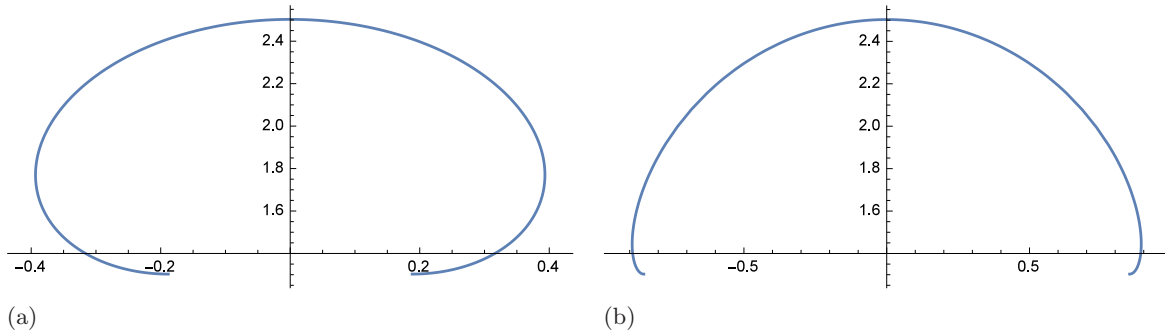


Figure 7:  $u(x)$  as a function of  $x$ : (a) overhanging solution  $F = -2.0$ , (b) overhanging solution  $F = -3.0$ .

and

$$J_2(\gamma) = \frac{\wp''(\gamma)}{\wp^3(\gamma)} 4\zeta(\omega_1)\gamma - \frac{4\zeta(\omega_1)}{\wp'^2(\gamma)} - 2\omega_1 \left( \frac{2\wp(\gamma)}{\wp'^2(\gamma)} + \frac{2\wp''(\gamma)\zeta(\gamma)}{\wp^3(\gamma)} \right).$$

This was determined by noting that

$$I_1(u + 2\omega_1, \gamma) = I_1(u, \gamma) + J_1(\gamma),$$

$$I_2(u + 2\omega_1, \gamma) = I_2(u, \gamma) + J_2(\gamma),$$

which we see from [28]:

$$\zeta(u + 2\omega_1) = \zeta(z) + 2\zeta(\omega_1),$$

$$\sigma(u + 2\omega_1) = -e^{2\zeta(\omega_1)(u + \omega_1)}\sigma(z).$$

Here  $T_x$  gives an analytical expression for the wavelength of the solution. If we wanted to force our solutions to be  $2\pi$  periodic, we could simply rescale  $x$  by  $2\pi/T_x$  and  $u$  by  $2\pi/T_x$  as this is the scaling symmetry of (1).

In order to better compare our results with those in [1], we would like to have the peak of the wave at  $x = 0$ . To achieve this we determine the value of  $s$  for which  $u(s)$  is at a peak and call this value  $T_s$ . Taking (11) we have

$$\wp((T_s + c_0)/4, g_2, g_3) = \frac{4(-QM^2\omega_0 + 2RM^2 + 6Q^2 - 6SM)}{M^2},$$

where we plugged in  $y = M$  and  $dy/ds = 0$  to be at the peak of the wave. This gives

$$T_s = 4\wp^{-1} \left( \frac{4(-QM^2\omega_0 + 2RM^2 + 6Q^2 - 6SM)}{M^2}, g_2, g_3 \right) - c_0.$$

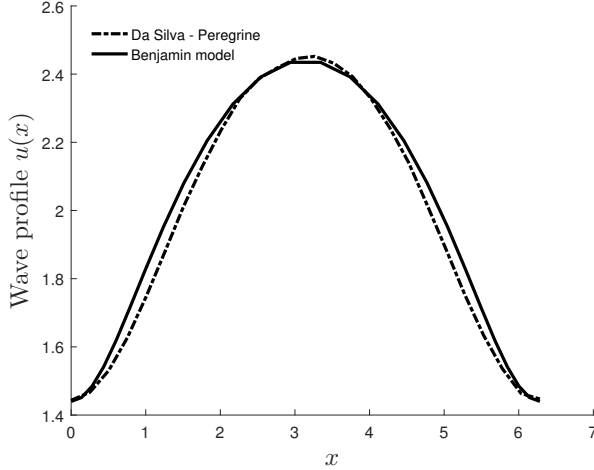


Figure 8: Comparing approximate solutions of the full Euler equations (dashed curve) to exact solutions of (1) (solid curve). The waves have waveheight  $H = 1$  and wavelength  $2\pi$ . The problem is normalized with  $g = 1$  and  $h_0 = 1$ , and the background vorticity is  $\omega_0 = -3$ .

Thus for solutions with the peak at  $x = 0$ , we rewrite (17), (19), and (21) as

$$\begin{cases} y = u(T_u(s - T_s)), & \text{given in (12),} \\ x = x(T_u(s - T_s)), & \text{given in (16),} \end{cases} \quad (29)$$

$$\begin{cases} y = P(u(T_u(s - T_s)), z), & \text{given in (18),} \\ x = x(T_u(s - T_s)), & \text{given in (16).} \end{cases} \quad (30)$$

$$\begin{cases} y = \psi(u(T_u(s - T_s)), z), & \text{given in (20),} \\ x = x(T_u(s - T_s)), & \text{given in (16).} \end{cases} \quad (31)$$

Additionally, we set

$$\begin{aligned} x_2 = T_u \left( Q(\tilde{s} + c_0) + \omega_0 B \left[ \frac{8(2A - CD) \arctan \left( \frac{D + 2\varphi((\tilde{s} + c_0)/4)}{\sqrt{-D^2 + 4E}} \right)}{(-D^2 + 4E)^{3/2}} \right. \right. \\ \left. \left. + \frac{-4AD + 8CE + (-8A + 4CD)\varphi((\tilde{s} + c_0)/4)}{(D^2 - 4E)(\varphi((\tilde{s} + c_0)/4)^2 + D\varphi((\tilde{s} + c_0)/4) + E)} \right] \right. \\ \left. + 2\omega_0 [J(m_1, n_1)I_2((\tilde{s} + c_0)/4, \alpha) + K(m_1, n_1)I_1((\tilde{s} + c_0)/4, \alpha) \right. \\ \left. + J(n_1, m_1)I_2((\tilde{s} + c_0)/4, \beta) + K(n_1, m_1)I_1((\tilde{s} + c_0)/4, \beta)] \right), \end{aligned} \quad (32)$$

where  $\tilde{s} = T_u(0 - T_s)$ . This  $x_2$  is chosen so that when  $s = 0$ ,  $x = 0$ . Additionally, note that we scale  $s$  by  $T_u$ . The scaling of  $s$  is so that as  $s$  ranges from  $-1/2$  to  $1/2$ , we plot exactly one period of wavelength  $T_x$ .

We compare some wave profiles presented in Fig. 6 of by Teles da Silva and Peregrine [31] with solutions of same parameters computed by the current explicit method. Note that in [31], the parameters  $g$  and  $h_0$  were normalized, so that we need to choose  $g = 1$  and  $h_0 = 1$ .

We first present a comparison of a traveling wave of waveheight  $H = 1$  and vorticity  $\omega_0 = -3$ . In order to get a good match with the plot from Fig. 6 of [31], we selected  $m = 1.44, M =$

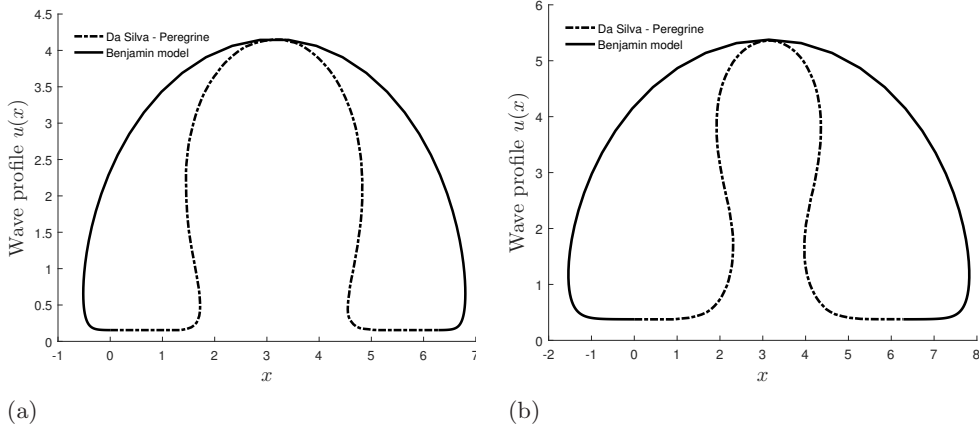


Figure 9: Comparing approximate solutions of the full Euler equations (dashed curve) to exact solutions of (1) (solid curve). The problem is normalized with  $g = 1$ ,  $h_0 = 1$  and wavelength  $2\pi$ . The background vorticity is  $\omega_0 = -3$ . (a) waveheight  $H = 4$ . (b) waveheight  $H = 5$ .

2.44,  $Q = 0.09$  Figure 8 shows an explicit solution of (1) compared to a solution of the full Euler equations shown in Fig. 6 in [31]. Even though the waveheight-depth ratio of  $1/2$  is not very small, the profiles match fairly closely.

Comparing higher-amplitude waves is more difficult since the solutions shown in [31] with waveheight larger than 1 are overhanging. Setting all parameters correctly yields the comparison shown in Figure 9. As can be seen, the wavelength matches, and the solutions of (7),(8) are also overhanging, but look very different nevertheless. One may conclude from this last comparison, that if solutions of (7),(8) are not single-valued, and therefore are beyond the validity of (1), they will not in general represent the physical reality of the surface-water wave problem.

## 4 Pressure contours and streamlines

In this section, we explore the flow underneath the surface as predicted by (1), with the help of the expression (18) for the pressure and (20) for the streamfunction.

First, pressure contours and streamlines are reviewed for positive Froude numbers  $F$ . This case corresponds to the case labelled 'upstream' in [31]. As mentioned in that work, it is in this case that a critical layer is possible. Examining figures 10-15, it appears that as the strength of the vorticity increases, first, the pressure becomes non-monotone (Figure 11). In other words, the pressure strongly departs from hydrostatic pressure, the bottom pressure is maximal under the sides of the wave (not the crest), and this goes hand in hand with the development of closed streamlines (Figure 12). For large enough Froude numbers, a critical layer (i.e., a closed circulation) develops in the interior of the fluid domain (Figure 13). In the extreme case of  $F = 3$ , pressure inversion occurs as regions of high pressure are above regions of low pressure in the fluid column (Figure 15).

For negative Froude numbers, the flow corresponds to the downstream case [31]. In this case non-monotone pressures also develop, but no critical layer occurs in the fluid domain. Figures 19 and 20 show strongly non-monotone pressures. Apparently, as the shape of the free surface approaches a cusped profile, non-physical features appear in the description of the flow.

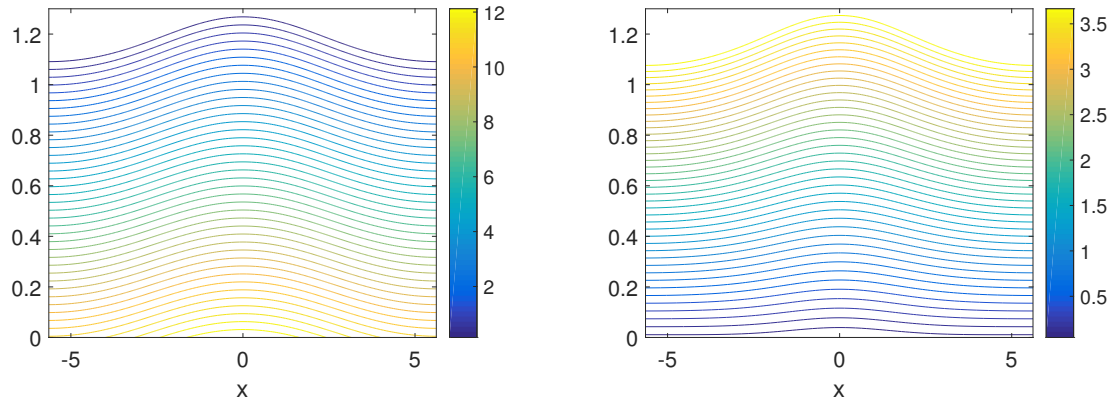


Figure 10: Traveling wave with  $m = 1.1$ ,  $M = 1.3$ , and  $F = 0.2$ . Left: pressure contours. Right: streamlines.

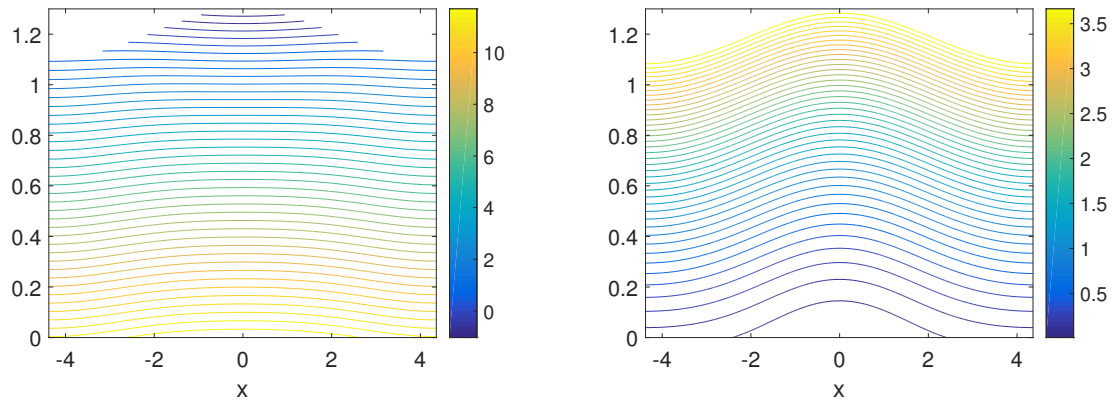


Figure 11: Traveling wave with  $m = 1.1$ ,  $M = 1.3$ , and  $F = 0.9$ . Left: pressure contours. Right: streamlines.

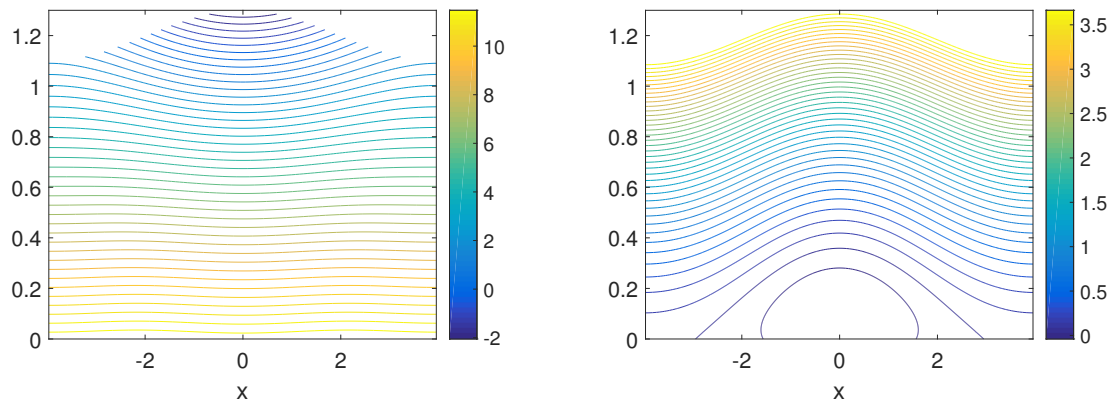


Figure 12: Traveling wave with  $m = 1.1$ ,  $M = 1.3$ , and  $F = 1.2$ . Left: pressure contours. Right: streamlines.

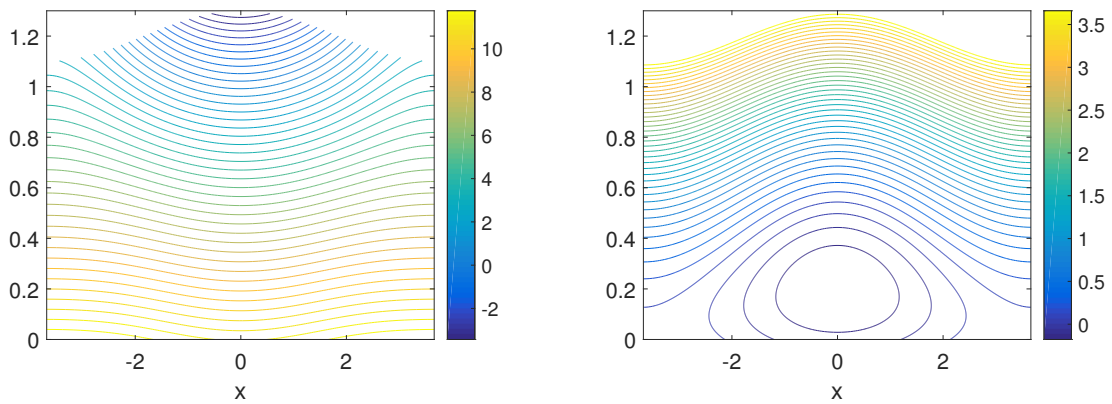


Figure 13: Traveling wave with  $m = 1.1$ ,  $M = 1.3$ , and  $F = 1.5$ . Left: pressure contours. Right: streamlines. Pressure highly non-monotone, critical layer appears.

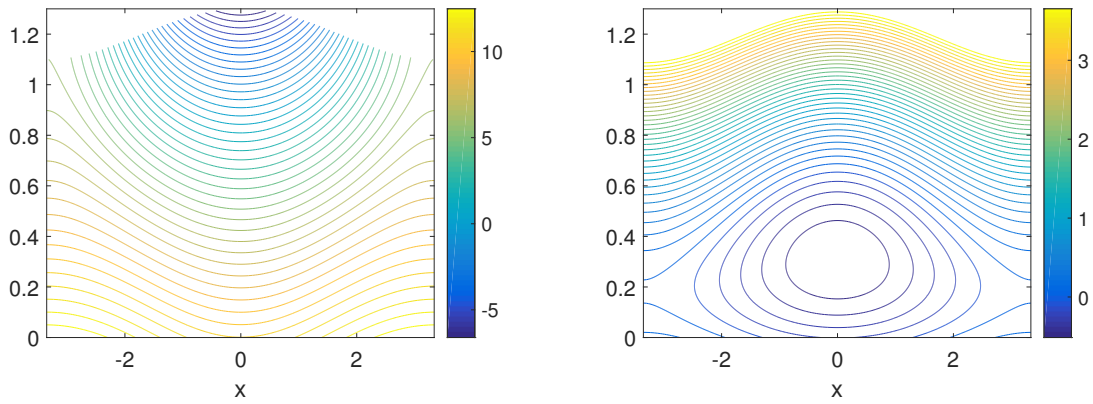


Figure 14: Traveling wave with  $m = 1.1$ ,  $M = 1.3$ , and  $F = 2.0$ . Left: pressure contours. Right: streamlines.

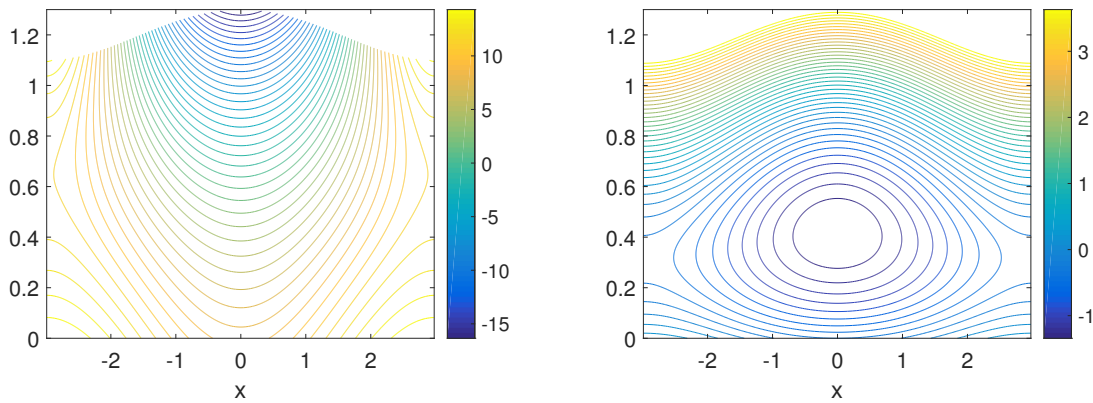


Figure 15: Traveling wave with  $m = 1.1$ ,  $M = 1.3$ , and  $F = 3.0$ . Left: pressure contours. Right: streamlines. Pressure inversion: high pressure above low pressure.

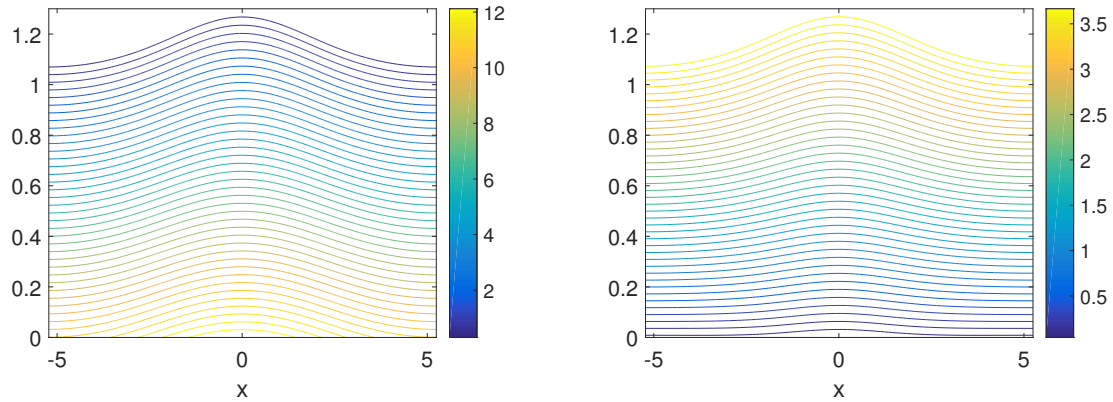


Figure 16: Traveling wave with  $m = 1.1$ ,  $M = 1.3$ , and  $F = -0.001$ . Left: pressure contours. Right: streamlines.

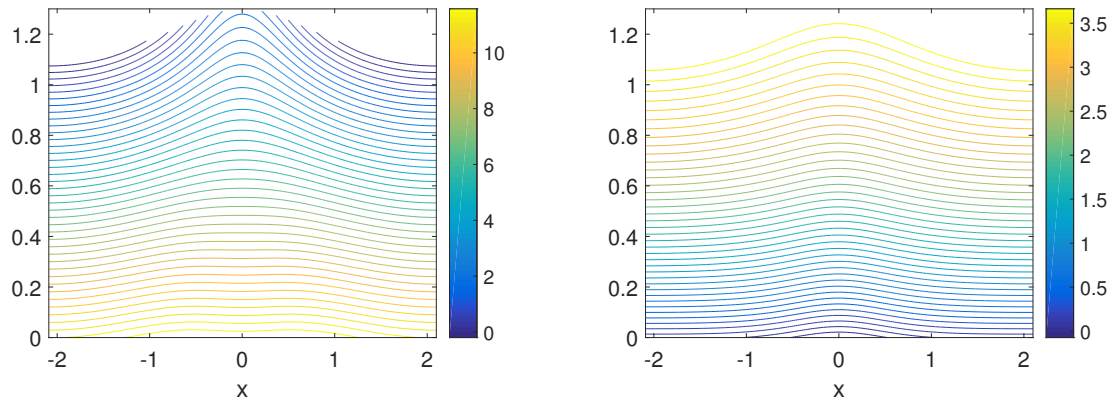


Figure 17: Traveling wave with  $m = 1.1$ ,  $M = 1.3$ , and  $F = -0.5$ . Left: pressure contours. Right: streamlines.

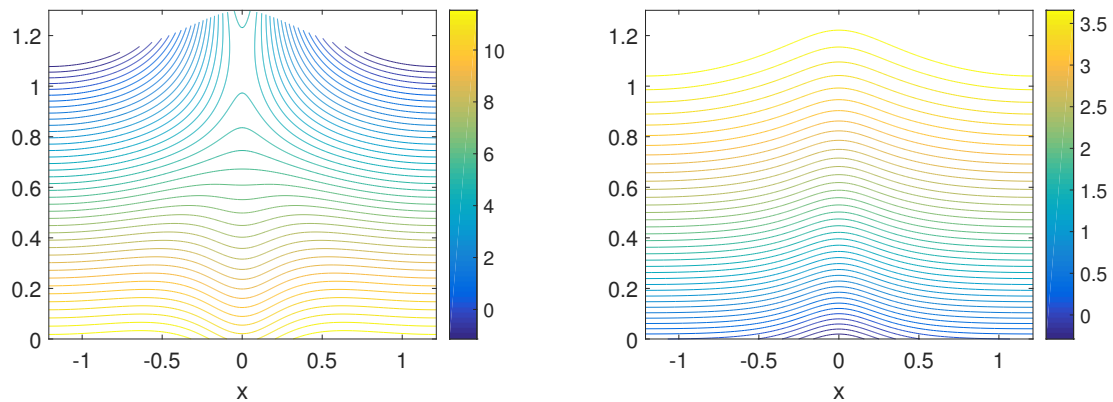


Figure 18: Traveling wave with  $m = 1.1$ ,  $M = 1.3$ , and  $F = -0.7$ . Left: pressure contours. Right: streamlines.

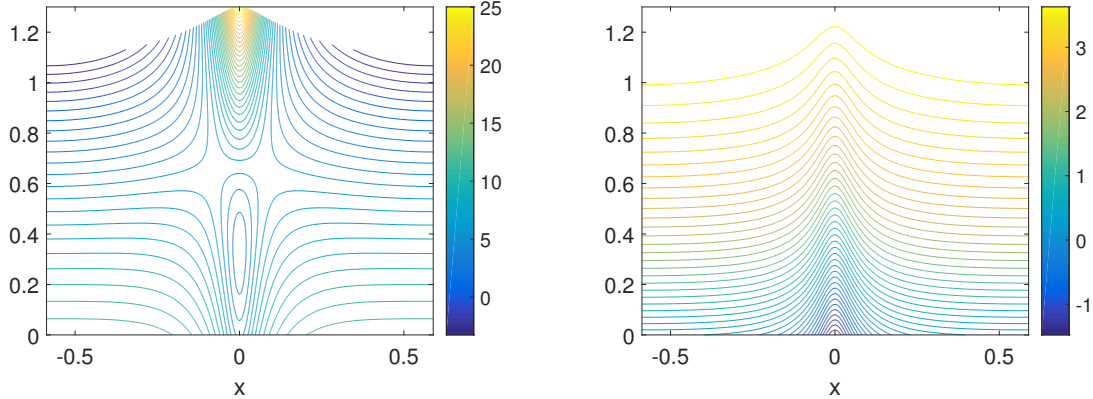


Figure 19: Traveling wave with  $m = 1.1$ ,  $M = 1.3$ , and  $F = -0.9$ . Left: pressure contours. Right: streamlines.

## 5 Conclusion

The nonlinear differential equation (1) is known to be a model for steady surface water waves on a background shear flow. The equation has been found to admit solutions given explicitly in terms of a parametric representation featuring the Weierstraß P, zeta and sigma functions. This representation is a convenient tool for obtaining a variety of wave profiles without having to resort to numerical approximation. In connection with the reconstruction of the pressure underneath the surface explained in [1], and the reconstruction of the streamfunction detailed in the appendix, a complete description of the flow can be obtained.

The exact solutions of (1) have been compared to wave profiles obtained from full Euler computations in [31], and fair agreement was found for regular waves. On the other hand, overhanging waves were found not to agree with the full Euler solutions. This is not surprising since the parametric representation enables the description of multi-valued profiles which transcends the collection of solutions of (1).

With a view towards the flow in the fluid column below the wave, a number of wave shapes with increasing strength of vorticity were exhibited. It was found in the case of steady waves propagating upstream that the flow underneath the waves may feature critical layers and non-monotone pressure profiles. In the case of waves propagating downstream, the development of cusped surface profiles goes hand in hand with unrealistic pressure profiles apparently conflicting with the long-wave approximation which is the basis for the model (1). Building on the results of this paper, future work may focus on detailed comparisons of the fluid flow as described by the methods of the current work to numerical approximations of the flow governed by the Euler equations with background vorticity. Such a study will cast more light on the limitations of the current model, especially as regarding the ability to describe properties of the flow in the bulk of the fluid.

## Acknowledgments

This research was supported in part by the Research Council of Norway under grant 213474/F20 and by the National Science Foundation under grant NSF-DMS-1008001. Any opinions, findings, and conclusions

or recommendations expressed in this material are those of the authors and do not necessarily reflect the views of the funding sources.

## A Reconstruction of the streamfunction

We want to reconstruct the streamfunction  $\psi(x, z)$  using the solutions  $u$  of the differential equation (1). This is done by using the ansatz

$$\psi = \frac{1}{2}z^2\omega_0 + zf - \frac{1}{3!}z^3f'', \quad (33)$$

for the streamfunction and the identity

$$Q = \frac{1}{2}u^2\omega_0 + \zeta f - u^3\frac{1}{6}f'',$$

both of which are valid to second order in the long-wave parameter  $\beta = h_0^2/\lambda^2$ , where  $h_0$  is the undisturbed depth of the fluid, and  $\lambda$  is the wavelength. To obtain an expression for  $f$  in terms of  $\zeta$ , one has to invert the operator  $1 - \frac{1}{6}\zeta^2\partial_{xx}$ , leading to

$$\left[1 - \frac{1}{6}\zeta^2\partial_{xx}\right]^{-1} \left(\frac{Q}{\zeta} - \frac{1}{2}\zeta\omega_0\right) = f.$$

In order to bring out the difference in scales between the undisturbed depth  $h_0$  and the wavelength  $L$ , we use the scaling

$$\tilde{x} = \frac{x}{L}, \quad \tilde{z} = \frac{z}{h_0}, \quad \tilde{\zeta} = \frac{\zeta}{h_0}, \quad \tilde{\psi} = \frac{1}{c_0 h_0} \psi, \quad \tilde{\omega}_0 = \frac{h_0}{c_0} \omega_0,$$

In addition,  $Q$  is scaled as

$$\tilde{Q} = \frac{Q}{h_0 c_0}.$$

In non-dimensional variables, the expression for  $\psi$  is

$$\tilde{\psi} = \frac{1}{2}\tilde{z}^2\tilde{\omega}_0 + \tilde{z}\tilde{f} - \frac{\beta}{3!}\tilde{z}^3\tilde{f}'' + \mathcal{O}(\beta^2).$$

The function  $\tilde{f}$  is written as

$$\begin{aligned} \tilde{f} &= \left[1 + \frac{\beta}{6}\tilde{u}^2\partial_{\tilde{x}}^2 + \mathcal{O}(\beta^2)\right] \left(\frac{\tilde{Q}}{\tilde{u}} - \frac{1}{2}\tilde{u}\omega_0\right) + \mathcal{O}(\beta^2). \\ &= \frac{\tilde{Q}}{\tilde{u}} - \frac{1}{2}\tilde{u}\tilde{\omega}_0 + \frac{\beta}{3}Q\frac{(\tilde{u}')^2}{\tilde{u}} - \frac{\beta}{6}Q\tilde{u}'' - \frac{\beta}{12}\omega_0\tilde{u}^2\tilde{u}'' + \mathcal{O}(\beta^2). \end{aligned}$$

The second derivative is

$$\tilde{f}'' = 2\frac{\tilde{Q}}{\tilde{u}^3}(\tilde{u}')^2 - \frac{\tilde{Q}}{\tilde{u}^2}\tilde{u}'' - \frac{1}{2}\omega_0\tilde{u}'' + \mathcal{O}(\beta).$$

Putting these together, we find the streamfunction in terms of  $\tilde{u}$ :

$$\begin{aligned} \tilde{\psi} &= \frac{1}{2}\tilde{z}^2\tilde{\omega}_0 + \tilde{z} \left[ \frac{\tilde{Q}}{\tilde{u}} - \frac{1}{2}\tilde{u}\tilde{\omega}_0 + \frac{\beta}{3}Q\frac{(\tilde{u}')^2}{\tilde{u}} - \frac{\beta}{6}Q\tilde{u}'' - \frac{\beta}{12}\omega_0\tilde{u}^2\tilde{u}'' \right] \\ &\quad - \frac{\beta}{3!}\tilde{z}^3 \left[ 2\frac{Q}{\tilde{u}^3}(\tilde{u}')^2 - \frac{Q}{\tilde{u}^2}\tilde{u}'' - \frac{\omega_0}{2}\tilde{u}'' \right] + \mathcal{O}(\beta^2). \end{aligned}$$

## References

- [1] A. Ali and H. Kalisch, *Reconstruction of the pressure in long-wave models with constant vorticity*, Eur. J. Mech. B Fluids **37** (2013), 187–194.
- [2] A. Ali and H. Kalisch, *On the formulation of mass, momentum and energy conservation in the KdV equation*, Acta Appl. Math. **133** (2014), 113–131.
- [3] T. B. Benjamin, *The solitary wave on a stream with an arbitrary distribution of vorticity*, J. Fluid Mech. **12** (1962), 97–116.
- [4] T. B. Benjamin and M. J. Lighthill, *On cnoidal waves and bores*, Proc. Roy. Soc. London Ser. A **224** (1954), 448–460.
- [5] H. Borluk and H. Kalisch, *Particle dynamics in the KdV approximation*, Wave Motion **49** (2012), 691–709.
- [6] P.F. Byrd and M.D. Friedman, *Handbook of elliptic integrals for engineers and scientists*, vol. 67. (Springer Berlin, 1971).
- [7] T.L. Clarke, B. Lesht, R.A. Young, D.J.P. Swift and G.L. Freeland, *Sediment resuspension by surface-wave action: An examination of possible mechanisms*, Marine Geology, **49** (1982) 43–59
- [8] T. Colin, F. Dias and J.-M. Ghidaglia, *On rotational effects in the modulations of weakly nonlinear water waves over finite depth*, Eur. J. Mech. B Fluids **14** (1995), 775–793.
- [9] A. Constantin, M. Ehrnström and E. Wahlén, *Symmetry of steady periodic gravity water waves with vorticity*, Duke Math. J. **140** (2007), 591–603.
- [10] A. Constantin and J. Escher, *Symmetry of steady periodic surface water waves with vorticity*, J. Fluid Mech. **498** (2004) 171–181.
- [11] A. Constantin and W. Strauss, *Exact steady periodic water waves with vorticity*, Comm. Pure Appl. Math. **57** (2004), 481–527.
- [12] A. Constantin and W. Strauss, *Pressure beneath a Stokes wave*, Comm. Pure Appl. Math. **63** (2010), 533–557.
- [13] A. Constantin and E. Varvaruca, *Steady periodic water waves with constant vorticity: regularity and local bifurcation*, Arch. Ration. Mech. Anal. **199** (2011), 33–67.
- [14] R. Conte and M. Musette, *The Painlevé Handbook* (Springer Science & Business Media, 2008).
- [15] W. Choi, *Strongly nonlinear long gravity waves in uniform shear flows*, Phys. Rev. E **68** (2003), 026305.
- [16] L. Debnath *Nonlinear Water Waves* (Academic Press, 1994).
- [17] S.H. Doole, *The pressure head and flowforce parameter space for waves with constant vorticity*, Quart. J. Mech. Appl. Math. **51** (1998), 61–72.
- [18] S.H. Doole and J. Norbury, *The bifurcation of steady gravity water waves in  $(R, S)$  parameter space*, J. Fluid Mech. **302** (1995), 287–305.
- [19] M. Ehrnström and G. Villari, *Linear water waves with vorticity: rotational features and particle paths*, J. Differential Equations **244** (2008), 1888–1909,
- [20] M. Ehrnström, J. Escher and E. Wahlén, *Steady water waves with multiple critical layers*, SIAM J. Math. Anal. **43** (2011), 1436–1456.
- [21] I. Gradshteyn and I. Ryzhik, *Table of Integrals, Series and Products*, 5th edn (Academic Press, New York, 1994).
- [22] V. M. Hur, *Exact solitary water waves with vorticity*, Arch. Ration. Mech. Anal. **188** (2008), 213–244.
- [23] H. Kalisch, *A uniqueness result for periodic traveling waves in water of finite depth*, Nonlinear Anal. **58** (2004), 779–785.
- [24] J. Ko and W. Strauss, *Large-amplitude steady rotational water waves*, Eur. J. Mech. B Fluids **27** (2008), 96–109.
- [25] P.K. Kundu and I.M. Cohen, *Fluid Mechanics*, 4th edition (Academic Press, 2008)

- [26] Y. Li and S.Å. Ellingsen, *Ship waves on uniform shear current at finite depth: wave resistance and critical velocity*, J. Fluid Mech. **791** (2016), 539–567.
- [27] C.C. Mei, S.-J. Fan and K.-R. Jin, *Resuspension and transport of fine sediments by waves*, J. Geophys. Res. Oceans **102** (1997), 15807–15821.
- [28] F.W.J. Olver, D.W. Lozier, D.F. Boisvert and C.W. Clark, Eds. NIST Handbook of Mathematical Functions, (Cambridge University Press, New York, 2010).
- [29] J.S. Ribberink and A.A. Al-Salem, *Sediment transport in oscillatory boundary layers in cases of rippled beds and sheet flow*, J. Geophys. Res. Oceans **99** (1994), 12707–12727.
- [30] R. Thomas, C. Kharif and M. Manna, *A nonlinear Schrödinger equation for water waves on finite depth with constant vorticity* Phys. Fluids **24** (2012), 127102.
- [31] A.F. Teles da Silva and D.H. Peregrine, *Steep, steady surface waves on water of finite depth with constant vorticity*, J. Fluid Mech. **195** (1988), 281–302.
- [32] J. Touboul, J. Charland, V. Rey and K. Belibassakis, *Extended mild-slope equation for surface waves interacting with a vertically sheared current*, Coastal Engineering **116** (2016), 77–88.
- [33] J. Touboul and E. Pelinovsky, *Bottom pressure distribution under a solitonic wave reflecting on a vertical wall*, Eur. J. Mech. B Fluids **48** (2014), 13–18.
- [34] G. Valiron and J. Glazebrook, The Geometric Theory of Ordinary Differential Equations and Algebraic Functions (Math Sci Press, 1984).
- [35] J.-M. Vanden-Broeck, *Periodic waves with constant vorticity in water of infinite depth*, IMA J. Appl. Math. **56** (1996), 207–217.
- [36] E. Wahlén, *Steady water waves with a critical layer*, J. Differential Equations **246** (2009), 2468–2483.
- [37] E. Wahlén, *Hamiltonian long-wave approximations of water waves with constant vorticity*, Phys. Lett. A **372** (2008), 2597–2602.